Neutrophil-Mediated Inflammation Linking Cigarette Smoke Exposure to Rheumatoid Arthritis Pathogenesis

By

Jeba Atkia Maisha

A thesis submitted to the Faculty of Graduate Studies of the University of Manitoba in Partial Fulfilment of the Requirements of the Degree of

MASTER OF SCIENCE

Department of Immunology

Rady Faculty of Health Sciences

University of Manitoba

Winnipeg, Manitoba, Canada

Abstract

Rheumatoid arthritis (RA) is a chronic autoimmune disorder marked by joint inflammation and progressive destruction, often preceded by the appearance of anti-citrullinated protein antibodies (ACPA). While genetic predisposition such as the presence of *HLA-DRB1* shared epitope alleles plays a major role in disease susceptibility, environmental factors are also critical in triggering disease onset. Among these, cigarette smoking is the most well-established risk factor, particularly in individuals who develop ACPA-positive RA. Despite this association, the precise mechanism linking cigarette smoke exposure to RA development remains incompletely understood. The "mucosal origins hypothesis" proposes that RA may initiate at mucosal surfaces, such as the lungs, where early immune dysregulation occurs. Notably, cigarette smoke induces lung inflammation that promotes the recruitment of neutrophils into the lungs. These neutrophils can release neutrophil extracellular traps (NETs) enriched with citrullinated proteins through activation of Peptidyl Arginine Deiminase (PAD), the enzyme that generates citrulline. Given this triad of cigarette smoking, lung neutrophilia, and the generation of citrullinated autoantigens, we aimed to investigate the contribution of cigarette smoking in the initiation of autoimmunity in RA. We hypothesized that neutrophils generate citrullinated proteins through the formation of NETs and activation of PAD4. This study investigated how cigarette smoke modulates neutrophil function and inflammation in the context of RA.

The *in vitro* findings suggested that, cigarette smoke extract (CSE) induces PAD4-dependent NETosis in the absence of microbial triggers and this pathway is likely mediated by the stable chemical components present in CSE medium. While CSE did not induce degranulation, it enhanced neutrophil responses in the presence of foreign particles, indicating selective functional modulation.

Using the collagen-induced arthritis (CIA) mouse model combined with cigarette smoke (CS) exposure we observed increased lung neutrophil infiltration and protein citrullination, with more pronounced effects after prolonged exposure. Elevated NE levels and increased CCL4 expression in the CIA-CS group, highlight a neutrophil-driven inflammatory lung environment.

Collectively, these findings reveal a complex interplay between CS exposure, neutrophil-mediated inflammation, and the development of inflammatory arthritis. Overall, our findings suggest that pulmonary neutrophil infiltration may drive differences in inflammatory arthritis through the formation of immunogenic citrullinated proteins in NETs.

Acknowledgements

I would like to commence by praising and thanking The Almighty Allah, by whose grace and mercy I was able to accomplish completion of my thesis work.

I would like to express my deepest gratitude to my supervisor, Dr. Liam O'Neil, for being a phenomenal mentor throughout my master's. Your support, insightful guidance, and encouragement gave me the confidence to grow as a researcher. I am incredibly thankful for your mentorship, which shaped my critical thinking and scientific communication, and for always believing in my potential. It has been an honor to be a part of your lab, and this experience will remain foundational for my future.

I extend my sincere appreciation to my co-supervisor, Dr. Neeloffer Mookherjee, for her valuable input and for providing me access to her lab facilities and resources. Your generosity, insightful feedback, and willingness to support my work whenever needed were crucial to the success of my project.

I would like to thank my advisory committee members, Dr. Janilyn Arsenio and Dr. Barbara Porto, for their expert guidance, constructive feedback, and thought-provoking discussions that helped refine my research and expand my scientific perspective. Your encouragement has been immensely helpful during key stages of this project.

I am deeply thankful to Dr. Hemshekhar Mahadevappa for his exceptional support, from training me in animal models to patiently walking me through each technical step, no matter how small. Your mentorship and assistance in the lab went far beyond expectations, and I am so grateful to have learned from you.

To Dr. Mario Navarrete, thank you for teaching me all the proteomics work involved in this project and for generously conducting several key experiments. Your expertise and support were vital to the successful completion of my thesis. However, our discussions about series and movies will remain one of the most important highlights of my time here at the lab.

Special thanks to Courtney Marshall and Tiffany Shen for teaching and helping me with the BAL collection procedure. Courtney, thank you for always being so approachable, especially

during the early days, for all the wisdom about graduate student life and for being so open to helping.

I gratefully acknowledge Dr. Deanna Santer for her generosity in allowing me to collect blood from their lab and Xinyun Liu (Leo), Vi Diep Vu, Jing (Maggie) Ouyang, Olamide Ogungbola and Richard Miller for their assistance with multiple things like donor acquisition, selection, and phlebotomy. Your collaboration was critical for the *in vitro* section of my thesis.

My sincere thanks to Haziqa Kassim for teaching me how to prepare the CSE medium and for preparing it for my experiments on multiple occasions.

I am also thankful to Dr. Christopher Pascoe for giving me access to the CSR machine and to Sriyani Ranatunga for taking the time to train me and helping troubleshoot issues when needed.

Dr. Christine Zhang, thank you for your help with flow cytometry training, acquisition, and all the support you offered along the way.

I would like to thank Angela Peloquin, Silvia Panameno, and Katie Poitras for their administrative support, which helped me navigate everything from registration to graduation with ease.

To my fellow lab mates and colleagues: Ramiza Nausheen Zaman, Kamali Kannan, Padmanie Ramotar, Jun Kim, Alina Semenenko, Michael Adeyemi, and Obinna Okeke, thank you for the many ways you have all supported me in and out of the lab. Your friendship made the long days brighter.

I am grateful for the financial support provided by the University of Manitoba Entrance Scholarship, Faculty of Graduate Studies, Rady Faculty of Health Sciences Graduate Studentship, Research Manitoba, MSHRF, and the Department of Immunology.

Lastly, I would like to thank my loving parents and my husband, Raiyan. Your unwavering support, encouragement, and sacrifices made this entire journey possible. Thank you for being my strength, my comfort, and my biggest cheerleaders.

Dedication

This dissertation is dedicated to my loving parents, my nieces and my husband for all their encouragement and support throughout.

Table of Contents

Abstract ..... **I**
Acknowledgements ..... **III**
Dedication ..... **V**
Table of Contents ..... **VI**
List of Figures ..... **IX**
List of Tables ..... **X**
List of Abbreviations ..... **XI**
Copyright and Licensing ..... **XIV**
Chapter 1: General Introduction **1**
1.1 Rheumatoid Arthritis: An Overview 2
1.1.1 Disease Mechanisms and Immune Dysregulation 2
1.1.2 Genetic and Environmental Risk Factors 3
1.1.3 Role of Autoantibodies and Citrullinated Proteins 5
1.2 Neutrophils and NETosis 8
1.2.1 Neutrophil Effector Functions 8
1.2.2 NETs and PAD Enzymes in RA 12
1.3 Cigarette Smoking as a Modifiable Risk Factor 14
1.3.1 Smoking and RA Susceptibility 14
1.3.2 Mechanisms of Cigarette Smoke-Induced Inflammation 16
1.4 Role of Lung Inflammation in RA 18
1.5 Collagen-Induced Arthritis (CIA) Model and CS Exposure 19
Chapter 2: Thesis Overview **21**
2.1 Study Rationale 22
2.2. Gap in Knowledge 22
2.3 Overall Hypothesis 22
2.4 Specific Aims 22
Chapter 3: Materials & Methods **23**
3.1 Healthy Donor 24
3.1.1 Blood Collection from Healthy Donors 24
3.1.2 Neutrophil Isolation from Healthy Donor Blood 24
3.2 Cigarette Smoke Extract (CSE) Medium Preparation 25
3.3 *In Vitro* Experiments for Neutrophil Functions 26
3.3.1 Flow Cytometry to Detect Neutrophil Activation and Degranulation 26

3.3.2 Enzyme Activity Assay 27
3.3.3 Phagocytosis Assay (IgG and heat-killed *E. coli*) 28
3.3.4 Detection of extracellular DNA release from Neutrophils 29
3.3.5 Immunofluorescence Imaging to Detect NETosis/Phagocytosis 30
3.3.6 Isolation of NETs 31
3.3.7 Detection of Citrulline in NETs 32
3.3.8 PAD4 Inhibition Assay 33
3.4 Animal Models and Experimental Design 3.4.1 Mice 35
3.4.2 Collagen-Induced Arthritis Cigarette Smoke Exposure Model (Synchronized and Non-Synchronized) 35
3.4.3 Bronchoalveolar Lavage Fluid (BALF) Collection 37
3.4.4 Blood (Serum) Collection 37
3.4.5 Immunophenotyping of BAL Cells 38
3.4.6 of Cytokines and Chemokines 39
3.4.7 Anti-Mouse Collagen Antibody ELISA with BALF and Serum 39
3.4.8 Anti-NE ELISA with BALF and Serum 40
3.4.9 Detection of Citrulline in BALF 40
3.5 Statistical Analyses 40
Chapter 4: Results **41**
4.1 *In Vitro* Findings on the Effect of CSE on Neutrophilic Functions 42
4.1.1 CSE does not lead to Neutrophil Degranulation 42
4.1.2 CSE Increases Phagocytic Activity of Neutrophils 44
4.1.3 Neutrophils undergo NETosis when stimulated with CSE 45
4.1.4 CSE Induces Citrullinated Protein Production via PAD4-mediated NETosis 47
4.2 *In Vivo* Findings on the Effects of CS in Synchronized CIA Mouse Model 50
4.2.1 Clinical Score, Disease Incidence, and Anti-Mouse Collagen II Autoantibody 50
4.2.2 Lung Neutrophil Recruitment and Neutrophils Associated Chemokines and Cytokines 52
4.2.3 Neutrophil-associated Chemokines and Cytokines in the Serum at Various Time Points 55
4.2.4 NE in BALF and Serum at Various Time Points 57
4.2.5 Citrullination in the BALF 58
4.3 *In Vivo* Findings on Effects of CS in Non-Synchronized CIA Mouse Model 60
4.3.1 Clinical Score, Disease Incidence, and Anti-Mouse Collagen II Autoantibody 60
4.3.2 Lung Neutrophil Recruitment and Neutrophils Associated Chemokines and Cytokines 62

4.3.3 Neutrophil-associated Chemokines and Cytokines in the Serum at Various Time Points 64
4.3.4 NE in BALF and Serum at Different Time Points 66
4.3.5 Citrullination in the BALF 67
Chapter 5: Discussion, Conclusions, and Limitations **70**
5.1 Discussion 71
5.1.1 Effect of CSE on neutrophil functions in the presence or absence of foreign particles and potential mechanism of CSE-induced NETosis 71
5.1.2 CS and neutrophils in the synchronized and non-synchronized CIA models 72
5.2 Limitations 77
Chapter 6: Future Directions **78**
6.1 Elucidate the Potential Receptor of CSE component on Neutrophils that Induces NETosis .. 79
6.2 Mechanistic Studies of PAD Regulation with BB-Cl Amidine and a *PAD4* Deficient Mouse Model 79
6.3 Exploring Autoantibody Development Prior to Disease Manifestation 79
6.4 Increase the Power of Analyses 80
References **81**

List of Figures

Figure 1: Two forms of Neutrophil Extracellular Traps (NETs) formation 12
Figure 2: List of epidemiological studies showing the association between cigarette smoking and RA 15
Figure 3: Working Principle of the Citrulline Phenylglyoxal-Rhodamine Probe 33
Figure 4: Collagen-Induced Arthritis Cigarette Smoke Exposure Models (with and without LPS) 36
Figure 5: CSE-stimulated neutrophils behave similarly to untreated neutrophils after 1 hour of stimulation as shown by surface markers and granular enzyme activities 43
Figure 6: CSE-treated neutrophils show enhanced phagocytosis of IgG-latex beads and heat-killed E. coli 44
Figure 7: CSE-treated neutrophils go through enhanced NETosis 46
Figure 8: CSE induces citrullinated protein release in NET in a PAD4-dependent pathway 48
Figure 9: Clinical score and anti-mouse collagen antibodies in pre-LPS, post-LPS (day 29) serums and day 29 BALF (synchronized model) 51
Figure 10: Neutrophil recruitment and neutrophil-related biomarkers in day 29 BALF (synchronized model) 54
Figure 11: Chemokines and cytokines in pre-LPS and post-LPS (day 29) serum samples (synchronized model) 57
Figure 12: Neutrophil Elastase (NE) abundance in pre-LPS, post-LPS (day 29) serums and day 29 BALF (synchronized model) 58
Figure 13: Citrullination in BALF (synchronized model) 59
Figure 14: Clinical score, disease incidence, and anti-mouse collagen antibodies in day 14, and day 58 serums and day 58 BALF (non-synchronized model) 61
Figure 15: Neutrophil recruitment and neutrophil-related biomarkers in day 58 BALF (non-synchronized model) 63
Figure 16: Chemokines and cytokines in day 14 and day 58 serum samples (non-synchronized model) 66
Figure 17: Neutrophil Elastase (NE) abundance in day 14, day 58 serums and day 58 BALF (non-synchronized model) 66
Figure 18: Citrullination in BALF (non-synchronized model) 68
Figure 19: Graphic Summary of the Overall Results 76

List of Tables

Table 1: Media Composition for Neutrophil Stimulation 26
Table 2: Human Neutrophil Surface Marker Panel 27
Table 3: Media Composition for Extracellular DNA Detection 30
Table 4: Composition for DTT + Sample Buffer + milliQ Water in Citrullination Probing 32
Table 5: Media Composition for PAD/4 Inhibition Assay 34
Table 6: Panel for Immunophenotyping Mouse BAL Cells 39
Table 7: Specificity of Human Neutrophil CD Markers 42

List of Abbreviations

RA	Rheumatoid Arthritis
TNF	Tumor Necrosis Factor
IL	Interleukin
IFN	Interferon
M-CSF	Macrophage Colony Stimulating Factor
FGF	Fibroblast Growth Factor
ROS	Reactive Oxygen Species
PAD	Peptidyl Arginine Deiminase
PTM	Post-Translational Modification
NET	Neutrophil Extracellular Trap
NK	Natural Killer Cell
ILC	Innate Lymphoid Cell
Treg	Regulatory T Cell
Th	Helper T Cell
APC	Antigen Presenting Cell
Tfh	Follicular Helper T Cell
RF	Rheumatoid Factor
ACPA	Anti-Citrullinated Protein Antibody
SE	Shared Epitope
HLA	Human Leukocyte Antigen
MHC	Major Histocompatibility Complex
GWAS	Genome-Wide Association Studies
SNP	Single Nucleotide Polymorphism
OR	Odds Ratio
CCL2	C-C Motif Ligand 2
ACR	American College of Rheumatology
Ig	Immunoglobulin
BMD	Bone Mineral Density
IC	Immune Complex
ADCC	Antibody-Dependent Cellular Cytotoxicity
TLR	Toll-Like Receptor
CIA	Collagen-Induced Arthritis
MPO	Myeloperoxidase
NE	Neutrophil Elastase
BPI	Bactericidal/Permeability-Increasing Protein
MMP	Matrix Metalloproteinase
PRR	Pattern Recognition Receptor
TLR	Toll-Like Receptor
NLR	NOD-Like Receptor
LPS	Lipopolysaccharide
LTA	Lipoteichoic Acid
Syk	Spleen Tyrosine Kinase
PI3K	Phosphoinositide 3-Kinase
PLCγ	Phospholipase Cγ

GTP	Guanosine Triphosphate
HOCl	Hypochlorous Acid
fMLP	N-Formylmethionyl-Leucyl-Phenylalanine
PKC	Protein Kinase C
MAPK	Mitogen-Activated Protein Kinase
ERK	Extracellular Signal-Regulated Kinase
PAMP	Pathogen-Associated Molecular Pattern
DAMP	Damage-Associated Molecular Pattern
ATP	Adenosine Triphosphate
DNase	Deoxyribonuclease
EIRA	Epidemiological Investigation of Rheumatoid Arthritis
PAH	Polycyclic Aromatic Hydrocarbons
PM	Particulate Matter
RNS	Reactive Nitrogen Species
CS	Cigarette Smoke
HMGB1	High Mobility Group Box 1
DNA	Deoxyribonucleic Acid
DC	Dendritic Cell
iBALT	Inducible Bronchus-Associated Lymphoid Tissue
ILD	Interstitial Lung Disease
COPD	Chronic Obstructive Pulmonary Disease
BAL	Bronchoalveolar Lavage
CFA	Complete Freund's Adjuvant
CSC	Cigarette Smoke Condensate
RBC	Red Blood Cell
CSE	Cigarette Smoke Extract
EDTA	Ethylenediaminetetraacetic Acid
PBS	Phosphate Buffered Saline
FBS	Fetal Bovine Serum
RT	Room Temperature
MM	Master Mix
PR3	Proteinase 3
BCA	Bicinchoninic Acid
ZEN	ZEISS Efficient Navigation
HEPES	N-2-hydroxyethylpiperazine-N'-2-ethanesulfonic acid
PFA	Paraformaldehyde
PMA	Phorbol 12-myristate 13-acetate
TCA	Trichloroacetic Acid
CHRIM	The Children’s Hospital Research Institute of Manitoba
FA	Fresh Air
CII	Collagen II
NPX	Normalized Protein Expression
CXCL	Chemokine (C-X-C motif) Ligand
CSF	Colony Stimulating Factor
CCL4	C-C Motif Chemokine Ligand
ELISA	Enzyme-Linked Immunosorbent Assay

ANOVA	Analysis of Variance
MFI	Mean Fluorescence Intensity
RFU	Relative Fluorescence Unit
NS	Not Significant
kDa	Kilo Dalton
TPM	Total Particulate Matter
NO	Nitric Oxide
TRPA1	Transient Receptor Potential Ankyrin 1
PAH	Polycyclic Aromatic Hydrocarbon
AhR	Aryl Hydrocarbon Receptor
nAChR	Nicotinic Acetylcholine Receptor
NF-κB	Nuclear Factor kappa B

Copyright and Licensing

Figure 1: Two forms of Neutrophil Extracellular Traps (NETs) formation

Papayannopoulos, V. Neutrophil extracellular traps in immunity and disease. *Nat Rev Immunol* 18, 134–147 (2018). https://doi.org/10.1038/nri.2017.105

Figure 3: Working Principle of the Citrulline Phenylglyoxal-Rhodamine Probe

Bicker, K. L., Subramanian, V., Chumanevich, A. A., Hofseth, L. J., & Thompson, P. R. (2012). Seeing citrulline: development of a phenylglyoxal-based probe to visualize protein citrullination. *Journal of the American Chemical Society*, 134(41), 17015–17018. https://doi.org/10.1021/ja308871v

Chapter 1: General Introduction

1.1 Rheumatoid Arthritis: An Overview

1.1.1 Disease Mechanisms and Immune Dysregulation

Rheumatoid arthritis (RA) is a systemic autoimmune disorder marked by continued synovial inflammation, ongoing joint damage, and involvement of tissues beyond the joints. An estimated 1% of people worldwide are affected by it.[1,2,3] While the pathogenic mechanisms of RA remain incompletely understood, a complex interplay between genetic and environmental factors leads to the development of autoimmunity and a targeted inflammatory response directed at synovial joints.[4,5] As such, RA involves a break of immune tolerance due to the dysregulation of the adaptive immune system.[6] However, recent studies have demonstrated that the innate immune system contributes substantially to the onset and progression of the disease.[7] For example, in RA monocytes and macrophages produce pro-inflammatory cytokines such as TNF, IL-1β, IL-6 and matrix-degrading enzymes, which lead to joint inflammation and destruction.[8] Various subsets of dendritic cells also release cytokines known to be important in RA such as TNF, IL-1, IL-12, IL-6, interferons (IFNs), and differentiation factors such as macrophage colony-stimulating factor (M-CSF) and fibroblast growth factor (FGF).[9]

Neutrophils remain a key player in the innate immune response as the most abundant leukocyte in the human body. They are found in high abundance in inflamed RA joints. Here, they interact with immune complexes via Fcγ receptors, prompting neutrophils to degranulate and produce reactive oxygen species (ROS).[10,11] The excessive ROS production, while important for host defense, contributes to bystander tissue damage. Within neutrophils a key enzyme known as peptidyl arginine deiminase (PAD4) is activated during neutrophil extracellular traps (NETs) formation.[12] PAD4 converts arginine to citrulline, which is a post-translational modification of proteins (PTM).[13] Deletion of the gene coding for this enzyme leads to decreased levels of pro-inflammatory cytokines, autoantibodies, and disease severity in a collagen-induced arthritis (CIA) mouse model, a model of human RA.[14] Natural killer (NK) cells also play a role in the pathophysiology of RA by producing cytokines, causing cytotoxicity, and interacting with monocytes to promote inflammation and tissue damage.[15,16] Moreover, different innate lymphoid cell (ILC) subsets play roles in RA.[7] There is evidence that the lymph node population skews towards pro-inflammatory ILCs (ILC1 and ILC3)[17] in the early stage of RA and ILC3s produce increased IL-17 and IL-22 that promote inflammation[18]. On the other hand, ILC2s in the synovium

of RA patients are decreased resulting in impaired regulatory T (Treg) cell function worsening the disease.[19]

While the innate immune cells play significant roles in the development of the disease, adaptive immune cells also contribute critically. Studies have suggested that the chronic manifestation of joint symptoms in RA may be due to the imbalance between pro-inflammatory Th1 and anti-inflammatory Th2 cells (termed Th1/Th2 imbalance).[20] Th1 cells maintain the inflammation in the synovium in RA by secreting pro-inflammatory proteins such as IFN-γ, TNF-α, and IL-2, subsequently leading to cartilage destruction and bone erosion.[21] Th17 cells produce IL-22, which stimulates synovial fibroblast proliferation through CCL2 and supports osteoclastogenesis.[22] On the other hand, B cells play a multifaceted role in the pathogenesis of RA via antigen presentation, autoantibody formation, and pro-inflammatory cytokine secretion.[23] In RA, B cells act as antigen presenting cells (APCs) to CD4+ T helper cells, activating the T cells to promote inflammation but also promote affinity maturation of B cells via follicular helper T (Tfh) cells.[24] The presence of autoantibodies such as rheumatoid factor (RF) and anti-citrullinated protein antibody (ACPA) prior to symptomatic disease is a hallmark of RA. Autoreactive B cells produce these autoantibodies, contributing to immune complex formation and tissue damage.[25] In addition to these two roles, peripheral B cells in RA patients secrete pro-inflammatory cytokines IFN-γ, TNF-α, IL-6, IL-17, IL-1β, and IL-10.[26] The combination of accumulated immune complexes in the synovium along with the cytokine signaling modulates the microenvironment, resulting in severe inflammation and erosion of adjacent cartilage and bone. While the roles of various immune cells have been studied in the context of RA, the complete order of mechanistic events from the break of immune tolerance to disease manifestation is not completely understood.

1.1.2 Genetic and Environmental Risk Factors

RA results from a complex interplay between genetic and environmental factors. The heritability of RA is approximately 60%, indicating the significant role of genetic predisposition in this disease.[27] The *HLA-DRB1* gene encodes a component of the major histocompatibility complex class II (MHC II) involved in antigen presentation. The "shared epitope" (SE) which is a collection of alleles within the *HLA-DRB1* gene, is the most important genetic risk factor for RA accounting for 11-37% of the disease heritability.[28] It has been closely linked to the risk of developing RA, more prominent joint destruction, and higher mortality.[29,30,31] Over the past two

decades, GWAS have revealed several SE risk alleles. Individuals carrying one or two SE alleles are estimated to have a 4 to 8 times higher risk of developing RA.[32] Among the various SE coding alleles, *DRB1 *0401* and **0404* have been linked early-onset RA (≤40 years), but *DRB1*0101* has been linked to late-onset RA (≥60 years).[33] In addition to the *HLA-DRB1* gene, other HLA loci have been independently associated with RA, such as: amino acid positions 9 of *HLA-DPB1*, 9 of *HLA-B* and 77 of *HLA-A*.[34,35] Non-HLA genes have also been correlated with RA susceptibility. One notable example is *PTPN22*, which encodes a lymphoid-specific phosphatase that regulates T cell activation.[36] A single-nucleotide polymorphism (SNP) *rs2476601* at the minor allele R620W of the *PTPN22* gene has been shown to double the risk of RA.[37] Certain haplotypes of the *PADI4* have been associated with a 1.5-2 fold increased risk of RA.[38] Additionally, a recent GWAS focusing on non-HLA genes confirmed association of *PTPN22, STAT4, TRAF1-C5, CTLA4* and *PADI4* with RA susceptibility.[39] Taken together, these genes highlight how antigen presentation, T cell dysregulation, and protein citrullination contribute to the pathophysiology of RA. Although the presence of these alleles does not guarantee the onset of RA, they can lead to an immune system susceptible to environmental triggers that initiate the development of the disease.

Of all the known environmental triggers of RA, cigarette smoking has emerged as the most important risk factor of RA. Several epidemiological studies have demonstrated that a greater cumulative smoking history increases the likelihood of developing RA. In a meta-analysis, it was observed that cigarette smokers have ~2x the risk of developing RA compared to non-smokers, and the risk was almost 1.3 times greater for female smokers than for non-smokers.[40] Another study reported that individuals with relatively low lifetime exposure (less than 10 pack years, that is, 1 pack of cigarettes per day for 10 years) also had a higher risk of RA.[41] In a Swedish cohort, individuals who smoked and carried the SE had a substantially higher odds ratio (OR) of developing seropositive RA (OR 10.0) compared to those with only one of the risk factors - either the SE alone (OR 4.8) or smoking alone (OR 1.9) suggesting a critical gene-environment interaction.[42] Apart from cigarette smoking, an inhaled occupational exposure, silica dust, also significantly elevates RA risk.[43] Silica exposure is widespread in industries such as mining, construction, and sandblasting. Alveolar macrophages are activated by silica exposure, which results in the release of IL-1β, lysosomal rupture, ROS, and inflammasome activation.[44,45] Additionally, neutrophil recruitment and NET formation occur in pulmonary silicosis.[46] Beyond these two, other exposures such as air pollution, textile dust, pesticides, solvents, and farming

agents have also been linked to the risk of RA development.[47] In addition to the different kinds of inhaled exposures, RA susceptibility has been linked to variables such as periodontal infections and nutrition. Various epidemiological studies have shown a correlation between periodontal disease and RA.[48,49] The oral bacterium *Porphyromonas gingivalis* (*P. gingivalis*) is the most thoroughly researched in relation to RA. It expresses an endogenous PAD enzyme called PPAD that can citrullinate proteins to act as RA autoantigens.[50] Interestingly, recent literature suggests that oral bacteria may enter the systemic circulation and expose citrullinated antigens to B cells, thereby activating inflammatory monocytes in RA patients during a disease flare.[51] Other risk factors for RA include dietary factors and obesity. These environmental exposures increase the risk of RA by influencing the immune system to evolve into a pro-inflammatory microenvironment. For many RA patients, the disease develops over several years where detectable autoimmunity remains clinically quiescent. Precisely how an individual transitions from autoimmunity to clinical disease remains unclear. However, it remains possible that repeated environmental insults and genetic susceptibility leads to a cascade of immunological dysregulation which targets the synovium.

1.1.3 Role of Autoantibodies and Citrullinated Proteins

The hallmark of seropositive RA is the presence of autoantibodies, which often precede the onset of clinical symptoms by several years. Rheumatoid Factor (RF) was the first serological marker identified in RA patients and was included in the 1987 ACR classification criteria for the disease.[52] RFs are autoantibodies that recognize the Fc portion of IgG and are released by B cells within the inflamed joint.[53,54] There are several isotypes of RF: IgM, IgA, and IgG. Among these, IgM RF is the most often tested antibody in clinical settings and is present in 60–80% of RA patients.[55] Interestingly, low-affinity IgM RF is produced transiently in healthy individuals under normal conditions.[56] However, high-affinity RF found in the RA synovium plays a specific pathogenic role, forming immune complexes with IgG in the joints. This leads to activation of the complement cascade and in turn recruits immune cells that lead to chronic inflammation and joint damage.[57] In addition to secreting these antibodies, B cells that produce RF also serve as APCs, activating autoreactive T cells and amplifying the autoimmune response. As a result, these pathogenic B cells maintain a cycle of sustained inflammation within the inflamed joint.[53] To explain the contrasting characteristics of RF in health and RA, a recent study has shown that RF only binds to antigen-bound IgG and not unbound IgG (due to its closed conformation).[58] The

specificity of the RF test is limited as it can also be found in other autoimmune conditions, chronic infections or even in a proportion of healthy individuals. However, poorer disease prognosis, aggressive articular symptoms, along with worse morbidity and mortality have all been linked to high titers of RF in RA patients.[59,60]

The other extensively studied autoantibody in RA is anti-citrullinated protein antibodies (ACPA). Studies have indicated that ACPA manifests considerably earlier than RF before RA onset [61,62] About two-thirds of RA patients have ACPA and it has a much higher diagnostic specificity compared to RF (>90%).[57] Importantly, ACPA positivity in individuals can be detected as early as 10 years before the onset of RA.[63–65] This "preclinical phase" indicates a heightened risk for progression to symptomatic RA. The risk at this stage is further strengthened by the presence of genetic factors, particularly with *HLA-DRB1*04* alleles, and other environmental triggers such as cigarette smoking. The finding that these antibodies are present much earlier in disease onset is consistent with the observational association between ACPAs and bone loss in the preclinical phase. Studies have shown that individuals with ACPA positivity display reduced bone mineral density (BMD).[66,67] By directly binding to citrullinated vimentin that is expressed on the surface of osteoclast precursors, ACPAs can mechanistically promote the activation and development of these bone-resorbing cells.[68] ACPAs can activate macrophages through immune complexes, which trigger the release of pro-inflammatory cytokines and in turn promote bone destruction. Macrophages reside in the synovial tissue while at resting state and are potent immune effectors that, when triggered, can cause inflammation and joint injury.[69,70] Apart from the effects on bone, ACPAs also contribute to immune activation and joint inflammation through multiple mechanisms. As briefly mentioned earlier, ACPAs recognize proteins that have undergone citrullination catalyzed by PAD enzymes. Commonly described citrullinated autoantigens for ACPA include histones, type II collagen, filaggrin, fibrinogen, vimentin, and α-enolase.[71–74] Studies have shown that NETs in RA patients contain α-enolase and citrullinated vimentin, which can serve as autoantigens triggering the production of ACPAs.[75] ACPAs are likely produced when NETs release citrullinated antigens in into the extracellular space. Interestingly, the immune complexes (ICs) that contain ACPAs can not only induce further NET formation but also release of pro-inflammatory cytokines such as TNF-α, IL-1β, IL-6 by neutrophils, and dendritic cells.[76,77] Further, ACPAs can induce neutrophils to release PAD enzymes in the peripheral blood of RA patients. Upon PAD4 activation, citrullinated histones are released locally, which serve as

autoantigens and promote clonal expansion of B cells, ultimately increasing the synthesis of ACPA.[78] Therefore, there appears to be a self-perpetuating cycle between ACPAs and innate cell stimulation that sustains the chronic inflammation observed within the joint. Moreover, according to recent research, ACPAs have a higher affinity for FcγRIIIa on immune cells due to their improved Fc-glycan alterations.[79] These glycan alterations intensify downstream pathways such as complement activation, pro-inflammatory cytokine release, and antibody-dependent cellular cytotoxicity (ADCC). In parallel, citrullinated proteins themselves are being increasingly recognized as contributors to RA pathogenesis. For example, citrullinated fibrinogen enhances the activation of synovial macrophages via TLR4, promoting IL-6 and TNF-α secretion.[80] *In vivo* studies have demonstrated strong evidence for the pathogenic synergy between ACPAs and citrullinated antigens. In the CIA mouse model, immunization of mice with citrullinated proteins, such as citrullinated fibrinogen or α-enolase, leads to robust T and B cell responses and exacerbates arthritis, particularly when combined with ACPA transfer.[81,82] In humanized mouse models expressing RA-susceptible HLA alleles, ACPAs accelerate arthritis onset and severity by enhancing Th17 polarization, synovial inflammation, and osteoclast activity.[83]

Aside from ACPA, other autoantibodies that target PTMs have been described in RA. For example, the recent discovery of anti-carbamylated protein (anti-CarP) can also act as an autoantibody in RA. The target proteins of anti-carP are altered by the PTM named carbamylation, where lysine residues are converted into homocitrulline by cyanate.[84] Anti-CarP antibodies are found in about 44% of RA patients.[85] These antibodies have been detected in multiple RA cohorts and are notably more prevalent in RA than in healthy controls.[86–88] Like ACPA, these antibodies can also appear years before RA develops[89] and are linked to disease progression and joint damage, particularly in ACPA-negative patients. Evidently, various autoantibodies and citrullinated proteins play a significant role in the development of RA.

1.2 Neutrophils and NETosis

1.2.1 Neutrophil Effector Functions

Neutrophils are the most abundant immune cells in the blood, representing about 50%-70% of all circulating leukocytes.[90] They are the first responders of the innate immune system in the event of an infection or inflammatory response. Neutrophils have a characteristic nucleus, which is usually divided into three to five linked lobes which is where the term "polymorphonuclear leukocytes" is derived. In addition, this lobulated nuclear morphology serves a functional purpose by enhancing nuclear deformability. The nuclear envelope of neutrophils is composed of fewer components (lamins A/C, B1 and B2, LBR, emerin and LAP2β), allowing more flexibility.[91,92] Both of these features enable neutrophils to pass through narrow intercellular junctions during transendothelial migration, which is essential for their rapid recruitment to inflammatory or infected tissues. Inside the cytoplasm, actin filaments and microtubules are abundant, and these are required for the coordinated shape changes necessary for different effector functions.[93] Neutrophils are also part of a specialized cell family termed “granulocytes” due to the wide range of granules present in their cytoplasm. Granules are membrane-bound vesicles that act as stores of strong antibacterial and immunoregulatory proteins. At least four subsets of these granules have been distinguished: primary or azurophilic, secondary or specific, tertiary or gelatinase, and secretory vesicles.[94] These subsets are generated successively during neutrophil maturation within the bone marrow. The primary granules are enriched in MPO, serine proteases (neutrophil elastase or NE, proteinase 3, cathepsin G, and azurocidin), α-defensins, lysozyme, and Cap57 (bactericidal/permeability-increasing protein, BPI).[95,96] Secondary granules include lactoferrin, NADPH oxidase components, lipocalin/NGAL, and other bacteriostatic proteins. In contrast, tertiary granules are abundant in matrix-degrading enzymes such as MMP-9, collagenase, and antibacterial proteins such as cathelicidin.[94] Secretory vesicles, however, are rapidly mobilized to the plasma membrane and include receptors crucial for pathogen recognition, endothelial adherence, and extravasation.[96] Apart from being structurally unique, neutrophils also have a distinct metabolic profile. Their primary source of energy is anaerobic glycolysis rather than mitochondria-derived ATP, which enables them to operate under the hypoxic conditions observed in inflammatory tissues.[97] Neutrophils are short-lived, with a typical lifespan of 6 to 12 hours in circulation. However, neutrophils are thought to live for prolonged periods under inflammatory conditions. Upon the resolution of inflammation, they go through apoptosis via macrophages,

thereby restoring tissue homeostasis.[98] Neutrophils' primary effector functions for host defense include phagocytosis, degranulation, and NET formation (or NETosis). These mechanisms work synergistically to contain infections during the early immune response. However, dysregulation of these functions can lead to immunopathology, including chronic inflammation and autoimmune diseases.

Phagocytosis is a fundamental mechanism through which neutrophils eliminate invading pathogens. The cascade of phagocytosis is initiated upon recognition of a foreign pathogen as an invader This recognition is mediated either directly via pattern recognition receptors (PRRs) or indirectly through opsonins. An array of PRRs including toll-like receptors (TLRs), NOD-like receptors (NLRs), and scavenger receptors, are expressed by neutrophils. These receptors can identify bacteria, fungi, and viruses by detecting conserved microbial components such as lipopolysaccharide (LPS), lipoteichoic acid (LTA), and β-glucans.[99] Neutrophils can also indirectly recognize opsonized pathogens, whereby pathogens are coated with IgG or complement component C3b to flag them for killing.[100] Opsonins bind to specific receptors on the surface of neutrophils to improve phagocytosis. While complement receptors like CR1 and CR3 recognize C3b and iC3b, neutrophil Fcγ receptors like FcγRIIA and FcγRIIIB bind to IgG.[101] Neutrophils use actin-mediated membrane remodeling to start the engulfment process after identifying the pathogen.[102] The cascade involves spleen tyrosine kinase (Syk), phosphoinositide 3-kinase (PI3K), phospholipase Cγ (PLCγ), and small GTPases, including Rac1, RhoA, and Cdc42 and thus cytoskeletal changes required for particle internalization are made.[103] As a result, a membrane-bound structure called a phagosome is formed surrounding the engulfed microbe. The phagosome fuses with lysosomal compartments and neutrophilic granules. Within the phagolysosomes, both oxidative and non-oxidative processes are utilized for intracellular killing. The NADPH oxidase complex on the phagosomal membrane transforms molecular oxygen into ROS, facilitating the oxidative burst. Hydrogen peroxide created from superoxide anions via NADPH oxidase is used up by the granular enzyme MPO to form hypochlorous acid (HOCl), a strong microbicidal oxidant.[104] Non-oxidative processes are also important and typically involve antimicrobial peptides and proteases. Defensins break down microbial membranes by creating pores, while lysozyme breaks down bacterial peptidoglycan, and serine proteases such as NE and cathepsin G break down microbial proteins and render virulence factors inactive.[105,106]

Another crucial effector function of neutrophils is degranulation, which is the controlled exocytosis of granule contents into the phagosome or extracellular space. When an infection or tissue damage occurs, this procedure enables neutrophils to release antibacterial compounds and immunomodulatory proteins.[107] Degranulation of neutrophils can be triggered by various stimuli. Granule exocytosis is triggered by immune complexes, IgG-coated pathogens, and bacterial products engaging the Fcγ receptors and PRRs, respectively. Chemoattractants such as N-formylmethionyl-leucyl-phenylalanine (fMLP), IL-8, and complement component C5a can activate downstream signaling cascades that involve intracellular calcium mobilization, protein kinase C (PKC), and the MAPK/ERK pathway, which coordinates membrane fusion and granule trafficking.[108] Interestingly, secretory vesicles are the first and quickest to be released, whereas azurophilic granules require the highest threshold of stimulant. This ensures that potentially harmful enzymes are only released under conditions of severe infection or tissue damage. The intracellular vesicle transport mechanism that facilitates granule exocytosis includes Rab GTPases like Rab27a and Rab27b.[109] Degranulation of neutrophils serves as both an immunomodulatory and antibacterial function. For instance, cathepsin G and NE break down microbial components and also serve to restructure host tissue, whereas lactoferrin chelates iron, limiting its availability to bacteria. Matrix metalloproteinases, such as MMP-9, break down extracellular matrix components to promote immune cell motility. On the other hand, cathelicidin can play immunomodulatory roles. Certain granular proteins, such as azurocidin, also have chemotactic qualities that can attract monocytes and other immune cells to the site of infection.

The comparatively newly discovered effector function of neutrophils is NETosis. NET formation can be triggered by a wide range of stimuli and thus it is involved in an array of immunological defense mechanisms. For example, bacteria, viruses, fungi, and parasites, pathogen-associated molecular patterns (PAMPs) like LPS, damage-associated molecular patterns (DAMPs) like extracellular ATP, and pro-inflammatory cytokines like IL-8, TNF-α, and GM-CSF can all trigger NETosis. Additionally, immune complexes, nitric oxide, and monosodium urate crystals can also serve as stimuli.[110,111] Two types of NETosis have been described: lytic (or suicidal) NETosis and non-lytic (or vital) NETosis. The lytic NETosis, also known as classical NETosis, occurs over hours and causes the neutrophils to perish. Based on the participation of NADPH oxidase, lytic NETosis is further divided into NADPH-dependent and NADPH-independent types.[112] The stimulus plays an important role in NET formation since proteomic

analyses have revealed an array of PTMs and NET constitution depending on the type of stimulus received.[113] However, complement proteins including C3b and C5a, other cytokines, and ligands that interact with TLRs or IgG-Fc receptors are frequently responsible for the initiation of typical lytic NETosis..[114] The endoplasmic reticulum releases calcium when a receptor is activated. By activating PKC through the RAF-MEK-MAPK/ERK signaling cascade, the resultant increase in cytoplasmic calcium causes gp91phox to become phosphorylated. This starts the synthesis of ROS by making it easier for membrane-bound NADPH oxidase subunits to assemble at the phagosomal or cytoplasmic membranes.[115,116] Following this, MPO, NE and other lytic enzymes are released into the cytosol. MPO aids in the release NE into the cytoplasm by oxidizing it.[117] The influx of calcium also promotes the disintegration of actin and vimentin molecules. Calpain is activated by citrullination and an increase in calcium levels which plays a role in nuclear lamin and filaments decondensation. Simultaneously, NE attaches to and breaks down actin fibers in order to reach the nucleus. Once there, NE breaks down the nuclear membrane allowing water infiltration.[117] NE cleaves histones present on the tightly wound chromatin called nucleosomes, ultimately leading to chromatin decondensation. Furthermore, PAD4 becomes activated by binding to calcium ions or by ROS. Within the nucleus, PAD4 citrullinates arginine (positively charged), converting the amino acid to citrulline (neutral charged) of histones which relaxes the histone-DNA bond. As a result, there is further chromatin decondensation.[118] Ultimately, DNA, cytosolic, and granular proteins extrude through gasdermin D-mediated pores formed on the plasma membrane.[119]

During vital or non-lytic NETosis, neutrophils release the nuclear (or mitochondrial) DNA and continue to be viable to perform antimicrobial activities such as recruitment, chemotaxis, and phagocytosis. The identification of complement receptor and activated platelet serve as stimuli for non-lytic NETosis. *Staphylococcus aureus*, *Escherichia coli*, and *Candida albicans* can serve to activate complement receptors and TLRs to initiate vital NETosis. In this case, the small conductance potassium channel member three (SK) is where calcium influx begins, activating both PAD4 and NE. These enzymes translocate to the nucleus and cause chromatin decondensation as above. After the chromatin is expelled via vesicular transportation, the blebs re-fuse with the plasma membrane. As a result, the plasma membrane remains intact and the now anucleated neutrophils continue their antimicrobial activities such as phagocytosis and migration.[112] Lytic NETosis takes roughly 3-4 hours, however, non-lytic NETosis takes approximately 5-60 minutes.[120] NETs typically consist of a DNA backbone adorned with a variety of antimicrobial

and immunologically active proteins derived from neutrophil granules and cytoplasm. These consist of lactoferrin, gelatinase, lysozyme, defensins, MPO, NE, cathepsin G, histones (H1, H2A, H2B, H3, and H4), and PAD4. A large number of these substances have direct antibacterial properties. While enzymes such as NE break down bacterial virulence components, histones and MPO have microbicidal effects. Nevertheless, if NETs persist or are not adequately removed, these cytotoxic molecules may also harm host tissues.

Lytic (slow cell death) and non-lytic NETosis. This figure was obtained from *Nat Rev Immunol*

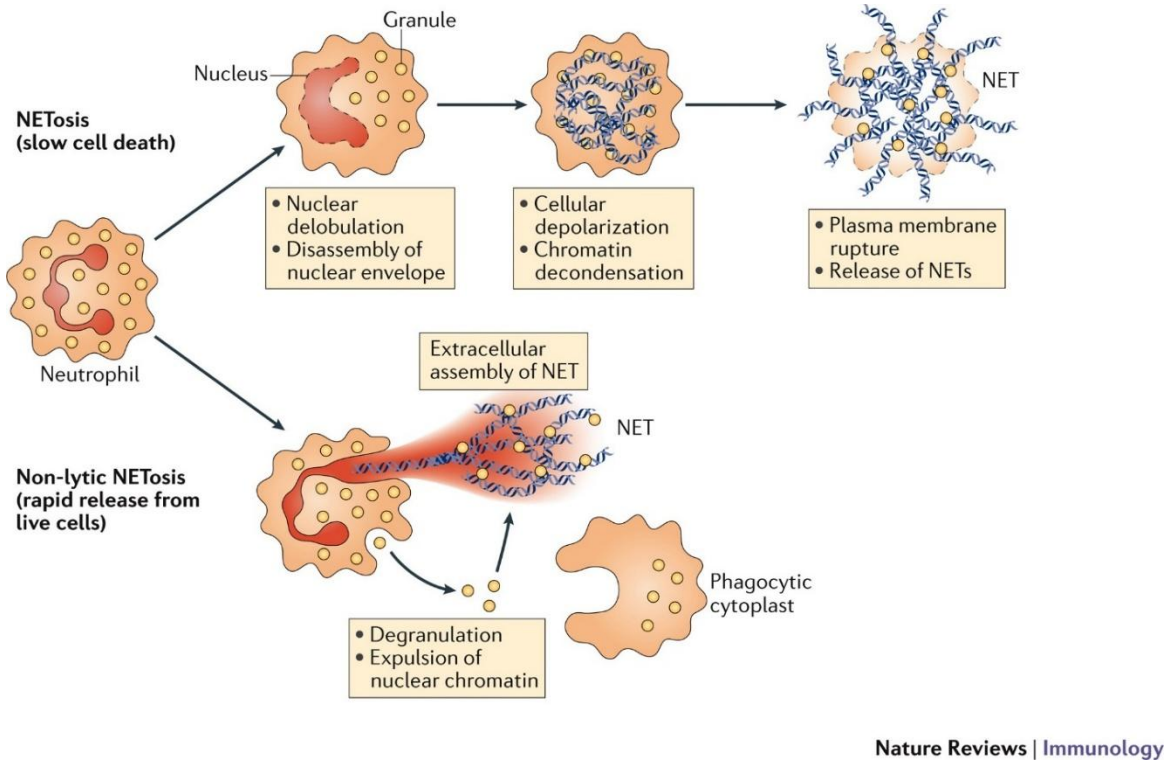

Figure 1: Two forms of Neutrophil Extracellular Traps (NETs) formation

18, 134–147 (2018)[121]

1.2.2 NETs and PAD Enzymes in RA

NET formation serves as a rich source of citrullinated autoantigens such as citrullinated histones (H3, H4), vimentin, α-enolase, fibrinogen, and myeloperoxidase which are known ACPA targets.[75] Interestingly, neutrophils from RA patients have increased levels of the PAD4 enzyme, which is required during NETosis and aids in the production of these neoepitopes.[122] Citrullination in NETs enables the break of immunological tolerance, particularly in genetically predisposed

individuals with HLA-DRB1 shared epitope alleles. As discussed in a previous section, these citrullinated peptides are preferentially presented to autoreactive CD4+ T cells in these individuals. In fact, by binding citrullinated targets on the neutrophil surface and activating Fcγ receptors, ACPAs themselves have been demonstrated to intensify NETosis, resulting in increased ROS generation and PAD4 activation.[123] This creates a feed-forward loop in which NETs stimulate the formation of ACPAs, which in turn intensify NETosis. This inflammatory circuit reinforces itself, worsening tissue damage and the uncontrolled autoantibody production. Additionally, NETs can also serve as a pro-inflammatory stimulus within the synovial joint. Pro-inflammatory cytokines such as TNF-α, IL-1β, and IL-6 which are key contributors to RA pathology are released when extracellular DNA and related proteins in NETs activate PRRs such as TLR9, TLR4 on dendritic cells and macrophages.[124,125] Moreover, NETs interact with synovial fibroblasts, causing them to release chemokines and MMPs, which aid in the destruction of joints and immune cell recruitment.[126] Ineffective NET clearance in RA further exacerbates this loop. Under normal circumstances, nucleases such as DNase I break down NETs, and macrophages remove the resultant DNA-protein complexes. However, in RA, this mechanism is often impaired either due to anti-NET antibodies, DNase resistance, or macrophage dysfunction – resulting in ongoing exposure to citrullinated autoantigens and further immunological activation.[127] Persistent NETs in the synovial environment sustain joint inflammation and destruction leading to the production of ICs that deposit in tissues, trigger complement pathways, and chemoattract in more neutrophils. The paradox of immunological responses RA is best exemplified by NETosis, which begin as a defense mechanism, but develops into a pathological process that triggers and maintains autoimmune inflammation.

1.3 Cigarette Smoking as a Modifiable Risk Factor

1.3.1 Smoking and RA Susceptibility

Cigarette smoking continues to be the most widely recognized risk factor for the development and severity of RA, particularly in genetically predisposed individuals. Over the past 20 years, immunological and mechanistic research has established smoking as a major factor in the pathophysiology of RA, particularly due to its ability to disrupt immune tolerance at mucosal surfaces.[128,129] Several other epidemiological studies have shown that there is an established association between cigarette smoking and RA. As mentioned in a previous section, according to a seminal study from the Swedish Epidemiological Investigation of Rheumatoid Arthritis (EIRA), ever-smokers were twice as likely as never-smokers to develop ACPA-positive RA, and there was a dose-response relationship between smoking duration and intensity.[130] These findings are corroborated by further data from the Nurses' Health Study I and II in the United States, which showed that smoking for ten years or more raises the chance of developing RA even after stopping, with the risk continuing for up to 20 years after quitting.[131] All of these data points to smoking as a significant avoidable contribution to the burden of RA in addition to being a risk factor. Figure 2 represents a list of studies establishing a strong association between cigarette smoking and RA.

The bioactive and hazardous compounds found in tobacco smoke are primarily responsible for the molecular pathways via which smoking cigarettes causes RA. Roughly 70 recognized carcinogens and a wide range of immunomodulatory and pro-inflammatory compounds are among the more than 7,000 chemicals found in cigarette smoke. Among these, the main alkaloid in tobacco, nicotine, has intricate immunological consequences. In some situations, nicotine can have immunosuppressive effects, but long-term exposure has been linked to dendritic cell activation and an increase in pro-inflammatory cytokines such TNF-α and IL-6.[132] In RA, IL-6 is essential for Th17 cell differentiation and B-cell activation, both of which are necessary for the production of autoantibodies. Acrolein which is a highly reactive aldehyde is produced during the burning of organic material, can bond with proteins to produce neoantigens. The immune system is more likely to identify these altered proteins as foreign, which might result in autoreactive reactions. Additionally, acrolein depletes glutathione, which weakens antioxidant defenses and prolongs oxidative stress, which is known to have a role in the pathophysiology of RA.[133,134] Polycyclic aromatic hydrocarbons (PAHs) are strong ligands of the aryl hydrocarbon receptor

(AhR), a transcription factor that affects the development of immune cells. PAH-induced AhR activation stimulates Th17 cell growth and increases IL-22 production, both of which are linked to RA and mucosal immunological dysregulation.[135] Moreover, PAHs encourage epigenetic modifications and DNA damage, which may activate autoreactive immune responses. Cigarette smoke is also a major source of particulate matters which can penetrate deep into the lungs and systemic circulation. Exposure to PM_{10} increases the expression of neutrophils and changes lung histopathology, which may connect cigarette smoking to the breakdown of self-tolerance in RA.[136] Notably, ROS and reactive nitrogen species (RNS), which harm proteins, lipids, and DNA, are abundant in cigarette smoke. As a result, persistent cigarette smoking leads to an oxidative stress within the microenvironment which may be crucial for the formation of citrulline. Therefore, cigarette smoking plays a central role in RA susceptibility, particularly in ACPA-positive disease.

Exposure	First Author	Study type	Cohort	Outcome	Risk of exposure	# RA cases	Reference
Cigarette Smoking	Di Giuseppe	Meta-analysis (3 prospective cohorts, 7 case-control)	Multiple	RF +/- RA	Ever smoking: RF+ RA RR 2.47, RF- RA RR 1.58	4552	(28)
Cigarette Smoking	Hedstrom	Case-Control	Sweden (EIRA)	ACPA +/- RA	Ever smoking: ACPA+ RA OR 1.9, ACPA- RA OR 1.3	3655	(29)
Cigarette Smoking	Too	Case-Control	Malaysia (MyEIRA)	ACPA +/- RA	Ever smoking: ACPA+ RA OR 4.1	1076	(30)
Cigarette Smoking	Bang	Case-Control	Korea	RA	Ever smoking: RA OR 2.7	1482	(31)
Cigarette Smoking	Pederson	Case-Control	Denmark	ACPA +/- RA	Ever smoking: ACPA+ RA OR 1.22 to 57.4; stratified by pack-year exposure AND SE+/-	515	(32)
Cigarette Smoking	Kochi	Case-Control	Japan	RA	Ever smoking: RA OR 1.15 to 1.35	2015	(33)
Cigarette Smoking	Karlson	Retrospective Cohort	USA (Women's Health Cohort)	RA	Ever smoking: RA RR 1.10 to 1.32; stratified by pack-year	7697	(25)
Cigarette Smoking	Costenbader	Retrospective Cohort	USA (Nurses Health Study)	RA	Ever smoking: RA RR 1.47	680	(26)
Cigarette Smoking	Di Giuseppe	Retrospective Cohort	Sweden (Swedish Mammography Cohort)	RA	Ever smoking: RA RR 2.31	219	(27)
Cigarette Smoking	de Hair	Prospective Cohort	Netherlands (IgM RF or ACPA + at-risk)	RA	Ever smoking: Sero+ RA HR 9.6	15	(34)
Cigarette Smoking	Ponchel	Prospective Cohort	United Kingdom (Leeds; RF or ACPA+ with joint pain)	RA	Ever smoking: Sero+ RA OR 3.1	125	(35)

ACPA, anti-citrullinated protein antibodies; RF, Rheumatoid Factor; EIRA, Epidemiological Investigation of Rheumatoid Arthritis; RR, Relative Risk; OR, Odds Ratio; HR, Hazards Ratio. All RR/OR/HR are statistically significant unless otherwise stated.

Figure 2: List of epidemiological studies showing the association between cigarette smoking and RA

This table was obtained from Front. Immunol. 14:1221125.[137]

1.3.2 Mechanisms of Cigarette Smoke-Induced Inflammation

Cigarette smoke (CS) can contribute to RA development by a series of pathogenic mechanisms which begin at the lung mucosa, and progress to systemic inflammation and autoimmunity. As mentioned in the previous section, cellular and molecular changes including oxidative stress, epithelial damage, immune cell activation, post-translational modifications of proteins like citrullination, and a loss of immunological tolerance serve as the foundation for this transformation. The mucosal surface of the respiratory tract serves as a first line of defense against toxins like CS, and the lungs are a vital interface between the immune system and the environment. Components of CS have the ability to directly harm airway epithelial cells, interfere with the epithelial barrier, and cause a local inflammatory reaction when inhaled. DAMPs such as high mobility group box 1 protein (HMGB1) are released as a result of the oxidative stress caused by CS, which also damages epithelial cells and causes mitochondrial malfunction.[138] PRRs such as TLRs and NLRs on dendritic cells (DCs), alveolar macrophages, and airway epithelial cells recognize these signals and start pro-inflammatory signaling cascades.[139,140] Pro-inflammatory cytokines like IL-1β, IL-6, and TNF-α, as well as chemokines CXCL8 (IL-8), are released when the TLR4/MyD88 pathway is activated in response to DAMPs induced by CS.[141] As discussed earlier, the two main early events that connect smoking to the production of autoantigens are increased NET formation and pulmonary PAD activity. Additionally, it has been demonstrated that CS increases the production of PAD enzymes in macrophages and lung epithelial cells, which caused enhanced citrullination of cytoskeletal and structural proteins such histone, fibrinogen, vimentin, and enolase.[142] An overabundance of citrullinated proteins may lead to DCs engulfment and processing to present them in the context of MHC class II molecules, especially those that are highly linked to the HLA-DRB1 common epitope allele. Citrullinated antigens and HLA-DRB1 SE molecules interact with activated CD4+ T cells, which in turn create Th17 and Tfh cells, that are critical for ACPA formation. The connection between innate and adaptive immunity appears to be mediated by lung-resident DCs. DCs exposed to CS exhibit enhanced antigen presentation capacity, increased expression of co-stimulatory molecules (CD80, CD86), and production of Th17 polarization-promoting cytokines IL-6 and IL-23.[143] After migrating from the inflammatory lung to draining lymph nodes, these DCs prime autoreactive T cell responses by presenting naïve T cells with citrullinated peptides. The pro-inflammatory cytokine IL-17A, which is produced by Th17 cells produced in this setting, activates neutrophils, synoviocytes, and osteoclast precursors.

Additionally, IL-17 maintains a feed-forward loop of inflammation by acting on lung epithelial and endothelial cells, which prolongs tissue damage and propagates inflammation.[144] Smokers have reduced Treg function, which may serve to increase autoreactivity and a lack of peripheral tolerance.[145,146] The altered pro-inflammatory and regulatory T cell balance in the lungs may accelerate the autoimmune process by encouraging immunological dysregulation and epitope dissemination. Several intertwined pathways are likely involved in the transition from mucosal to systemic inflammation due to CS. First, pro-inflammatory cytokines such as IL-6, TNF-α, and IL-1β that are generated in the lungs may enter the systemic circulation leading to persistent low-grade inflammatory condition. Moreover, autoreactive cells that have been activated in pulmonary lymphoid tissues may migrate via the blood to secondary lymphoid organs. Research has shown that the lungs of smokers and preclinical RA patients have inducible bronchus-associated lymphoid tissue (iBALT), indicating that the lung's tertiary lymphoid structures might be potential sites for antigen presentation and affinity maturation.[147] Furthermore, ACPA produced in the lungs can reach the bloodstream and combine with citrullinated antigens in other parts of the body, such as the joints, to create immune complexes. These immune complexes lead to tissue inflammation, complement activation, and cytokine production by activating the Fcγ receptors on neutrophils and macrophages. Additionally, CS leads to epigenetic changes such as DNA methylation, histone alterations, and microRNA dysregulation in local cells. As such, even with smoking cessation, these modifications can result in immune cell reprogramming and long-term changes in gene expression patterns and cell function. For example, smokers have been shown to have DNA hypomethylation of immune-related genes in monocytes and T cells, which is linked to increased production of MHC molecules and pro-inflammatory cytokines.[148] Hence, CS is heavily involved in inducing immune responses across almost all kinds of immune cells.

1.4 Role of Lung Inflammation in RA

The lung and other mucosal sites remain crucial for autoimmunity development in RA. This is particularly true for genetically predisposed people who are exposed to environmental risk factors such as cigarette smoke. Long-term lung diseases such as chronic obstructive pulmonary disease (COPD) and interstitial lung disease (ILD) have been shown to increase the risk of developing RA. Furthermore, even before clinical arthritis appears, anti-citrullinated protein antibody (ACPA)-positive individuals have been shown to have subclinical pulmonary abnormalities, such as airway wall thickening, ground-glass opacities, and bronchiectasis.[149] These changes are often accompanied by abnormal pulmonary function tests (e.g., reduced diffusion capacity), even in the absence of respiratory symptoms. Investigations using bronchoalveolar lavage (BAL) have found that at-risk patients had higher amounts of neutrophils, lymphocytes, and inflammatory cytokines such as IL-6 and IL-8, suggesting that lung mucosal inflammation might be a site of autoimmune priming.[149,150] According to the mucosal origins hypothesis of RA, autoantibodies are produced as a result of immune dysregulation that starts in mucosal locations such the gut, oral cavity, and lung.[151] The lung has attracted special attention among them due to the various immune cells and the clear role for inhaled exposures in the development of the disease. The lung epithelium, particularly the distal airways, has innate immune receptors such as TLRs, which can identify pollutants, microbial products, and CS components. Once activated, alveolar macrophages release TNF-α and IL-6.[152] These cytokines aid autoreactive B cells by promoting local development of Th17 and Tfh cells and increasing PAD expression. It is possible that the draining lymph nodes of the lungs act as a bridge connecting systemic and pulmonary immunity. Additionally, antigen-loaded DCs from the lung can migrate to mediastinal lymph nodes, where they activate autoreactive T and B cells that can subsequently settle in synovial tissues.[150] Beyond its role in disease initiation, the lung is also a major site of RA-associated morbidity. One common extra-articular symptom that can appear before, during, or following the development of arthritis is RA-associated interstitial lung disease (RA-ILD).[153] In RA patients, ILD is linked to a worse prognosis and a lower survival rate. Fibrosis, immune complex deposition, and chronic inflammation are some of the pathogenic processes of RA-ILD. It is noteworthy that individuals with RA-ILD frequently exhibit elevated ACPA titers, indicating that systemic autoimmunity persists in targeting pulmonary tissues.[154]

1.5 Collagen-Induced Arthritis (CIA) Model and CS Exposure

One of the most popular and well-studied experimental models for studying human RA is the Collagen-Induced Arthritis (CIA) model. The CIA model was first created in the early 1980s and first reported by Trentham and associates in 1977. It was shown that immunizing susceptible rodent strains with type II collagen (CII), the main collagen component of articular cartilage, would lead to a polyarthritis that resembled human RA in many clinical and histological aspects.[155] Researchers now have a repeatable, immune-mediated platform to investigate the pathophysiology of autoimmune arthritis to study RA. In this model, the disease usually appears after receiving a second injection (booster) of type II collagen emulsified in incomplete Freund's adjuvant (IFA) from a cow, chicken, or mouse. The ensuing immune response mimics some of the pathological features observed in RA patients. Importantly, the CIA model requires both innate and adaptive immunological responses, such as autoreactive T cells, B cells, and pro-inflammatory cytokines including TNF-α, IL-6, and IL-17.[156] A critical feature of the CIA model is its dependence on genetic susceptibility, similar to human RA. Strikingly, similar to human RA, the disease does not develop consistently among mice strains, and only those with certain MHC class II alleles (such as $H\text{-}2^q$ or $H\text{-}2^r$) exhibit considerable vulnerability.[157] Because of this genetic requirement, CIA is a valuable model for investigating gene-environment interactions and their role in autoimmune arthritis. The significance of the microbiome in regulating the onset and course of CIA has come into focus more recently.[158,159]

Outside of genetic alterations, there are a variety of modifications that may be used to induce CIA in susceptible mice. To overcome the variability of arthritis onset, many have turned to a synchronized model of CIA where LPS, a component of Gram-negative bacterial cell walls, is used to synchronize disease onset and severity after the booster injection.[160] Mechanistically, LPS is a TLR4 agonist, which amplifies inflammation by activating innate immune pathways such as NF-κB signaling and cytokine production. Hence, LPS co-administration is particularly helpful in experimental design when arthritis development is required. Additionally, it may replicate an environmental trigger in human RA, such as microbial dysbiosis and infections.

In the CIA model, CS exposure has been shown in many studies to lead to more severe arthritis. When mice are given cigarette smoke condensate (CSC) at the time of collagen immunization, for example, the severity of their rheumatoid arthritis like symptoms increase. Both

young and elderly mice display a dose-dependent increase, suggesting that CSC has a systemic influence on the development of arthritis.[161] Consistent with this, nasal exposure to CSC also increases the development and progression of joint abnormalities in CIA mice.[162] In contrast, other research has found that exposure to CS delays the onset of RA like symptoms. In a study, it was observed that there was a substantial delay in the onset of these symptoms in DBA/1 mice that were exposed to CS for 16 weeks in comparison with non-smoking controls prior to collagen immunization. Interestingly, these mice also exhibited lower levels of anti-collagen type II (anti-CII) and anti-cyclic citrullinated peptide (aCCP) antibodies, suggesting an immunomodulatory effect of CS when given prior to the first injection of collagen.[163] Mice treated with nicotine alone showed a similar delay, suggesting that nicotine may act as a mediator of this protective effect, which may be due to reduced Th17 responses and IL-6 production, both of which are important in the pathophysiology of human RA. Another study showed that nicotine suppressed Th17 responses by activating the cholinergic anti-inflammatory pathway, which in turn decreased CIA.[164] Overall, the literature suggests that CS exposure prior to injection of collagen reduces inflammatory arthritis severity, while the disease is more severe when provided after collagen exposure.

Chapter 2: Thesis Overview

2.1 Study Rationale

Rheumatoid arthritis (RA) is a chronic autoimmune disease characterized by joint inflammation and destruction, often preceded by the development of ACPA.[61,62] While genetic predisposition especially *HLA-DRB1* shared epitope alleles play a significant role in the disease[29–31], environmental triggers are also crucial triggers. The most well-known and modifiable risk factor among the environmental triggers is cigarette smoking, particularly for ACPA-positive RA.[137] However, the underlying mechanism of this association is not clearly understood. On the other hand, neutrophils are abundant in inflamed joints and by activating PAD enzymes during NETosis aid in the production of citrullinated proteins. Citrullinated antigens, if dysregulated, can cause break of immune tolerance. CS directly impacts neutrophils in the lungs by encouraging neutrophil recruitment through ROS and chemical irritants. CS exposure has also been associated with increased PAD expression and activity. Therefore, CS may prime neutrophils to play a role in the break of immune tolerance via dysregulated PAD production that occurs before established arthritis. This study aims to investigate how cigarette smoke influences neutrophil survival, PAD activation, and NET formation in the lungs, driving the production of citrullinated autoantigens and potentially promoting RA development.

2.2. Gap in Knowledge

Despite strong epidemiological evidence linking CS to RA, the precise immunological mechanisms by which smoke-induced activity in the lungs initiates autoimmunity remain unclear.

2.3 Overall Hypothesis

Cigarette smoke stimulates neutrophils to undergo NET formation which leads to RA autoimmunity and development.

2.4 Specific Aims

1. Examine the influence of cigarette smoke extract (CSE) on neutrophil mediated inflammation.

    a. Determine the effect of CSE on neutrophil degranulation, NET formation and phagocytosis.

    b. Elucidate the intracellular cascade that regulates CSE-induced NET formation.

2. Characterize the effect of cigarette smoking on NET formation and protein citrullination *in vivo*.

Chapter 3: Materials & Methods

3.1 Healthy Donor

3.1.1 Blood Collection from Healthy Donors

The human blood collection procedure was approved by the University of Manitoba Biomedical Research Ethics Board (#HS25252). In compliance with the Declaration of Helsinki, written informed consent was obtained from each blood donor. The donor's demographic data (age and sex) was collected with their consent and managed following the University of Manitoba's guidelines regarding the Personal Health Information Act. Healthy donors between the ages of 18 and 65 with no reported serious health issues were selected. Donors were given a comprehensive checklist to assess their eligibility for the study prior to blood draw. The checklist included questions about any possible chronic conditions (e.g., diabetes, cancer, inflammatory bowel diseases, celiac disease, and rheumatoid arthritis), fear of needles and/or bruising, any long-term medications, possible smoking habit, and the possibility of a recent infection within the previous few weeks. Donors who answered no to all of the aforementioned questions were eligible to participate in the research.

3.1.2 Neutrophil Isolation from Healthy Donor Blood

Blood collected from healthy donor samples was separated using the Ficoll-Paque PREMIUM (Cytvia) density gradient medium followed by centrifugation (acceleration 1, deceleration 0, 1440 RPM, 24°C, 20 minutes). From the resulting layers, the erythrocyte/granulocyte fraction was collected and subjected to further purification using the EasySep™ RBC Depletion Reagent, following the manufacturer’s protocol (Stemcell Technologies). In brief, 5 mL of the erythrocyte/granulocyte layer was mixed with 5 mL of 12 mM Ethylenediaminetetraacetic acid (EDTA) (Sigma-Aldrich) prepared in 1X PBS (pH 7.2, Gibco), yielding a final EDTA concentration of 6 mM. This suspension was then diluted with 10 mL of 2% FBS (Thermo Fisher Scientific) in 1X PBS (pH 7.2). Next, 500 µL of the RBC depletion reagent was added, and the mixture was incubated at room temperature (RT) on a magnet with the tube lid open for 10 minutes. After incubation, the clear fraction along with 1 mL of the RBC fraction was transferred to a new tube (Falcon), followed by the addition of 250 µL of the reagent. The tube was placed back on the magnet, and the incubation step was repeated as before. After this, only the clear fraction was transferred again to a new tube and incubated on the magnet for

an additional 10 minutes at RT. Finally, the clear fraction was collected into another fresh tube, and the cells were manually counted using a hemocytometer. The resulting neutrophil population was at least 98% pure, based on nuclear morphology observed under a microscope (Nikon, Japan).

3.2 Cigarette Smoke Extract (CSE) Medium Preparation

The CSE medium was prepared according to a previously published method with minor modifications.[165] In brief, the smoke of one 1R6F research-grade cigarette (University of Kentucky, Lexington, KY) was passed through 50 mL of RPMI 1640 medium (without phenol red, Gibco) using a vacuum pump. This medium was then filtered through a 0.22 μm filter (Merck Millipore) to remove any particles and bacteria. This was considered a stock medium of 100% CSE and was stored at -80°C in aliquots for using in experiments.

3.3 *In Vitro* Experiments for Neutrophil Functions

3.3.1 Flow Cytometry to Detect Neutrophil Activation and Degranulation

To assess neutrophil activation and/or degranulation following CSE stimulation, flow cytometry was conducted using a panel of surface marker antibodies. A stock cell suspension was prepared at a cell density of 1×10^6 cells/mL for this assay. Following neutrophil isolation, cells were counted and aliquoted into triplicates of 100,000 cells each (equivalent to 100 µL of the stock) into round-bottom polystyrene tubes (Falcon) under four conditions: (i) unstained; (ii) stained – untreated; (iii) stained – Ionophore (A23187, Sigma-Aldrich); and (iv) stained – CSE. Here, Ionophore serves as a positive control as it is a potent trigger of NETosis. The medium composition for each condition is outlined in Table 1.

Table 1: Media Composition for Neutrophil Stimulation

Medium	Reagent	Volume (in 1 mL)
Unstained	RPMI 1640	1 mL
Stained – untreated	RPMI 1640	1 mL
Stained – Ionophore	Ionophore A23187 (5 µM)	1 µL
	RPMI 1640	999 µL
Stained – CSE	100% CSE medium	1 mL

The tubes were centrifuged at 1500 RPM for 5 minutes, after which the supernatant was carefully decanted to preserve the cell pellet. Each pellet was then resuspended in its respective treatment medium (RPMI 1640, Ionophore, or 100% CSE) and incubated at 37°C and 5% CO_2 for 60 minutes. After incubation, cells were centrifuged again at 1500 RPM for 5 minutes, and the supernatant was collected into separate microcentrifuge tubes (Bio-Rad) without disturbing the pellet. The supernatant was used for the enzyme activity assay discussed in section 3.3.2. The pellets were subsequently fixed in 4 mL of a fixing solution (1:10 dilution of FACS™ Lysing Solution (BD Biosciences) in MilliQ water) and incubated at room temperature (RT) for 10 minutes. During fixation, a master mix (MM) of antibodies was prepared by adding 1 µL of each antibody per sample: FITC CD11b (BioLegend), BV786 CD16 (BD Biosciences), V450 CD63 (BD Biosciences), APC CD32 (BioLegend), BUV737 CD64 (BD Biosciences), and PE-Cy7 CD66b (Invitrogen by Thermo Fisher), all diluted in 100 µL per sample of eBiosciences™ Flow

Cytometry Staining Buffer (Invitrogen by Thermo Fisher). Following fixation, cells were centrifuged at 1500 RPM for 5 minutes, and the fixing solution was gently aspirated. Each pellet was then resuspended in 100 µL of MM, while the unstained control was resuspended in 100 µL of staining buffer without antibodies. In addition to these, compensation controls were also prepared before the first experiment to set up accurate voltage and gating parameters. For that, one tube was used per antibody where each tube contained one drop of UltraComp eBeads™ Compensation Beads (Invitrogen by Thermo Fischer) and the 1 µL of the corresponding antibody. All tubes were kept on ice and protected from light for 30 minutes. After this incubation, 1 mL of the flow buffer was added to each tube, followed by another centrifugation at 1500 RPM for 5 minutes. Finally, supernatants were removed, and cell pellets were resuspended in 500 µL of the flow buffer. Samples were promptly analyzed using the LSRFortessa flow cytometer (BD Biosciences). For each sample, 10,000 events were collected, and mean fluorescence intensity (MFI) was measured for each marker using BD FACSDiva software (BD Biosciences) on granulocytes gated based on FSC-A vs. SSC-A and single cells gated on SSC-A vs. SSC-H. FlowJo Software (v10.9.0, BD Biosciences) was used for subsequent data analysis.

Table 2: Human Neutrophil Surface Marker Panel

Surface Marker	Fluorophore	Laser (Detection Range)
CD11b	FITC	Blue (515-545)
CD16	BV786	Violet (750-810)
CD63	V450	Violet (425-475)
CD32	APC	Red (663-667)
CD64	BUV737	UV (723-757)
CD66b	PE-Cy5	Yellow Green (655-685)

3.3.2 Enzyme Activity Assay

Neutrophils release granular proteases upon degranulation, so assessing protease activity in the supernatants can serve as an indicator of degranulation, particularly by measuring the activity of the activity serine proteases such as neutrophil elastase (NE) and proteinase 3 (PR3). To evaluate this, supernatants were collected following treatment with the various media described in the previous section (3.3.1). These supernatants were centrifuged at 11,000 RPM for 5 minutes

at 4°C to eliminate any remaining cellular debris. The cleared supernatants were then aliquoted and stored at -80°C until used for the assay. To ensure equal protein input across samples, the total protein concentration in each sample was first quantified using the Pierce™ Bicinchoninic Acid (BCA) Protein Assay Kits (Thermo Fisher Scientific), following the manufacturer's protocol. For the enzyme activity assay, a Greiner 96-well flat-bottom black plate (Millipore Sigma) was prepared with reagents added in the following sequence: 80 µL of 100 µM HEPES buffer (pH 7.6, containing 1.5M NaCl) was dispensed into all wells, followed by 8 µL of IGEPAL detergent (Sigma Aldrich) diluted 1:100 in 1X PBS. Next, 47 µL of the respective sample supernatants (Untreated/Ionophore/CSE) were added to designated wells in duplicate. Purified PR3 (Athens Research & Technology) and purified NE (Athens Research & Technology) were also included in the assay plate as controls to confirm the assay was working. The plate was incubated at 37°C for 5 minutes. After incubation, either fluorescent PR3 substrate (Biosynth) or fluorescent NE substrate (Biosynth) was added to the wells, and the plate was immediately subjected to kinetic reading for 45 minutes, with measurements taken every 1 minute at 37°C using excitation/emission wavelengths of 320/420 nm in the Synergy H1 microplate reader (BioTek).

3.3.3 Phagocytosis Assay (IgG and heat-killed *E. coli*)

The impact of CSE stimulation on neutrophil phagocytic function was initially assessed using the IgG Phagocytosis Assay Kit (Cayman), following the manufacturer's protocol. For this assay, a stock cell suspension at a cell density of 3.5×10^6 cells/mL was prepared. There were three conditions: (i) unstained; (ii) untreated; and (iii) CSE. Neutrophils were aliquoted into six replicates, each containing 350,000 cells (100 µL of the stock cell suspension) in round-bottom polystyrene tubes for each condition. All tubes were centrifuged at 1500 RPM for 5 minutes. Simultaneously, FITC-labeled IgG beads provided in the kit were diluted 1:400 in either pre-warmed RPMI 1640 or 100% CSE medium. For immunofluorescence imaging, 50 µL of each cell suspension was placed onto coverslips pre-coated with 0.01% poly-L-lysine (Sigma-Aldrich) placed in separate wells of a Costar® 24-well flat bottom plate (Corning Inc.). Both the tubes and the coverslip containing plate were incubated at 37°C and 5% CO_2 for 5 minutes. After incubation, tubes were centrifuged again under the same conditions, while the coverslips were fixed with 500 µL of 4% paraformaldehyde (PFA) in PBS (Thermo Fisher Scientific) for 10 minutes after

removing the excess media. Supernatants from the tubes were gently aspirated, followed by a single wash with 200 µL of the wash buffer provided in the kit. The wash buffer was then decanted, and the neutrophils were resuspended in 300 µL of flow cytometry staining buffer. Samples were analyzed using the LSRFortessa flow cytometer (BD Biosciences). A total of 10,000 events were acquired for each sample, and data analysis was performed using FlowJo Software (v10.9.0, BD Biosciences). Meanwhile, PFA was removed from the coverslips and replaced with 300 µL of 1X PBS. The coverslips were then stored at 4°C overnight for further staining and immunofluorescence imaging (discussed in 3.3.5). This experiment was repeated using the heat-killed *E. coli* phagocytosis assay kit (Cayman) but with a 1:2 dilution for the *E. coli* suspension in the respective medium.

3.3.4 Detection of extracellular DNA release from Neutrophils

During NETosis, neutrophils release extracellular DNA, which was detected in this experiment using SYTOX™ Green (Invitrogen by Thermo Fisher), a fluorescent nucleic acid stain. Since this dye cannot permeate intact cell membranes, it selectively stains extracellular nucleic acids, allowing fluorescent detection of DNA released during NETosis. In brief, following neutrophil isolation and counting, cells were divided into round-bottom polystyrene tubes at a density of 1×10^6 cells/mL under the following conditions: (i) untreated; (ii) Ionophore; (iii) CSE; and (iv) negative control (as described in Table 3). The tubes were centrifuged at 1500 RPM for 5 minutes. While centrifugation was in progress, media specific to each condition were prepared. After centrifugation, the supernatants were carefully decanted, and cell pellets were resuspended in their respective media. The resuspended cells were then immediately plated on to a Nunc 96-well optical bottom black plate (Thermo Fischer Scientific), with 6-8 replicate wells for each condition. Fluorescence was measured kinetically using the Synergy H1 microplate reader (BioTek) under the following parameters: readings taken every hour over an 8-hour period at 37°C, with excitation/emission wavelengths set to 485/528 nm, and all wells scaled relative to high signal negative control wells.

Table 3: Media Composition for Extracellular DNA Detection

Medium	Reagent	Volume (in 1 mL)
Untreated	RPMI 1640	999 µL
	SYTOX™ Green (5 µM)	1 µL
Ionophore	Ionophore A23187 (5 µM)	1 µL
	SYTOX™ Green (5 µM)	1 µL
	RPMI 1640	998 µL
CSE	100% CSE medium	999 µL
	SYTOX™ Green (5 µM)	1 µL
Negative Control	RPMI 1640	1 mL

3.3.5 Immunofluorescence Imaging to Detect NETosis/Phagocytosis

For immunofluorescence imaging of NETs, neutrophils were first isolated and counted, then centrifuged at 1500 RPM for 5 minutes. The cell pellets were resuspended in either RPMI 1640 or 100% CSE medium. A volume of 500 µL from each suspension was placed onto the coverslips pre-coated with 0.01% poly-L-lysine, which were positioned in individual wells of a Costar 24-well flat-bottom plate. The plate was incubated at 37°C with 5% CO_2 for 3 hours, as neutrophils typically release NETs within 2–4 hours following stimulation[166]. After incubation, excess medium was carefully removed, and the cells on the coverslips were fixed using 500 µL of 4% paraformaldehyde (PFA) in PBS for 10 minutes. The PFA was then aspirated and replaced with 300 µL of 1X PBS. Coverslips were stored overnight at 4°C. The next day, PBS was removed from the wells, and the coverslips were blocked with 0.2% gelatin (Sigma Aldrich) in PBS at 37°C for 30 minutes. Following the blocking step, the coverslips were inverted on 10 µL drops of the primary antibody - Mouse ELA2 Monoclonal Antibody (4E11) (Abnova by Thermo Fisher Scientific) (1:50 diluted in 0.2% gelatin) and were incubated at 37°C for 1 hour. Afterward, coverslips were placed back in the wells and washed three times with 1X PBS for 5 minutes each on a shaker. Subsequently, coverslips were again inverted on 10 µL drops of the secondary antibody - Alexa Fluor™ Plus 488 Goat anti-Rabbit IgG (Invitrogen by Thermo Fisher) (1:100 diluted in 0.2% gelatin), followed by a 30-minute incubation at 37°C. The washing procedure was

then repeated as previously described. Next, the coverslips were counterstained with a DNA dye Hoechst 33258 (Invitrogen by Thermo Fisher) (1:1000 diluted in 1X PBS) at 37°C for 10 minutes. This was followed by three washes of milliQ water, each for 5 minutes. Finally, the coverslips were mounted on glass slides with ProLong™ Diamond Antifade Mountant (Invitrogen by Thermo Fisher), and images were captured using a Carl Zeiss Axio Lab A1 microscope (Carl Zeiss, Oberkochen, Germany). Images were obtained using a 20X magnification per slide. For the coverslips obtained from the phagocytosis assay, the blocking was followed by the DNA staining, and mounting steps as described above, and imaging was performed at 20X magnification using the same microscope. Image processing and overlaying were done on the ZEISS Efficient Navigation (ZEN) software.

3.3.6 Isolation of NETs

To identify the presence of citrullination in NETs induced by different stimulants (Ionophore, PMA, and CSE), NETs were isolated. Following neutrophil isolation and counting, cells were centrifuged at 1500 RPM for 5 minutes. The pellets were then resuspended in one of the following media: (i) Ionophore; (ii) Phorbol 12-myristate 13-acetate (PMA) (Thermo Fisher Scientific); or (iii) CSE, at a concentration of 3.5×10^6 cells/mL. Both Ionophore and PMA were used as alternative NETosis-inducing agents. The media compositions were consistent with the earlier experiments (1 µL of 5 µM Ionophore or PMA in 999 mL of RPMI, or 1 mL of 100% CSE medium). The neutrophil suspensions were seeded into individual wells of a Costar 12-well flat-bottom plate (Stemcell Technologies) and incubated for ~4 hours at 37°C with 5% CO_2. During this period, the neutrophils formed a thin, adherent layer at the bottom of each well. Care was taken to avoid disturbing this layer while carefully aspirating the excess media. To digest and release NETs, 330 µL of Micrococcal Nuclease Solution (≥100 U/µL, Thermo Scientific), diluted 1:5000 in RPMI 1640, was added to the center of each well. The plate was gently shaken and left undisturbed at RT for 10 minutes. Following incubation, the supernatants were carefully aspirated and transferred into microcentrifuge tubes (Bio-Rad). The tubes were then centrifuged at 11,000 RPM for 5 minutes at 4°C to remove any residual cell debris. The clear supernatants were subsequently collected into new microcentrifuge tubes and stored at -80°C in aliquots for downstream analyses.

3.3.7 Detection of Citrulline in NETs

To assess citrullination in NETs, the total protein concentration of the samples was first determined using the Pierce™ BCA Protein Assay Kits (Thermo Fisher Scientific), in accordance with the manufacturer's protocol. Subsequently, 40 µL sample volumes were prepared containing approximately 20 µg of protein, and the remaining volume was adjusted with milliQ water. Each sample then received 10 µL of 100% Trichloroacetic acid (TCA, Sigma Aldrich). Following this, 1 µL of 10 mM Citrulline-specific Probe-rhodamine (Rh-PG) (Cayman) was added to each tube. The samples were incubated at 37°C for 30 minutes. After incubation, 10 µL of 0.1M citrulline (Sigma Aldrich) was added to the tubes, which were then vortexed and placed on ice for 30 minutes. The samples were centrifuged at 10,000 × g at 4°C for 15 minutes. The supernatant was gently discarded, and the resulting pellet was resuspended in 500 µL of cold (-20°C) acetone (Sigma Aldrich). The centrifugation step was repeated under the same conditions, and the acetone wash was performed once more. After the final wash, the supernatant was discarded, and 20 µL of a mixture containing 0.1M dithiothreitol (DTT, Sigma Aldrich), NuPAGE™ LDS Sample Buffer (Thermo Fisher Scientific), and milliQ water (composition detailed in Table 4) was added to each pellet. The samples were boiled in a sand bath for 10 minutes and then sonicated for 15 minutes. Subsequently, the full contents of each sample were loaded into a 10-well NuPAGE™ Bis-Tris Mini Protein Gel (4-12%, Thermo Fisher Scientific). A 3 µL aliquot of the iBright™ Prestained Protein Ladder (Thermo Fisher Scientific), covering a molecular weight range of 11 to 155 kDa, was used as a marker. The gel electrophoresis was carried out with 20X Bolt™ MOPS SDS Running Buffer (Thermo Fischer Scientific) at 120 volts for 90 minutes. SYPRO™ Ruby protein gel stain (Thermo Fischer Scientific) was used to detect proteins. Gel images were captured using the Amersham™ Imager 680 (GE Healthcare).

Table 4: Composition for DTT + Sample Buffer + milliQ Water in Citrullination Probing

Reagent	Concentration	Volume (in 100 µL)
Dithiothreitol (DTT)	0.1 M	9.67 µL
NuPAGE™ LDS Sample Buffer	4X	64.5 µL
milliQ Water	-	25.8 µL

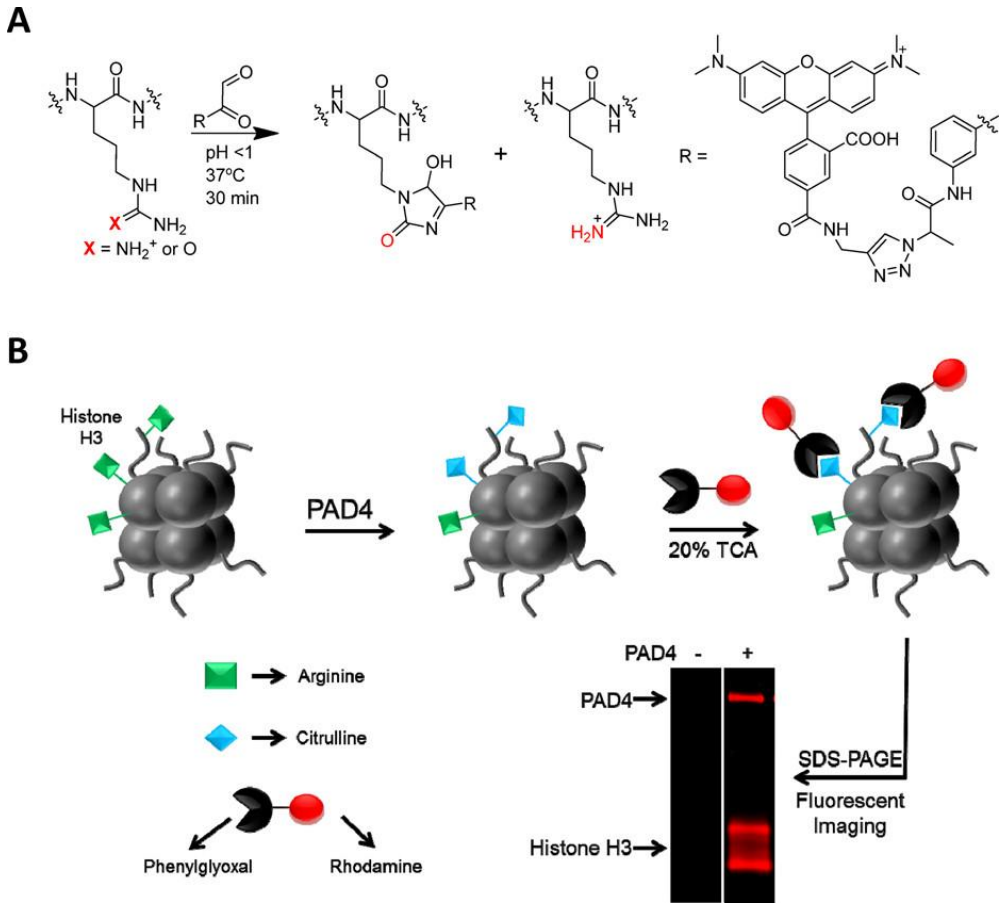

Figure 3: Working Principle of the Citrulline Phenylglyoxal-Rhodamine Probe

(A) The rhodamine–phenylglyoxal (Rh–PG) probe selectively targets citrulline over arginine under acidic pH conditions; **(B)** Arginine (green squares) residues of histone 3 (H3) that convert to citrulline (blue diamonds) by the action of PAD4 are labeled by the Rh-PG probe under acidic conditions. Fluorescent analysis in gel can then reveal citrullinated proteins. The figure was obtained from *J. Am. Chem. Soc*. 2012, 134, 41, 17015-17018[167]

3.3.8 PAD4 Inhibition Assay

Citrullination is catalyzed by PAD enzymes, with PAD4 specifically recognized as an important player in NET formation.[168] To determine whether PAD4 activation is required for NET generation when stimulated by CSE, a pan-PAD inhibitor called Cl-Amidine (Cayman), which targets multiple PAD isoforms, was initially used. Following the same experimental approach described in section 3.3.4, extracellular DNA release was assessed under the following conditions: (i) untreated; (ii) untreated + Cl-Amidine; (iii) CSE; (iv) CSE + Cl-Amidine; and (v) negative

control. The media composition for each condition is detailed in Table 5. Subsequently, a specific PAD4 inhibitor, GSK484 (Cayman), was also tested, given the known involvement of PAD4 in NETosis. Fluorescence readings were taken kinetically using the Synergy H1 microplate reader (BioTek) under the following settings: measurements every hour over an 8-hour period at 37°C, using excitation/emission wavelengths of 485/528 nm, with all wells normalized relative to high signal negative control wells.

Table 5: Media Composition for PAD/4 Inhibition Assay

Medium	Reagent	Volume (in 1 mL)
Untreated	RPMI 1640	999 µL
	SYTOX™ Green (5 µM)	1 µL
Untreated + Cl-Amidine/GSK484	RPMI 1640	998 µL
	SYTOX™ Green (5 µM)	1 µL
	Cl-Amidine (500 µM)/ GSK484 (10 µM)	1 µL
CSE	100% CSE medium	999 µL
	SYTOX™ Green (5 µM)	1 µL
CSE + Cl-Amidine/GSK484	100% CSE medium	999 µL
	SYTOX™ Green (5 µM)	1 µL
	Cl-Amidine (500 µM)/ GSK484 (10 µM)	1 µL
Negative Control	RPMI 1640	1 mL

3.4 Animal Models and Experimental Design

3.4.1 Mice

Male DBA/1J (~6 weeks old) were obtained from The Jackson Laboratory. Mice were housed in the Children's Hospital Research Institute of Manitoba (CHRIM) satellite animal care facility (an extension of the central animal care facility) at the University of Manitoba. Upon arrival, the mice were randomly housed by the animal care facility staff, with no more than five mice per cage, and were acclimatized for two weeks prior to the start of the experiment.

3.4.2 Collagen-Induced Arthritis Cigarette Smoke Exposure Model (Synchronized and Non-Synchronized)

The two CIA models used in this study were adapted with slight modification from previously published protocols.[169–171] The study received ethical approval from the University of Manitoba Animal Research Ethics and Compliance Board (protocol #B2024-010/1 (AC11885)).[172] In the first experimental setup which incorporated LPS (outlined in **Figure 4**), mice were divided into four groups: (i) Saline-FA (n = 5); (ii) Saline-CS (n = 5); (iii) CIA-FA (n = 5); and (iv) CIA-CS (n = 8). In addition to receiving either saline or collagen injections, mice were exposed to either fresh air (FA) or cigarette smoke (CS). Each group was housed in a separate cage. Because the CIA-CS group consisted of 8 mice, they were split into two cages, with 5 mice in one and 3 in the other. Mice in the CIA-FA and CIA-CS groups were anesthetized with 4% isoflurane and given a subcutaneous (s.c.) injection of 100 µg bovine collagen II (CII) (Chondrex Inc., Redmond, WA, USA) emulsified in complete Freund's adjuvant (Chondrex Inc.) at a site 1.5 cm from the base of the tail on day 0. This was followed by a booster injection (s.c.) on day 21 using 50 µg of bovine CII emulsified in incomplete Freund's adjuvant (Chondrex Inc.). To synchronize disease onset across animals, all mice received an intraperitoneal (i.p.) injection of 20 µg LPS (*E. coli* 0111:B4) (Chondrex Inc.) on day 25. For cigarette smoke exposure, Standard 1R6F research-grade cigarettes (University of Kentucky, Lexington, KY) were used. The smoke from 10 cigarettes was delivered using the SCIREQ InExpose® smoking robot (SCIREQ, Montreal, QC, Canada) at a rate of 2 L/min, with one puff per minute and five puffs per cigarette. Mice in the Saline-FA and CIA-FA groups were exposed to room air in a foreign cage during the CS exposure sessions. Smoke exposure was conducted for 1 hour daily at the same time, 5 days a week, from day 1 through day

28. Mice were monitored every other day for changes in body weight, grooming behavior, and activity levels. Joint thickness measurements were taken every 48 hours starting on day 22 using a digital slide caliper. Clinical scoring was performed based on previously established criteria.[173,174] Scoring was defined as follows: 0 = normal joint; 1 = paw swelling only; 2 = swelling with one affected joint; 3 = multiple affected joints in a limb; and 4 = all joints involved or limb fusion. Each mouse received a cumulative clinical score ranging from 0 to 16 by summing the scores of all four paws. On day 29, all mice were anesthetized with 4% isoflurane and euthanized via cardiac puncture.

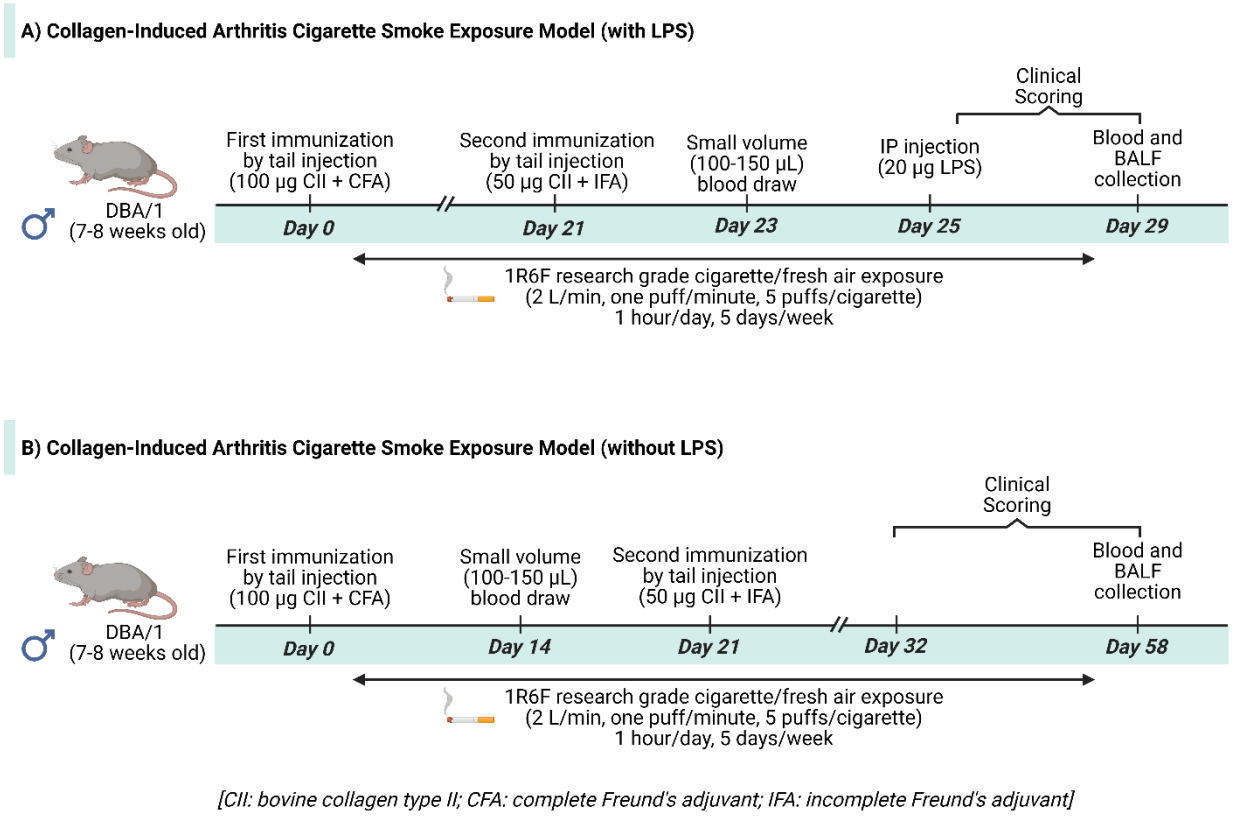

[CII: bovine collagen type II; CFA: complete Freund's adjuvant; IFA: incomplete Freund's adjuvant]

Figure 4: Collagen-Induced Arthritis Cigarette Smoke Exposure Models (with and without LPS)

(A) CIA – Cigarette Smoke Exposure model with LPS or, the synchronized model with an intraperitoneal (i.p.) LPS injection on day 25. **(B)** CIA – Cigarette Smoke Exposure model without any LPS injection, or the non-synchronized model which continued up to day 58 from the first CII injection. Image created with BioRender.com

In the second experimental setup, also illustrated in **Figure 3**, the intraperitoneal (i.p.) injection of LPS was omitted. As a result, this setup followed a conventional CIA model, in which the onset of arthritic symptoms occurs over a longer duration. As in the first setup, mice were assigned to four groups, though with different sample sizes: (i) Saline-FA (n = 3); (ii) Saline-CS (n = 3); (iii) CIA-FA (n = 6); and (iv) CIA-CS (n = 6). Each group was housed separately with 3 mice per cage, leading to two cages each for the CIA-FA and CIA-CS groups. The bovine CII injections were administered in the same manner as described in the previous model. Following each injection, mice were physically and visually assessed every other day for one week. Clinical scoring began on day 32 and continued through day 58. On day 59, all mice were anesthetized with 4% isoflurane and euthanized by cardiac puncture.

3.4.3 Bronchoalveolar Lavage Fluid (BALF) Collection

Immediately following euthanasia, the skin overlying the trachea was carefully dissected using dissecting scissors (VWR) to expose the trachea. A small incision was made to allow the insertion of a 20-gauge catheter (BD Biosciences) into the trachea. Once inserted, the catheter was secured in place by tying a thread around both the catheter and the trachea. A 1 mL syringe (BD Biosciences) containing saline (Fisher Scientific) was then attached to the catheter. Saline was gently instilled into the lungs and subsequently aspirated to collect the lavage fluid. This process of instillation and aspiration was repeated twice. Two separate washes were performed using 1 mL of saline each, and the resulting BALF was collected into a 2 mL microcentrifuge tube (Bio-Rad) and kept on ice. The collected BALF was centrifuged at 150 × g for 10 minutes at 10°C. The supernatant was then carefully transferred into fresh microcentrifuge tubes and stored at -80°C. The remaining cell pellets were used for immunophenotyping by flow cytometry.

3.4.4 Blood (Serum) Collection

In the first experimental setup, a small volume of blood (100–150 µL) was collected on day 23 as “pre-LPS” blood. In the second experimental setup, a similar volume (100–150 µL) was collected on day 14. On the day of euthanasia, the blood obtained through cardiac puncture was stored in 1.6 mL microcentrifuge tubes (Bio-Rad). Following the collection of BALF, the diaphragm was cut, and the heart was dissected to access any remaining blood. This additional

blood was collected using a syringe without a needle and added to the corresponding microcentrifuge tubes. For the post-processing, the blood samples were left undisturbed at RT for 1 hour. After incubation, the samples were centrifuged at 6000 RPM for 10 minutes. The resulting serum was carefully transferred into new microcentrifuge tubes. This centrifugation process was repeated once more before aliquoting the serum and storing the samples at -80°C for further analysis.

3.4.5 Immunophenotyping of BAL Cells

Cells obtained from the BAL were stained with a panel of antibodies to immunophenotype innate immune cell populations. Each tube was brought to volume with 1 mL of eBiosciences™ Flow Cytometry Staining Buffer (Invitrogen by Thermo Fisher), followed by centrifugation at 1200 RPM for 5 minutes at 4°C. During this step, the MM was prepared using the following antibodies: APC anti-mouse Ly-6G, FITC anti-mouse CD11c, PerCP-Cy5.5 anti-mouse F4/80, PE anti-mouse CD170 (Siglec-F), and PE-Cy7 anti-mouse/human CD11b (BioLegend). The MM was calculated as follows:

MM = amount of each antibody + amount of flow buffer

Where, Amount of each antibody = (number of samples + 1) × 0.5 µL

And, Amount of flow buffer = ((number of samples + 1) × 20 µL) – (number of antibodies × amount of each antibody)

For the first experimental setup, compensation controls were prepared using UltraComp eBeads™ Compensation Beads (Invitrogen by Thermo Fisher) and 0.5 µL of the respective antibody. After centrifugation and supernatant removal, the cells were resuspended in 20 µL of the prepared MM and gently vortexed. Both the compensation control and the sample tubes were incubated on ice and protected from light for 30 minutes. Following incubation, 1 mL of flow buffer was added to each tube, which were then centrifuged again at 1200 RPM for 5 minutes at 4°C. After aspirating the supernatant, 300 µL of 2% PFA in PBS (Thermo Fisher Scientific) was added to each tube. The samples were vortexed and incubated on ice in the dark for 15 minutes. Subsequently, 1 mL of flow buffer was added, and the tubes were centrifuged again under the same conditions. Finally, the supernatant was removed, and the cells were resuspended in 400 µL

of flow buffer. The stained samples were analyzed using the LSRFortessa flow cytometer (BD Biosciences). For each sample, 10,000 events were collected, and the data were analyzed using FlowJo Software (v10.9.0, BD Biosciences).

Table 6: Panel for Immunophenotyping Mouse BAL Cells

Marker	Fluorophore	Laser (Detection Range)
Ly-6G	APC	Red (663-667)
CD170 (Siglec-F)	PE	Green (578-594)
CD11c	FITC	Blue (515-545)
F4/80	PerCP-Cy5.5	Blue (685-735)
CD11b	PE-Cy7	Yellow Green (750-810)

3.4.6 of Cytokines and Chemokines

The total protein concentration in the BALF was quantified using the Pierce™ BCA Protein Assay Kits (Thermo Fisher Scientific) to ensure that sufficient protein was available for evaluating the expression of various biomarkers. Subsequently, the protein expression levels of a panel of cytokines and chemokines were assessed in both BALF and serum samples collected at different time points from both experimental models, using the multiplex Olink® Target 48/96 platform (Olink Biosciences), following the manufacturer's guidelines. A 48-plex panel was utilized for the first model, while a 96-plex panel was applied in the second model. The proteomic expressions of the following cytokines and chemokines were analyzed: CXCL1, CXCL2, IL1α, IL1β, CSF2, CSF3, IL17a, IL17f, TNF, and CCL4. The values obtained for analysis were expressed in normalized protein expression units (NPX).

3.4.7 Anti-Mouse Collagen Antibody ELISA with BALF and Serum

Mice produce high levels of serum antibodies against the injected CII, and due to the conserved amino acid sequences in type II collagen, these antibodies can cross-react with the body's own type II collagen, contributing to the development of arthritis. As a result, the levels of antibodies targeting autologous collagen serve as a reliable indicator of arthritis onset and severity in the experimental mice. Accordingly, antibody levels in both BALF and serum samples from both models were measured using an enzyme-linked immunosorbent assay (ELISA) with the

Mouse Anti-Mouse Type II Collagen IgG Antibody Assay Kit (Chondrex Inc.), following the manufacturer's protocol. For BALF samples, a 1:4 dilution was applied, whereas serum collected at various time points was diluted at a ratio of 1:10000.

3.4.8 Anti-NE ELISA with BALF and Serum

Considering the established role of NETs in the pathogenesis of rheumatoid arthritis[175], the possible presence of NETs was assessed by measuring neutrophil elastase (NE) levels in BALF and serum samples using an ELISA. The Mouse ELA2 Quantikine ELISA Kit (R&D Systems, Minnesota, USA) was used for this purpose following the manufacturer's instructions. BALF samples were diluted at a ratio of 1:2, while serum samples were diluted 1:25 for the assay.

3.4.9 Detection of Citrulline in BALF

Citrulline levels in the BALF samples from both models were measured following the same protocol described in section 3.3.7, with each sample containing approximately 20 µg of protein.

3.5 Statistical Analyses

All data analyses were conducted using GraphPad Prism version 10.4.0. For comparisons between two groups, such as in the degranulation flow cytometry, phagocytosis flow cytometry, and PAD4 inhibition experiments with sample size < 20, the non-parametric Mann-Whitney *U* test was applied. For comparisons involving more than two groups, including analyses of neutrophil percentages, cytokine and chemokine levels in BALF and serum, anti-NE ELISA, and anti-mouse collagen II antibody ELISA experiments, one-way ANOVA followed by Tukey's multiple comparison test was used. A *p*-value of less than 0.05 was considered statistically significant.

Chapter 4: Results

4.1 *In Vitro* Findings on the Effect of CSE on Neutrophilic Functions

4.1.1 CSE does not lead to Neutrophil Degranulation

The first aim was to evaluate the impact of 100% CSE medium on key neutrophil function and phenotype, including surface marker expression, degranulation, phagocytosis, and NET formation. Neutrophils were treated with 100% CSE medium, and the most relevant cluster of differentiation (CD) markers associated with neutrophil activation and degranulation were selected for analysis (as listed in Table 7).

Table 7: Specificity of Human Neutrophil CD Markers

Surface Marker	Specificity	Function
CD11b	Gelatinase Granules	β – integrin involved in neutrophil migration and adhesion[176]
CD16	FcγRIIIb	FcγRIIIb involved in neutrophil degranulation, phagocytosis and oxidative burst[177,178]
CD63	Azurophilic Granules	Tetraspanin involved in neutrophil activation, granule targeting and release[179,180]
CD32	FcγRII	FcγRII involved in immune complex interaction and neutrophil activation[181]
CD64	FcγRI	FcγRI involved in IgG binding, phagocytosis and ADCC during inflammation[177]
CD66b	Specific Granules	Protein involved in neutrophil activation, adhesion, degranulation and ROS production[182,183]

Flow cytometry showed that the expression levels of these markers in CSE-treated neutrophils did not increase relative to those in untreated neutrophils ($p = ns$) (**Figure 5A**). To validate these findings, the enzymatic activities of granular proteins NE and PR3, which are typically released during degranulation, were measured in the corresponding cell supernatants. Each sample generated a progress curve based on substrate consumption, recorded at one-minute intervals over a 45-minute period. Linear regression was applied to each curve, and the slope was used to quantify enzymatic activity.[184] Recombinant PR3 and HNE were included as positive

controls to confirm assay validity (data not shown). The results indicated that the activities of both NE and PR3 in CSE-treated samples were similar to those in supernatants from untreated neutrophils (*p = ns*) (**Figure 5B**). Each data point in the graphs represents an individual replicate.

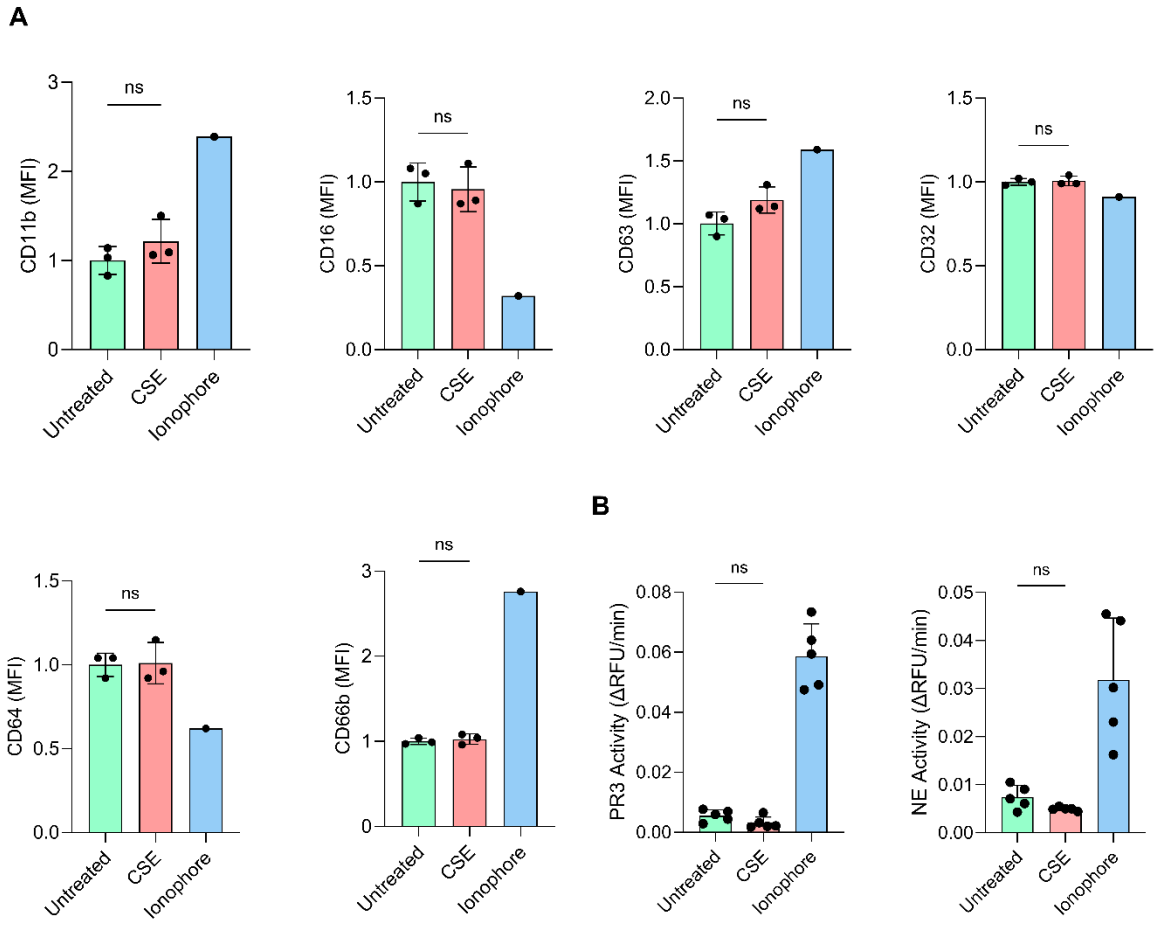

Figure 5: CSE-stimulated neutrophils behave similarly to untreated neutrophils after 1 hour of stimulation as shown by surface markers and granular enzyme activities

(A) Surface expression of degranulation and activation markers CD11b, CD16, CD63, CD32, CD64, and CD66b on neutrophils stimulated for 1 hour, analyzed by flow cytometry. Results are presented as relative mean fluorescence intensity (MFI). Data represent mean ± SEM from individual experiments (n = 3), and comparisons between untreated and CSE-treated groups were made using the Mann-Whitney *U* test; *ns* = not significant. **(B)** Enzymatic activity of PR3 and NE in cell supernatants after 60 minutes in culture at 37°C. Results are shown as ΔRFU/min, and comparisons between enzyme activities in the supernatants from untreated and CSE-treated neutrophils were performed using the Mann-Whitney *U* test; *ns*.

4.1.2 CSE Increases Phagocytic Activity of Neutrophils

To determine whether CSE influences neutrophils capacity to phagocytose foreign entities, fluorescently (FITC) labeled IgG-latex beads were used. IgG is recognized by the FcγR receptors on neutrophils[185], which allows for identification and engulfment of the latex beads. To assess non FCγR mediated phagocytosis, heat-killed *E. coli* was used.

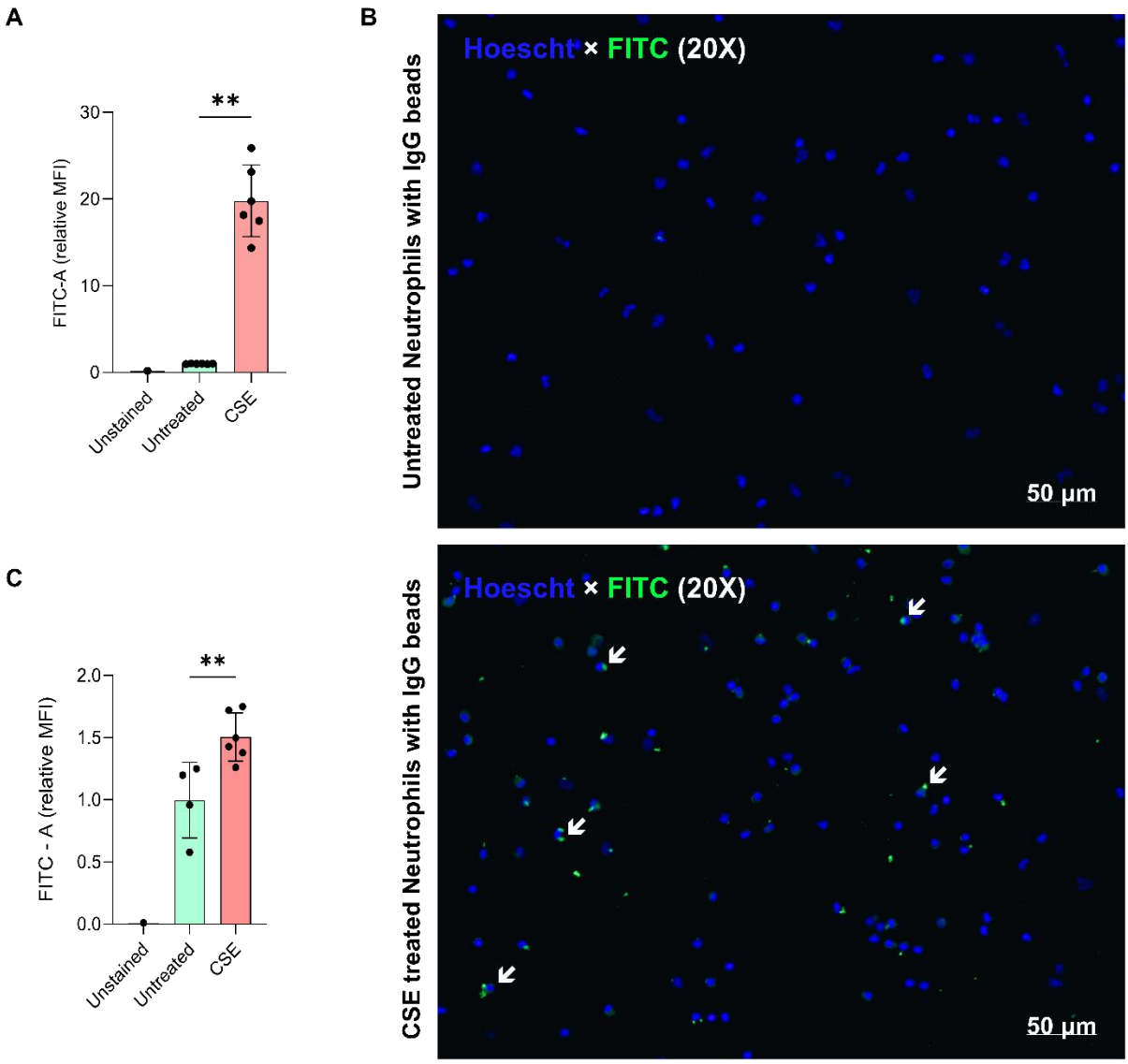

Figure 6: CSE-treated neutrophils show enhanced phagocytosis of IgG-latex beads and heat-killed *E. coli*

(A) Phagocytic activity of untreated and CSE-treated neutrophils (18.96 fold higher than untreated) measured in the presence of FITC IgG-labeled latex beads at a 1:400 dilution, following a 5-minute

incubation at 37°C. **(B)** Neutrophils were stained with Hoechst dye and incubated with 1:400 FITC IgG-labeled latex beads for 5 minutes. Fluorescence from chromatin stained with Hoechst (blue) and IgG-latex beads stained with FITC (green) was captured at 20X magnification, and images were overlaid using the ZEN software (scale bars, 50 µm). **(C)** Phagocytic activity of untreated and CSE-treated neutrophils (1.35 fold higher than untreated) in the presence of FITC-labeled heat-killed *E. coli* at a 1:2 dilution, incubated for 5 minutes at 37°C. Data in panels A and C are expressed as relative mean fluorescence intensity (MFI). Statistical comparison of relative MFI between untreated and CSE-treated neutrophils in panels A and C was performed using the Mann-Whitney *U* test; **, $p < 0.01$.

A comparison between untreated and CSE-treated neutrophils revealed about a 20-fold increase in the phagocytic capacity of the CSE-treated cells without any pre-treatment (**Figure 6A**). This finding was supported by immunofluorescence imaging: in the untreated condition, neutrophils appeared intact and stained only with the Hoechst (blue) dye, whereas in the CSE-treated group, cells showed increased uptake of the green FITC-labeled latex beads (**Figure 6B**). Although the difference in phagocytosis between untreated and CSE-treated neutrophils was less pronounced with heat-killed *E. coli* (1.35 fold versus 18.96 fold in the IgG-beads phagocytosis), the CSE-treated group exhibited a significantly higher phagocytic response (**Figure 6C**). These results suggest that CSE enhances the ability of neutrophils to phagocytose both artificial and physiologically relevant foreign particles.

4.1.3 Neutrophils undergo NETosis when stimulated with CSE

To investigate the effect of CSE on NET formation, the total DNA released from neutrophils upon stimulation with CSE was measured. Since DNA can also be released during spontaneous cell death, the measurement was performed kinetically to determine the specific time point at which DNA release begins. NET formation typically occurs after >120 minutes, while necrotic cells death occurs at earlier time points.[166] Immunofluorescence imaging was used to visualize DNA and NE and validate the findings from the plate assay.

The extracellular DNA release assay (8 hours with readings taken every 30 minutes), showed CSE-treated neutrophils begin to release DNA around 2.5 to 3 hours post-treatment (**Figure 7A**). This elevated release continued consistently throughout the kinetic measurement. The timing of the release was indicative of NETosis. To confirm that NETs were being formed, immunofluorescence imaging was performed after fixing untreated and CSE-treated neutrophils

(at 3 hour) and staining for DNA (Hoechst) and NE (AF488). Imaging revealed that untreated neutrophils retained intact chromatin and cell membranes, while CSE-treated neutrophils displayed extracellular DNA strands decorated with NE, consistent with NET formation (**Figure 7B**).

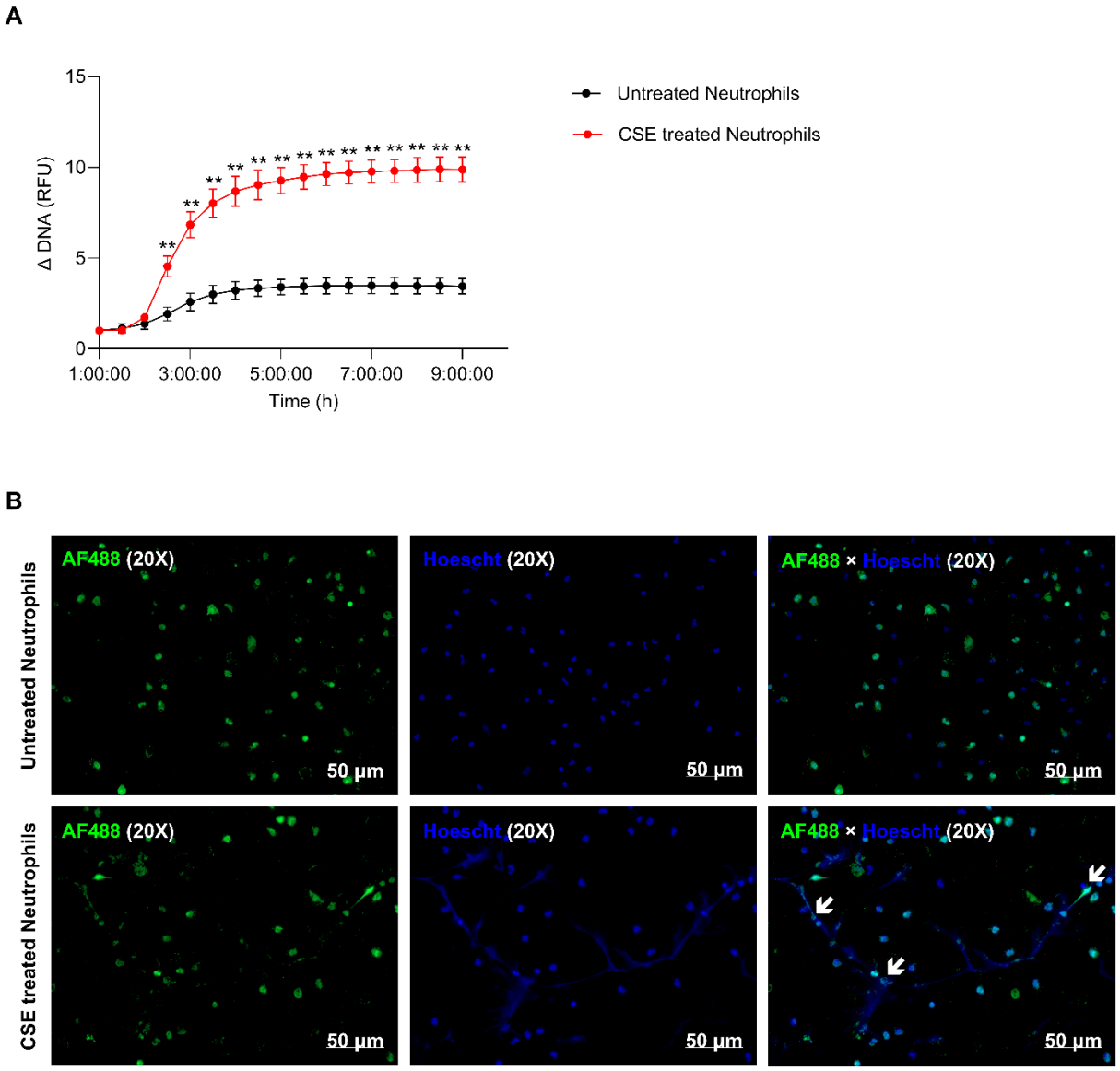

Figure 7: CSE-treated neutrophils go through enhanced NETosis

(A) Extracellular DNA release from untreated and CSE-treated neutrophils measured by fluorescence (SYTOX green) reads made over time at 37°C. The results are shown as relative fluorescence units (RFU), and statistical comparisons of DNA release between untreated and CSE-treated neutrophils at various time points were performed using multiple Mann-Whitney tests; **,

$p < 0.01$. **(B)** Immunofluorescence images of neutrophils stained with AF488 Neutrophil Elastase (green) and Hoechst-stained DNA (blue) were captured separately at 20X magnification and merged using the ZEN software (scale bars, 50 µm).

4.1.4 CSE Induces Citrullinated Protein Production via PAD4-mediated NETosis

The formation of NETs typically requires activation of the enzyme PAD4, which is responsible for the citrullination of histone and other proteins. To determine whether citrullinated proteins were generated in NETs derived from neutrophils stimulated with the CSE medium, in-gel fluorescence imaging was performed. The in-gel fluorescence revealed citrullination between the 21 kDa and 32 kDa bands, which corresponds to the expected molecular weights of neutrophil serine proteases such as NE, PR3, and cathepsin G.[186] Strong fluorescence was also detected around the 11 kDa region, possibly indicative of histone subunits (10-15 kDa).[187] Furthermore, a band at ~95 kDa was observed. These findings confirmed that citrullinated proteins were present in the NETs isolated from CSE-treated neutrophils (**Figure 8A**). In the SYPRO™ Ruby stained gel, a high level of protein deposition was also evident just above the 11 kDa marker, likely indicative of histone subunits, as these are found in high abundance in NETs (**Figure 8B**).

Given the observation that CSE-generated NETs are citrullinated, we next investigated the involvement of PAD enzymes. A pan-PAD inhibitor, Cl-Amidine, was first used to assess its effect on extracellular NET release. A 30-minute pre-treatment with 500 µM Cl-A significantly reduced ($p = 0.0286$) DNA release from neutrophils under CSE stimulation (**Figure 8C**). Given neutrophils contain both PAD4 and PAD2, 5 µM of GSK484, which is a PAD4-specific inhibitor was then used for pre-treatment prior to stimulation with CSE medium. GSK484 also significantly decreased ($p = 0.0286$) extracellular DNA release from neutrophils stimulated with CSE (**Figure 8D**).

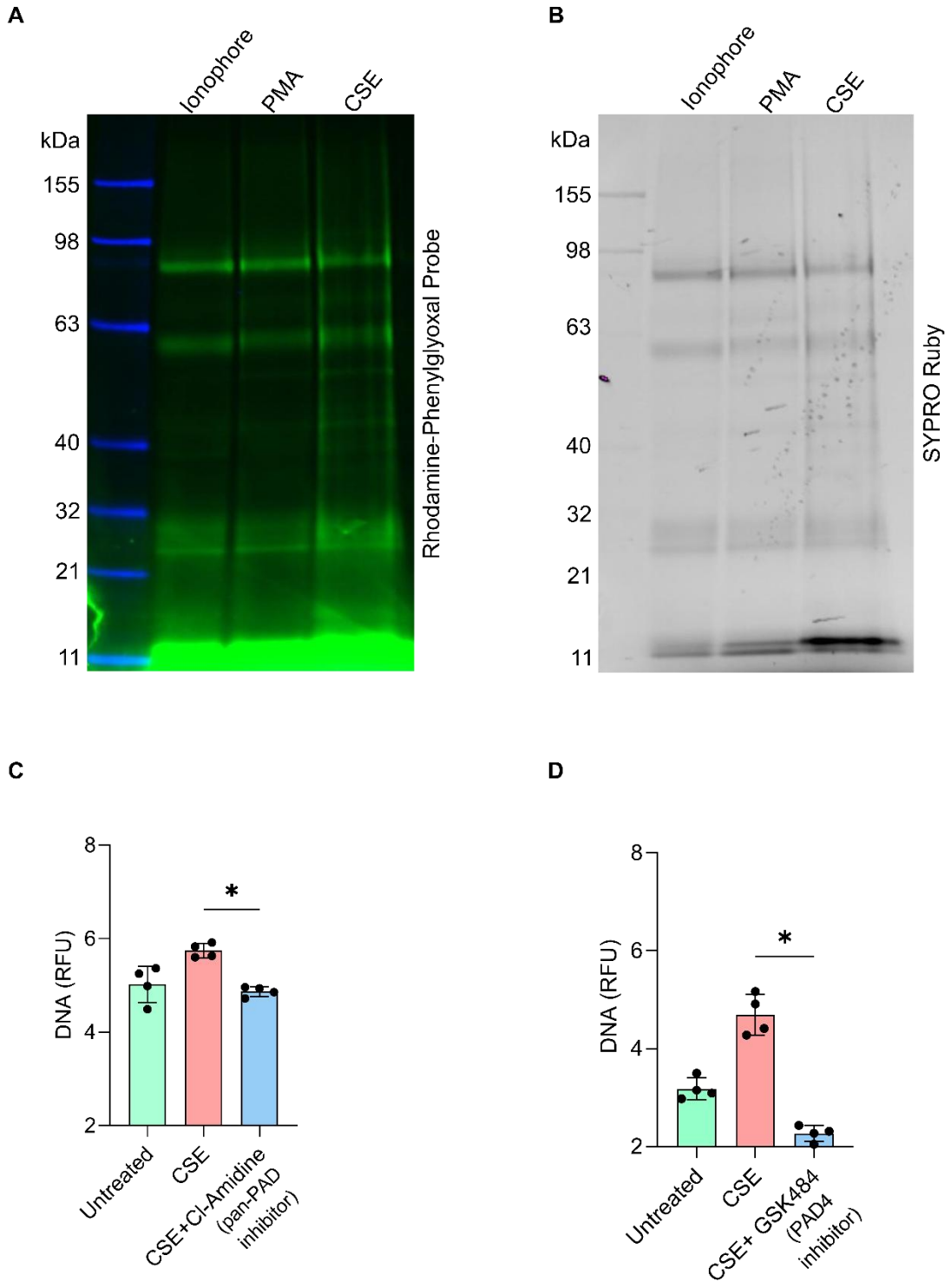

Figure 8: CSE induces citrullinated protein release in NET in a PAD4-dependent pathway

(A) In-gel fluorescence images of NETs derived from neutrophils stimulated with Ionophore, PMA, and CSE, using the Citrulline-specific Rhodamine-Phenylglyoxal probe. **(B)** The

corresponding gel stained with SYPRO™ Ruby to visualize overall protein content. **(C)** Measurement of extracellular DNA release from neutrophils pre-treated with 500 µM Cl-Amidine. **(D)** Measurement of extracellular DNA release from neutrophils pre-treated with 5 µM GSK484. Comparisons of DNA release between CSE-treated and inhibitor-pre-treated neutrophils in panels C and D were analyzed using the Mann-Whitney *U* test; *, $p < 0.05$.

4.2 *In Vivo* Findings on the Effects of CS in Synchronized CIA Mouse Model

4.2.1 Clinical Score, Disease Incidence, and Anti-Mouse Collagen II Autoantibody

To evaluate clinical scores, the thickness of the paws and joints was measured and summed to assign a total clinical score to each mouse. In this model, clinical scoring was conducted from day 22 to day 29. Following the LPS injection, disease progression appeared similar in both the CIA-FA (n = 4) and CIA-CS (n = 7) groups (**Figure 9A**). However, the trajectory of disease onset did appear to be different between the two groups. The CIA-FA group developed arthritis earlier (day 25) than the CIA-CS group. In spite of this, the CIA-FA clinical scores steadily increased until study end, with the CIA-CS group scores rising more rapidly between day 27 and day 29. All mice in both CIA groups expectedly developed arthritis, and there was no statistically significant difference in clinical scores between the two groups (**Figure 9A**). The levels of anti-mouse collagen autoantibodies between CIA-CS (n = 6) and CIA-FA (n = 4) in pre-LPS ($p = 0.87$), post-LPS ($p = 0.87$) serums and BALF ($p = 0.99$) were not significantly different (**Figures 9B**, **9C**, and **9D**).

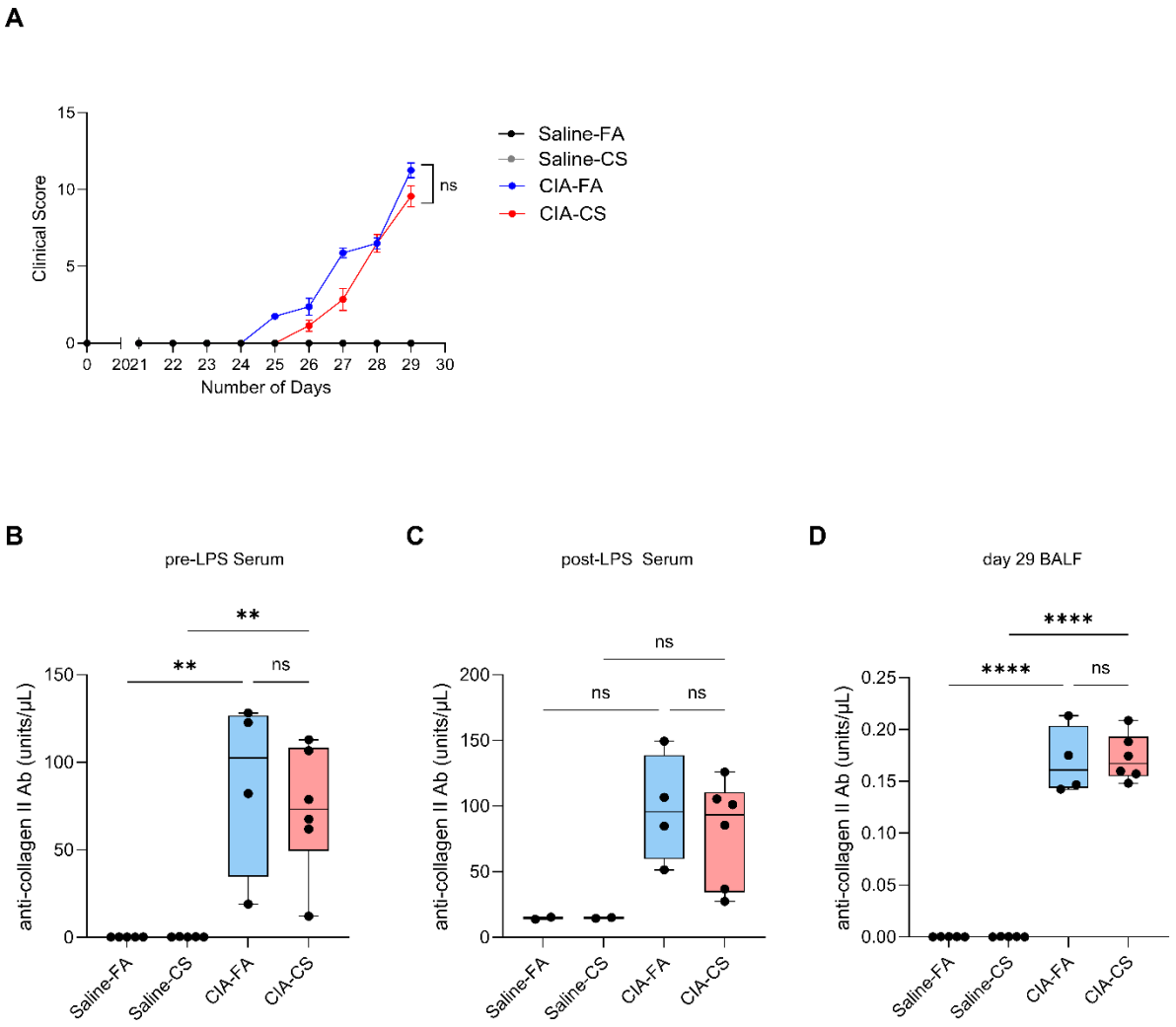

Figure 9: Clinical score and anti-mouse collagen antibodies in pre-LPS, post-LPS (day 29) serums and day 29 BALF (synchronized model)

(A) Clinical scores monitored from day 22 to day 29. The scoring was done using previously defined criteria as discussed in the methods. **(B-C)** Anti-mouse collagen antibody levels in pre-LPS, post-LPS (day 29) serums and day 29 BALF using anti-mouse collagen II antibody ELISA. Bars show median and the whiskers show all points (n = 2/4/5/6). Data were analyzed using one-way ANOVA with Tukey's correction for multiple comparisons. **, $p < 0.01$; ****, $p < 0.0001$; *ns*.

4.2.2 Lung Neutrophil Recruitment and Neutrophils Associated Chemokines and Cytokines

To determine whether neutrophils are similarly affected as the *in vitro* results in a pre-clinical model, the effect of cigarette smoking was observed in the synchronized CIA model. In that context, neutrophil infiltration was observed within the BAL and immunophenotyping of BAL cells was performed. Neutrophils were identified as the Siglec-F^{-}CD11c^{-}CD11b^{+}Ly6G^{+} population. We found that the CIA-CS group showed the highest neutrophil infiltration when compared to the remaining groups, although the comparison to CIA-FA was not significant (Saline-FA = 0.9%, Saline-CS = 0.57%, CIA-FA = 2%, CIA-CS = 4.4%). Neutrophil infiltration in the CIA-CS group was significantly higher than Saline-CS group ($p = 0.0033$), with the Saline-CS group showing minimal neutrophil infiltration (**Figure 10A**). Additionally, the levels of neutrophil-associated cytokines and chemokines were measured using the Olink® Target 48 platform (Olink Biosciences). The concentrations of the neutrophil chemoattractants CXCL1 and CXCL2 were highest in the CIA-CS group (n = 6), though the differences were not statistically significant ($p = 0.18$ and $p = 0.97$ respectively) compared to the CIA-FA group (n = 4) (**Figures 10B** and **10C**). The Saline-CS group (n = 5) exhibited the lowest levels of these chemokines, while the Saline-FA group (n = 5) displayed relatively higher levels, particularly for CXCL2, where levels were similar to those as seen in both CIA groups (**Figure 10C**). CSF3, also known as Granulocyte Colony Stimulating Factor (G-CSF) was found to be elevated in the CIA-CS group. However, the increase was not significant ($p = 0.64$) when compared to the CIA-FA group (**Figure 10D**). Nevertheless, CSF3 levels in the CIA-CS group were significantly higher than those in the Saline-CS group (**Figure 10D**). IL17f, another cytokine that facilitates neutrophil recruitment, also showed elevated levels in the CIA-CS group. However, the differences were not significant when compared to either the CIA-FA ($p = 0.93$) or Saline-CS ($p = 0.21$) groups (**Figure 10E**). Inflammatory IL1α levels were elevated ($p = 0.21$) in the CIA-CS group compared to CIA-FA, while low levels were observed in both the Saline-CS (n = 5) and CIA-CS groups ($p = 0.98$, **Figure 10F**). IL1β levels were comparable across both CIA groups irrespective of smoke exposure ($p > 0.99$, **Figure 10G**). TNF level was elevated ($p = 0.36$) in the CIA-CS group compared to CIA-FA and significantly increased ($p = 0.0013$) compared to Saline-CS groups (**Figure 10H**). CCL4 (also known as MIP-1β), which is involved in generating a pro-NETotic phenotype of neutrophils[188], was also elevated in the CIA-CS group. Although this elevation was not significant ($p = 0.2$) compared to the CIA-FA group, it was significantly higher ($p = 0.0029$) than in the Saline-CS

group (**Figure 10I**). Overall, these data suggest that, there was increased infiltration of neutrophils in the BAL fluid of the CIA-CS group along with overall elevated levels of pro-inflammatory and pro-NETotic biomarkers.

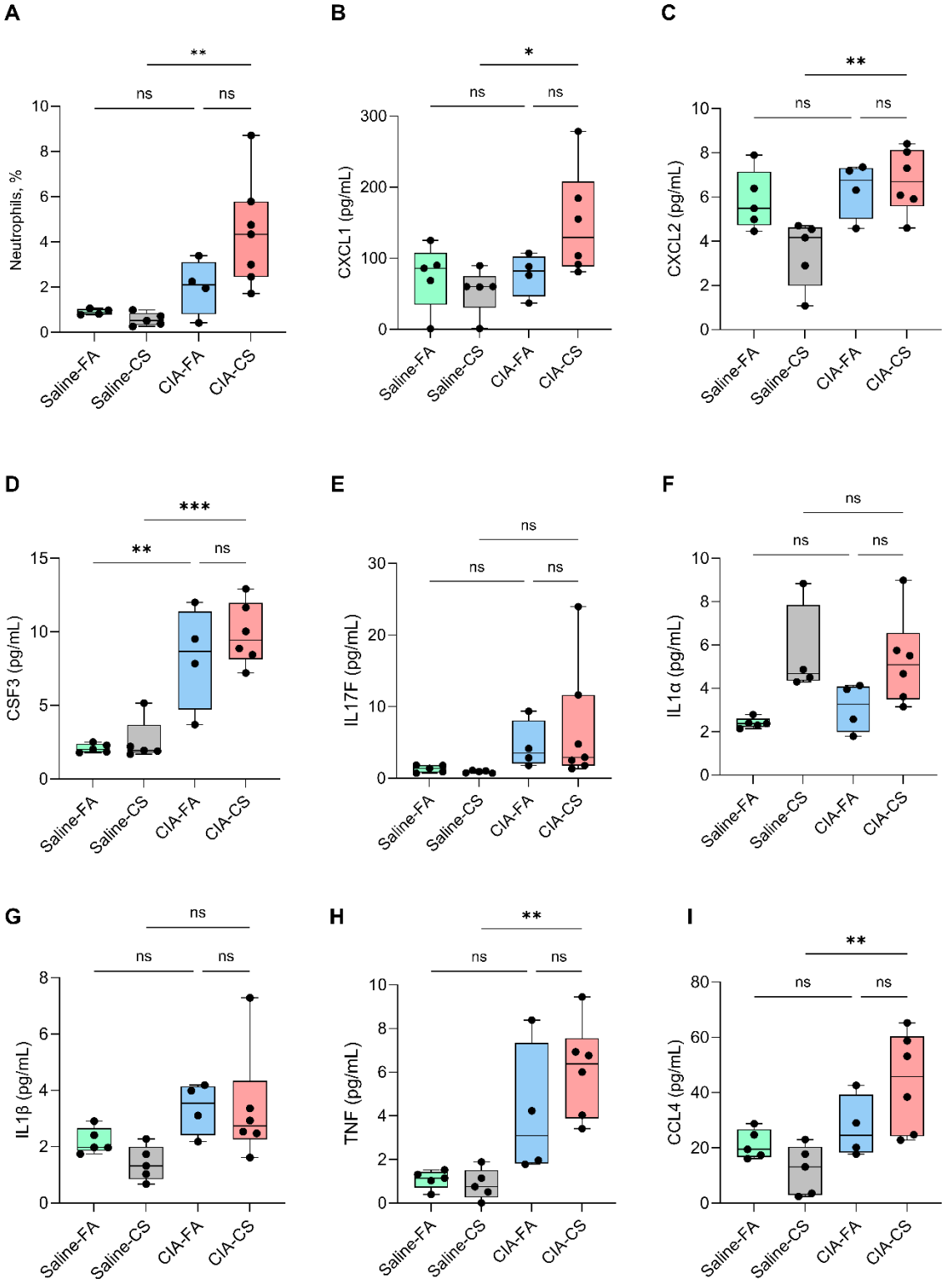

Figure 10: Neutrophil recruitment and neutrophil-related biomarkers in day 29 BALF (synchronized model)

(A) Percentage (%) of neutrophils (identified as Siglec-F−CD11c−CD11b+Ly6G+) in the BAL of different groups in the synchronized model. **(B-I)** CXCL1, CXCL2, CSF3, IL17f, IL1α, IL1β, TNF, and CCL4 levels in the BALF of different groups in the synchronized model as measured by Olink® Target 48 platform (Olink Biosciences). Bars show median and the whiskers show all points (n = 4/5/6/7). Data were analyzed using one-way ANOVA with Tukey's correction for multiple comparisons. *, $p < 0.05$; **, $p < 0.01$; ***, $p < 0.001$; *ns*.

4.2.3 Neutrophil-associated Chemokines and Cytokines in the Serum at Various Time Points

We next sought to evaluate the levels of neutrophil-related chemokines and cytokines in serum during the development phase of the CIA mouse model. Using serum drawn prior to the injection (s.c) of LPS we applied the Olink® Target 48 platform (Olink Biosciences). In the pre-LPS serum, levels of CXCL1, CSF3, and CCL4 were elevated in the CIA-CS group (n = 5). While these elevations were not statistically significant compared to the CIA-FA group, they were significantly higher than in the Saline-CS group (**Figures 11A**, **11B**, and **11F**). For IL17f, IL1β, and TNF, the two CIA groups showed comparable levels, but CIA-CS levels were significantly higher than those in the Saline-CS group (Figures **11C**, **11D**, and **11E**).

In the end point serum, CXCL1 levels were found to be similar among the Saline-CS (n = 5), CIA-FA (n = 4), and CIA-CS (n = 5) groups (**Figure 11G**). For CSF3 and IL17f, increased variability was noted within the CIA-FA group, though the differences between CIA-FA and CIA-CS remained statistically insignificant ($p = 0.16$ and $p = 0.8$ respectively). Interestingly, both the levels and variability of these cytokines increased substantially in the Saline-FA group (n = 5, **Figures 11H** and **11I**), although not significantly increased when compared to pre-LPS serum cytokine levels ($p = 0.55$ and $p = 0.42$ respectively). IL1β, TNF, and CCL4 levels continued to be elevated in the CIA-CS group, but the lack of statistical significance ($p = 0.67$, $p = 0.4$ and $p = 0.4$ respectively) between CIA-CS and CIA-FA persisted (**Figures 11J**, **11K**, and **11L**). Additionally, the differences between CIA-CS and Saline-CS became less pronounced post-LPS (**Figures 11J**, **11K**, and **11L**).

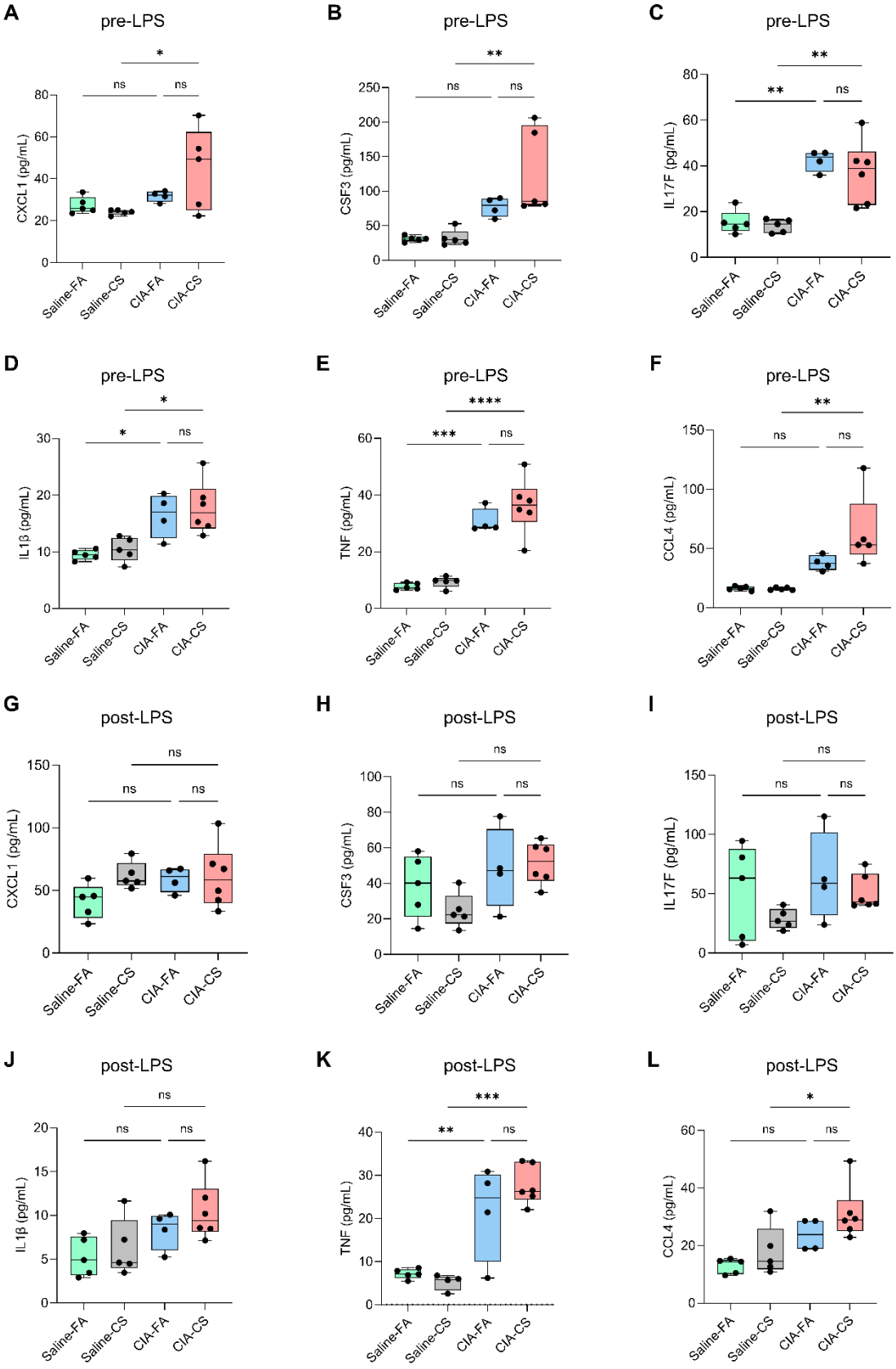
A
pre-LPS
CXCL1 (pg/mL)
B
pre-LPS
CSF3 (pg/mL)
C
pre-LPS
IL17F (pg/mL)
D
pre-LPS
IL1β (pg/mL)
E
pre-LPS
TNF (pg/mL)
F
pre-LPS
CCL4 (pg/mL)
G
post-LPS
CXCL1 (pg/mL)
H
post-LPS
CSF3 (pg/mL)
I
post-LPS
IL17F (pg/mL)
J
post-LPS
IL1β (pg/mL)
K
post-LPS
TNF (pg/mL)
L
post-LPS
CCL4 (pg/mL)
Saline-FA
Saline-CS
CIA-FA
CIA-CS
ns

Figure 11: Chemokines and cytokines in pre-LPS and post-LPS (day 29) serum samples (synchronized model)

(A-F) CXCL1, CSF3, IL17f, IL1β, TNF and CCL4 levels in the pre-LPS serum from different groups in the synchronized model. **(G-L)** CXCL1, CSF3, IL17f, IL1β, TNF and CCL4 levels in the pre-LPS serum from different groups in the synchronized model. Data quantified by Olink® Target 48 platform (Olink Biosciences). Bars show median and the whiskers show all points (n = 4/5/6). Data were analyzed using one-way ANOVA with Tukey's correction for multiple comparisons. *, $p < 0.05$; **, $p < 0.01$; ***, $p < 0.001$; ****, $p < 0.0001$; *ns*.

4.2.4 NE in BALF and Serum at Various Time Points

NE is released during NETosis and therefore to speculated on potential NETosis, the levels of NE were measured in both BALF and serum at various time points to assess its abundance in these samples. NE was significantly higher in the BALF of CIA-CS (n = 6) mice compared to both CIA-FA (n = 4, $p = 0.013$) and Saline-CS (n = 5, $p < 0.0001$) groups (**Figure 12C**). Similarly, in the pre-LPS serum, there was a significant difference in the serum NE levels between the CIA-CS and both CIA-FA ($p = 0.04$) and Saline-CS ($p < 0.0001$) groups (**Figure 12A**). In the post-LPS or, the end point serum however, we no longer observed a significant difference ($p = 0.86$) between CIA-CS and CIA-FA although the difference between CIA-CS and Saline-CS remained significant ($p < 0.0001$). (**Figure 12B**).

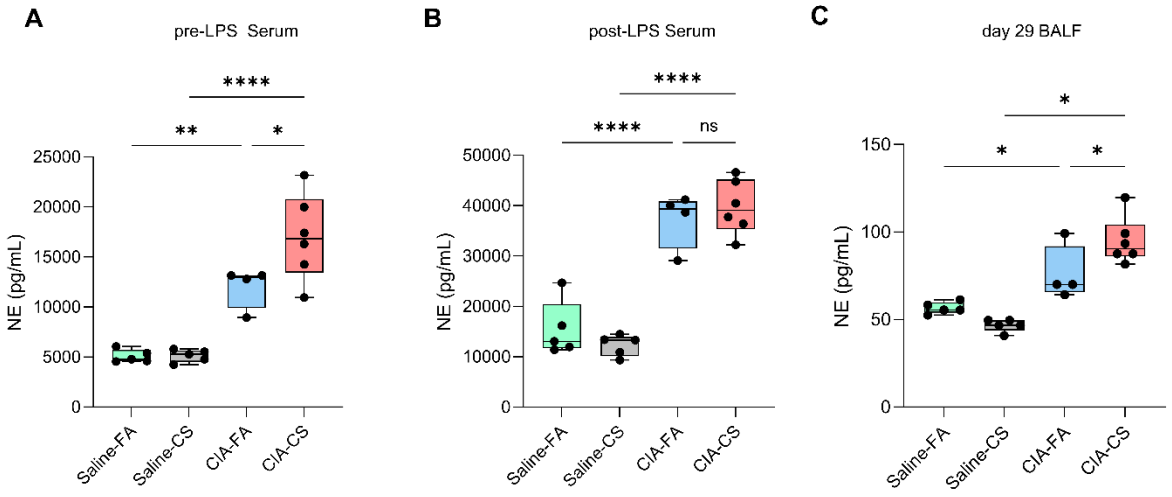

Figure 12: Neutrophil Elastase (NE) abundance in pre-LPS, post-LPS (day 29) serums and day 29 BALF (synchronized model)

(A-C) Abundance of NE assessed in pre-LPS, post-LPS (day 29) serums and day 29 BALF using Anti-NE ELISA. Bars show median and the whiskers show all points (n = 4/5/6). Data were analyzed using one-way ANOVA with Tukey's correction for multiple comparisons. *, $p < 0.05$; **, $p < 0.01$; ****, $p < 0.0001$; *ns*.

4.2.5 Citrullination in the BALF

Citrullinated proteins are typically released alongside NETs, serving as potential targets for ACPA autoantibodies. To assess the possible release of citrullinated proteins that could contribute to disease exacerbation, the citrullination profile in the BALF was analyzed using the citrulline phenylglyoxal-rhodamine probe. Equal amounts of protein were loaded into each well after quantification with BCA assay. In the BALF samples, the CIA-CS group showed greater citrullination within the 65–80 kDa range compared to the CIA-FA group (**Figure 13A** and **Figure 13C**). Additionally, citrullination was detected at 10 and 15 kDa, possibly corresponding to citrullinated histones (**Figure 13A**) which are abundant in NETs. Notably, the Saline-FA group also displayed dense bands near 65 kDa, whereas the Saline-CS group exhibited prominent bands in the 10–15 kDa range (**Figure 13A**).

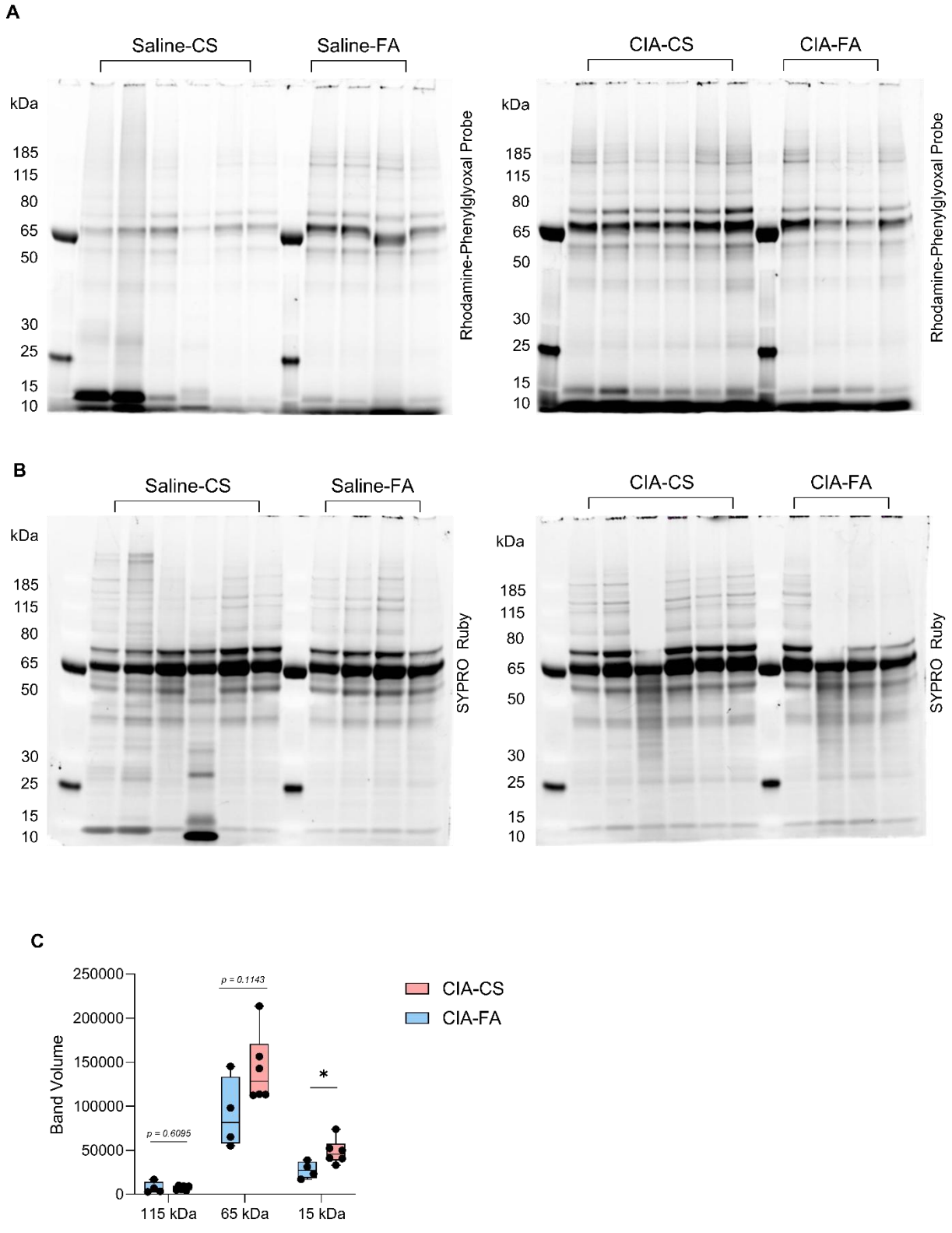

Figure 13: Citrullination in BALF (synchronized model)

(A) In-gel fluorescence images of BALF from all four groups using the Citrulline Phenylglyoxal-Rhodamine probe. **(B)** The corresponding gel stained with SYPRO™ Ruby to visualize overall protein content. **(C)** Band volume compared between CIA-CS and CIA-FA groups at 115 kDa, 65 kDa and 15 kDa.

4.3 *In Vivo* Findings on Effects of CS in Non-Synchronized CIA Mouse Model

Since the synchronized CIA mouse model did not yield definitive results regarding the effects of CS on disease progression and endpoint results, these effects were further examined in a non-synchronized model (without LPS injection) given the evidence from previous study showing CS worsens disease in a conventional (non-synchronized) CIA mouse model.[189]

4.3.1 Clinical Score, Disease Incidence, and Anti-Mouse Collagen II Autoantibody

In this model, clinical scoring began on day 32 and continued until the study endpoint on day 58. The clinical scores were, as expected, lower compared with the synchronized model and no significant differences observed between the CIA-CS (n = 6) and CIA-FA (n = 6) groups (**Figure 14A**). However, disease incidence did differ between groups: only 33.33% (2 out of 6) of the CIA-FA mice showed physical symptoms such as joint swelling, whereas 83.33% (5 out of 6) of the CIA-CS mice developed joint swelling (**Figure 14B**). When anti-mouse collagen autoantibodies were measured, BALF samples showed significantly higher levels ($p = 0.0234$) in the CIA-CS group compared to the CIA-FA group (**Figure 14E**). Autoantibody levels were elevated in the CIA-CS group compared to the CIA-FA group at day 14, although the difference was not statistically significant ($p = 0.13$) (**Figure 14C**). By day 58, the difference in autoantibody levels between CIA-CS and CIA-FA groups were no longer apparent ($p = 0.94$) (**Figure 14D**).

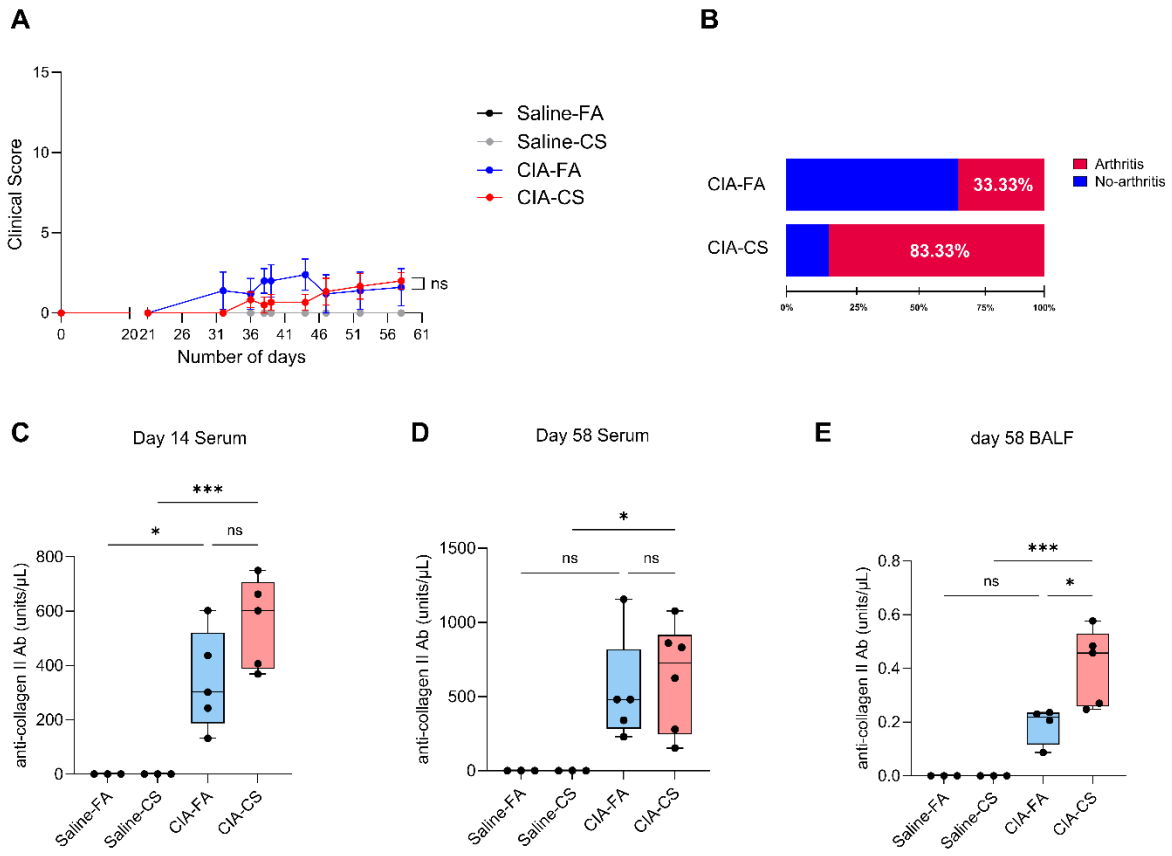

Figure 14: Clinical score, disease incidence, and anti-mouse collagen antibodies in day 14, and day 58 serums and day 58 BALF (non-synchronized model)

(A) Clinical scores monitored from day 32 to day 58. The scoring was done using previously defined criteria as discussed in the methods. **(B)** Disease incidence in CIA-FA and CIA-CS groups. **(C-D)** Anti-mouse collagen antibody levels in day 14, day 58 serums and day 58 BALF using anti-mouse collagen II antibody ELISA. Bars show median and the whiskers show all points (n =3/4/5/6). Data were analyzed using one-way ANOVA with Tukey's correction for multiple comparisons. *, $p < 0.05$; **, $p < 0.01$; ***, $p < 0.001$; *ns*.

4.3.2 Lung Neutrophil Recruitment and Neutrophils Associated Chemokines and Cytokines

In this model, the highest neutrophil infiltration in BAL was in the CIA-CS group (n = 6), which was significantly higher ($p < 0.0001$) than that in CIA-FA (n = 5) (**Figure 15A**). Interestingly, the neutrophil infiltration in the BAL of the Saline-CS group was comparable to that of the CIA-CS group (**Figure 15A**). To assess the levels of neutrophil-associated chemokines and cytokines, the Olink® Target 96 platform (Olink Biosciences) was utilized. CXCL1 levels were elevated in the CIA-CS group but were not significantly higher ($p = 0.64$) than those in the CIA-FA group (**Figure 15B**). Notably, the Saline-FA (n = 3) group also exhibited high levels of CXCL1, comparable ($p = 0.3$) to those seen in the CIA-CS group (**Figure 15B**). CSF2, also known as Granulocyte-Macrophage Colony-Stimulating Factor (GM-CSF), showed the highest levels in the Saline-FA group. However, the high variability within the CIA-CS group resulted in no statistically significant differences across the groups (**Figure 15C**). The pro-inflammatory cytokine IL1β did not show a significant increase in the CIA-CS group when compared to either the CIA-FA ($p = 0.73$) or Saline-CS (n = 3, $p = 0.145$) groups (**Figure 15D**). Interestingly, IL1β level in the Saline-FA group was higher ($p = 0.38$) than in the Saline-CS group. When TNF levels were compared across the groups, no statistically significant differences were observed (**Figure 15E**).

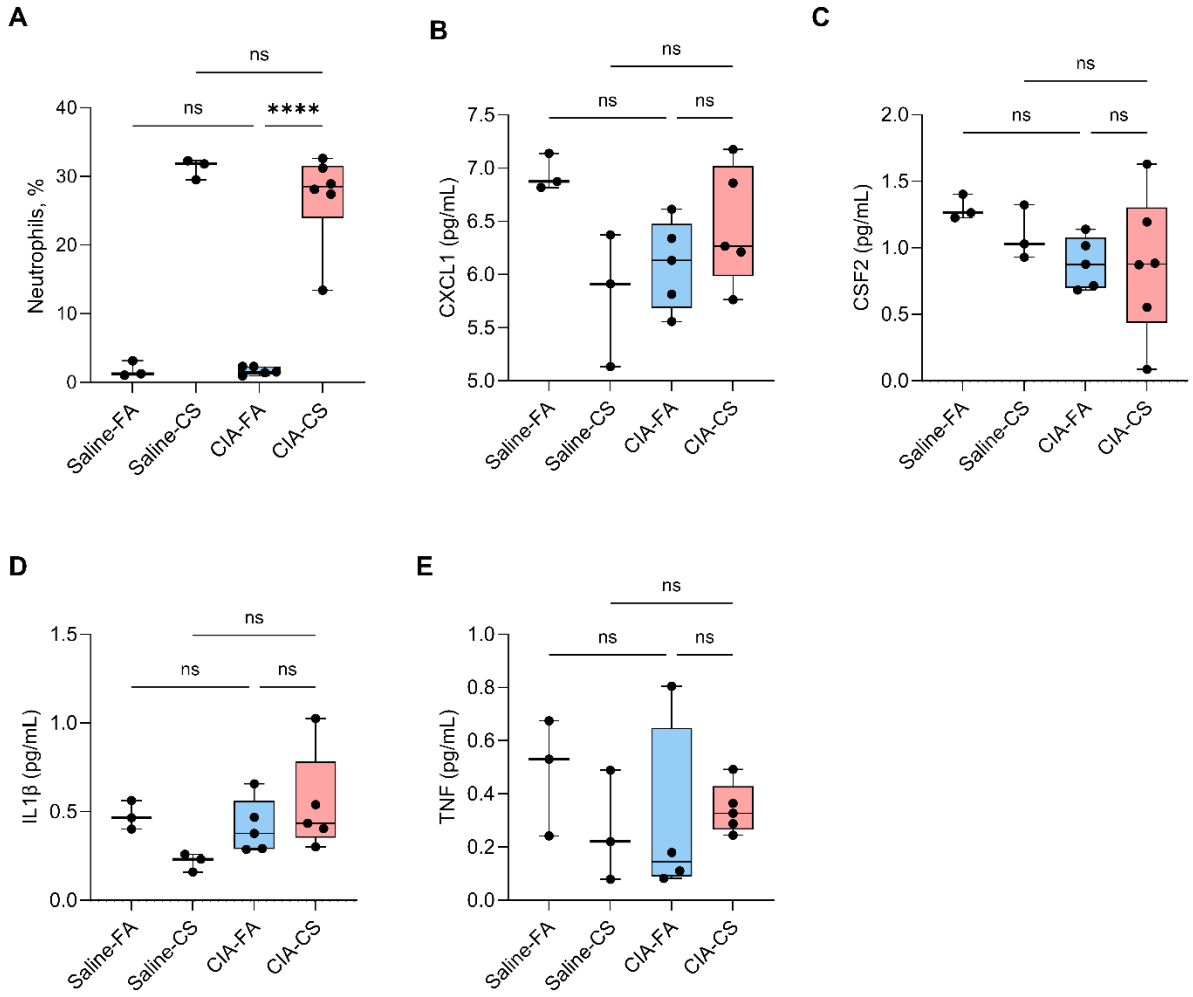

Figure 15: Neutrophil recruitment and neutrophil-related biomarkers in day 58 BALF (non-synchronized model)

(A) Percentage (%) of neutrophils (identified as Siglec-F−CD11c−CD11b+Ly6G+) in the BAL of different groups in the non-synchronized model. **(B-E)** CXCL1, CSF2, IL1β, and TNF levels in the BALF of different groups in the synchronized model as measured by Olink® Target 96 platform (Olink Biosciences). Bars show median and the whiskers show all points (n = 3/4/5/6). Data were analyzed using one-way ANOVA with Tukey's correction for multiple comparisons. ****, $p < 0.0001$; *ns*.

4.3.3 Neutrophil-associated Chemokines and Cytokines in the Serum at Various Time Points

The levels of CXCL1, CSF2, IL17a, IL1β, and TNF were comparable between the CIA-CS (n = 6) and CIA-FA (n = 6) groups on day 14 (**Figures 16A–E**). However, CXCL1, IL17a, and TNF levels were significantly higher ($p = 0.005$, $p = 0.02$, and $p < 0.0001$ respectively) in the CIA-CS group compared to the Saline-CS group (n = 3) on day 14 (**Figures 16A**, **16C**, and **16E**). The day 14 blood collection was intended to reflect the "pre-disease" or "induction" phase of collagen-induced arthritis in mice and to evaluate whether CS exposure had any notable impact during this early stage.

By day 58, CXCL1 levels in the CIA-CS group showed some variability, but there was no significant difference ($p = 0.99$) between the CIA-CS and CIA-FA groups (**Figure 16F**). Similarly, levels of CSF2, IL1β, and TNF remained statistically insignificant ($p = 0.99$, $p = 0.66$, and $p > 0.99$ respectively) between the CIA-CS and CIA-FA groups (**Figures 16G**, **16I**, and **16J**). While IL17a levels in the CIA-FA group displayed some variable values within the group (values ranging from 1.2 pg/mL to 2.3 pg/mL), they were not significantly elevated ($p = 0.5$) compared to the CIA-CS group (**Figure 16H**).

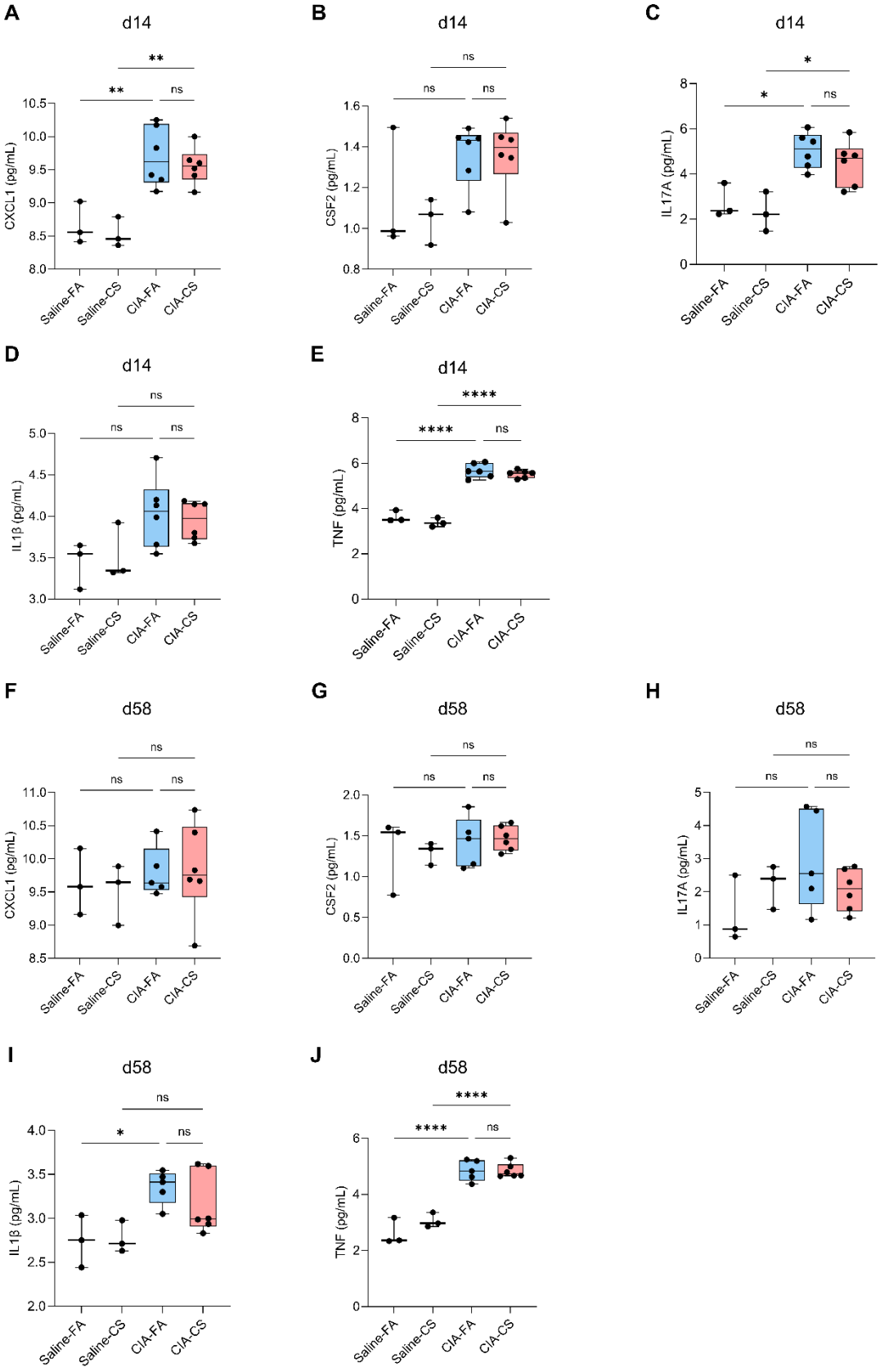
A
d14
CXCL1 (pg/mL)
B
d14
CSF2 (pg/mL)
C
d14
IL17A (pg/mL)
D
d14
IL1β (pg/mL)
E
d14
TNF (pg/mL)
F
d58
CXCL1 (pg/mL)
G
d58
CSF2 (pg/mL)
H
d58
IL17A (pg/mL)
I
d58
IL1β (pg/mL)
J
d58
TNF (pg/mL)
Saline-FA
Saline-CS
CIA-FA
CIA-CS
ns

Figure 16: Chemokines and cytokines in day 14 and day 58 serum samples (non-synchronized model)

(A-E) CXCL1, CSF2, IL17a, IL1β, and TNF levels in the day 14 serum from different groups in the non-synchronized model. **(F-J)** CXCL1, CSF2, IL17a, IL1β, and TNF levels in the day 58 serum from different groups in the non-synchronized model. Data quantified by Olink® Target 96 platform (Olink Biosciences). Bars show median and the whiskers show all points (n = 3/4/5/6). Data were analyzed using one-way ANOVA with Tukey's correction for multiple comparisons. *, $p < 0.05$; **, $p < 0.01$; ****, $p < 0.0001$; *ns*.

4.3.4 NE in BALF and Serum at Different Time Points

In this model, NE levels in the BALF were higher in the CIA-CS group (n = 6) compared to the CIA-FA (n = 5), although this did not reach statistical significance ($p = 0.99$) (**Figure 17C**). In the serum collected on both day 14 and day 58, NE levels were not significantly different ($p = 0.6$ and $p = 0.4$ respectively) between the two CIA groups. (**Figures 17A** and **14B**).

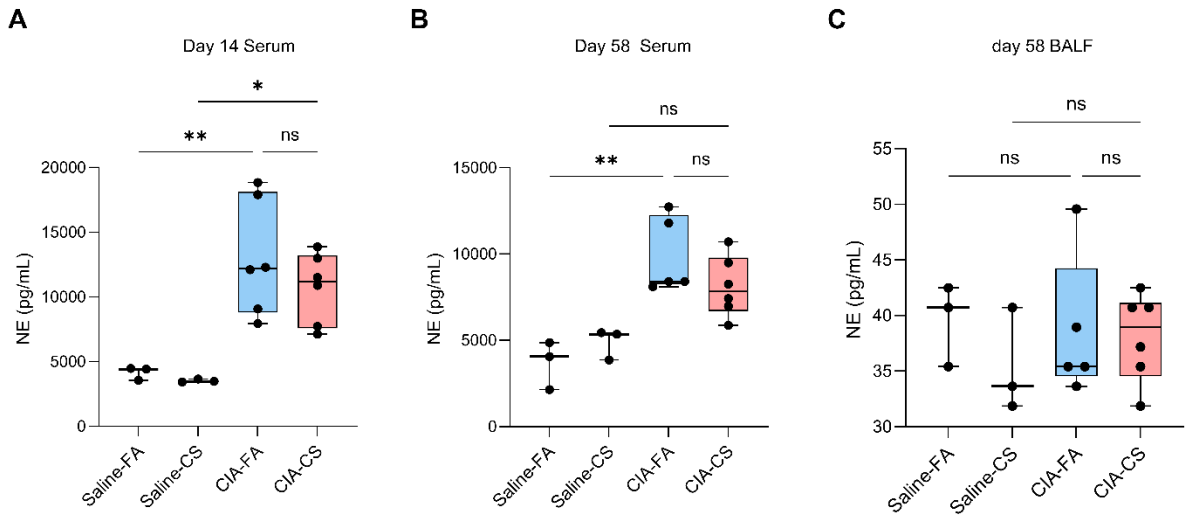

Figure 17: Neutrophil Elastase (NE) abundance in day 14, day 58 serums and day 58 BALF (non-synchronized model)

(A-C) Abundance of NE assessed in day 14, day 58 serums and day 58 BALF using Anti-NE ELISA. Bars show median and the whiskers show all points (n = 3/5/6). Data were analyzed using one-way ANOVA with Tukey's correction for multiple comparisons. *, $p < 0.05$; **, $p < 0.01$; *ns*.

4.3.5 Citrullination in the BALF

For the non-synchronized model's BALF samples, the CIA-CS group exhibited some variability in the intensity of bands around the 50–65 kDa and 10–15 kDa ranges (**Figure 18C**); however, the overall citrullination bands were more prominent compared to the CIA-FA group (**Figure 18A**). Consistent with the synchronized model, the Saline-FA group showed dense bands than the Saline-CS group, with prominent bands appearing in similar ranges as those observed in the CIA-CS group (**Figure 18A**).

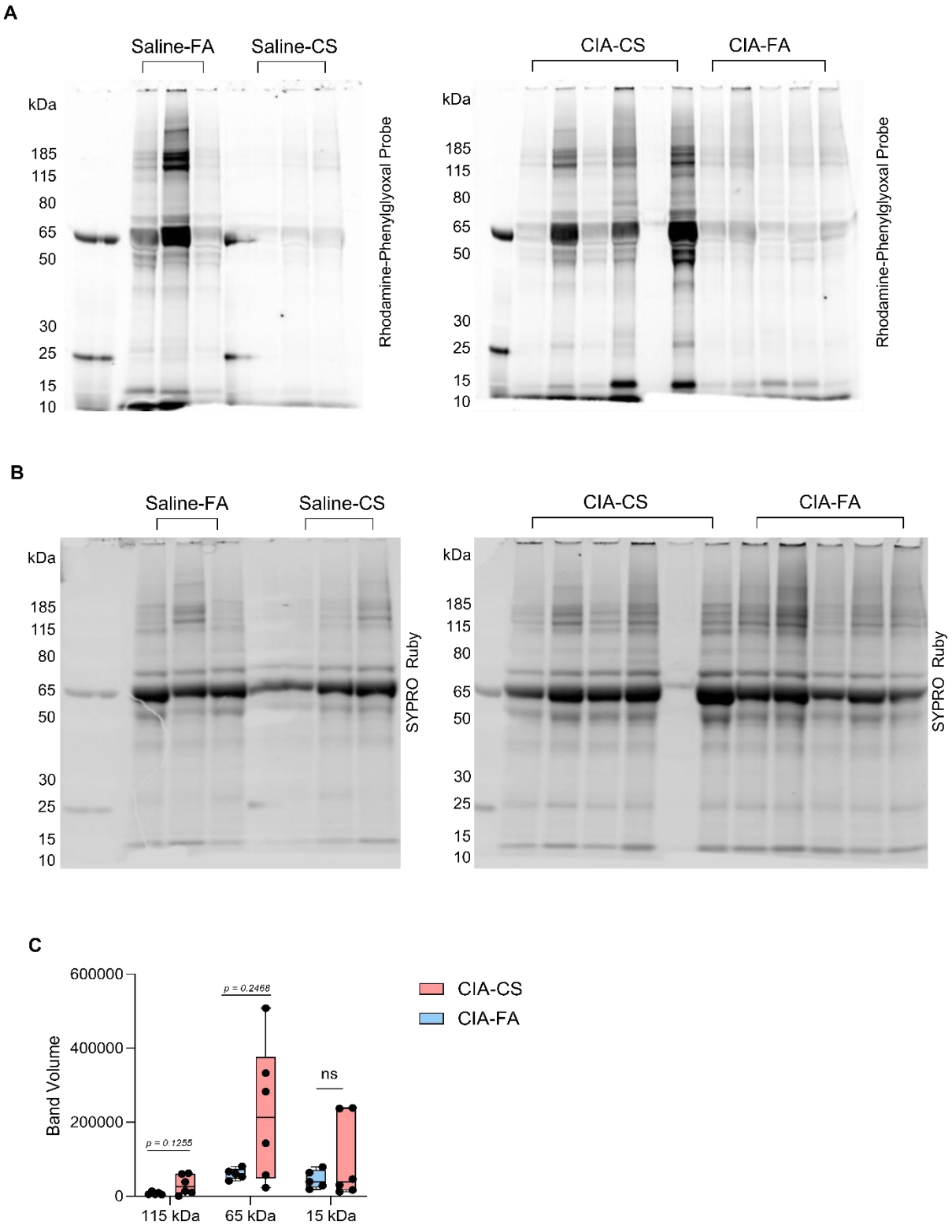

Figure 18: Citrullination in BALF (non-synchronized model)

(A) In-gel fluorescence images of BALF from all four groups using the Citrulline Phenylglyoxal-Rhodamine probe. **(B)** The corresponding gel stained with SYPRO™ Ruby to visualize overall protein content. **(C)** Band volume compared between CIA-CS and CIA-FA groups at 115 kDa, 65 kDa and 15 kDa.

Chapter 5: Discussion, Conclusions, and Limitations

5.1 Discussion

5.1.1 Effect of CSE on neutrophil functions in the presence or absence of foreign particles and potential mechanism of CSE-induced NETosis

This study revealed that the CSE medium does not directly trigger neutrophil degranulation yet promotes NETosis through the activation of PAD4. Many of the known stimuli to form NETs in neutrophils, such as PMA or Calcium Ionophore, also typically lead to degranulation. CSE is a complex medium with over 7,000 known chemicals.[190] CSE medium is passed through a 0.22 µm filter, particulate matter and any potential bacterial contaminants in the CSE are removed. As such, it is unlikely that this observation is due to a contaminating microbial stimulus. Interestingly, when IgG-coated latex beads or heat-killed *E. coli* were introduced in the presence of the CSE medium, neutrophils displayed robust phagocytic activity. These results indicate that while the CSE medium alone may not act as a trigger for degranulation, it does appear to enhance neutrophils' immune response in the presence of opsonized entities or foreign pathogens through robust phagocytosis and NET formation. This finding contrasts with previous published research, which has shown that total particulate matter (TPM) from cigarettes suppresses the bactericidal activity of neutrophils.[191] The best-characterized pathway of NETosis involves the activation of NADPH oxidase leading to ROS production, which in turn facilitates the nuclear translocation of NE and MPO, and in some cases, activation of PAD4. While CS contains reactive molecules such as nitric oxide (NO), nitrogen dioxide, oxygen free radicals, peroxynitrite, and ROS[192,193], these compounds are short-lived and decompose rapidly in aqueous environments. Thus, these are unlikely to cause NADPH oxidase activation *in vitro*. Instead, more stable chemical constituents of the CSE medium, such as acrolein and α, β-unsaturated aldehydes like crotonaldehyde (as reported in the certificate of analysis[194] of the 1R6F reference cigarette), are capable of activating NADPH oxidase.[195] This likely represents the initiating signal by which CSE induces NETosis. The observation that NETs form in response to CSE in the absence of external pathogens supports the concept of "frustrated phagocytosis," where neutrophils lacking viable targets respond to chemical stimuli by undergoing NETosis.[196]

Although some NETosis stimuli do not require PAD4 activation (e.g., *Candida albicans*, Group B *Streptococcus*, or cytosolic Gram-negative ligands[197]), this study observed that CSE-mediated NETosis is dependent on PAD4. Given that PAD4 is a calcium-dependent enzyme, it is likely that the CSE medium facilitates Ca^{2+} influx into neutrophils, leading to PAD4 activation.

Prior research has demonstrated that both CS and CSE can induce calcium entry through TRPA1 channels in primary human airway smooth muscle cells.[198] Since TRPA1 is also expressed on neutrophils[199] and functions as a broad chemo-sensor, it is plausible that its activation contributes to CSE-induced NETosis. Interestingly, TRPA1 can be activated by acrolein[200], nicotine[201], or low molecular weight organic matter such as acetaldehyde[202], all of which are present in the CSE medium. This suggests a potential mechanism where stable compounds like acrolein and crotonaldehyde activate NADPH oxidase to generate ROS, while acrolein, nicotine, and acetaldehyde stimulate TRPA1 channels to mediate Ca^{2+} influx, thereby activating PAD4. Together, these converge to induce PAD4-dependent NETosis in neutrophils exposed to CSE. An alternate possibility is that CSE medium may induce hypoxia-like conditions *in vitro.* Cigarette smoke exposure is known to reduce oxygen availability in tissue, leading to systemic hypoxia.[203,204] It is unclear if a similar microenvironment is replicated *in vitro* with CSE exposure or whether it impacts the degree of NETosis. Notably, hypoxia has been associated with both upregulation and suppression of NETosis in various contexts[205,206] suggesting a stimulus-dependent effect. Whether hypoxic conditions influence CSE-mediated NETosis warrants further investigation.

5.1.2 CS and neutrophils in the synchronized and non-synchronized CIA models

In the synchronized and non-synchronized CIA models, we observed that neutrophil infiltration was highest in the CIA-CS group. This suggests that prolonged CS exposure amplifies lung inflammation in inflammatory arthritis. We observed that the total neutrophil counts across the groups were elevated in the non-synchronized model, this may be due to prolonged CS exposure of 8 weeks as opposed to 4 weeks in the synchronized model. We also observed interesting differences between the two models, namely that neutrophil infiltration in the synchronized model's Saline-CS group was comparable to the neutrophil infiltration in the CIA-CS group of the non-synchronized model. It is notable that, the length of smoke exposure is different between the synchronized (4 weeks) and non-synchronized models (8 weeks). Acute model of CS exposure (1 hour twice per day) has been shown to induce neutrophil infiltration and upregulation of chemokines in mice lungs after only 3 consecutive days.[207] However, the comparatively longer duration of exposure in the non-synchronized model may impact the degree

of lung injury, which in turn may lead to elevated neutrophil retention. In the synchronized model, BALF collection was performed after a 4-week long exposure and approximately 19-20 hours after last smoke exposure, potentially allowing the transiently recruited neutrophils to return to the circulation. Based on our results, the 4-week exposure may not have been enough for neutrophil retention within the lungs. However, the increased chronicity of the exposure in the non-synchronized model may have led to longer and persistent vascular inflammation, as well as impaired clearance, thus enhancing neutrophils in the lungs. Interestingly, nicotine has been shown to prolong neutrophil survival by suppressing apoptosis[208] which may have caused the retention of neutrophils within the lungs independent of arthritis. Second, Chronic CS exposure can induce vascular damage, oxidative stress, and epithelial dysfunction.[209] All of these can promote neutrophil retention in the alveolar and perivascular spaces by upregulation of adhesion molecules such as ICAM-1. These findings suggest that the duration of CS exposure and the extent of neutrophil priming can have a critical influence on neutrophil dynamics in these models.

We also observed that within the BALF, CXCL1, CXCL2, CSF2, CSF3, IL-1α/β, and TNF which were elevated in the CIA-CS group across both models. CXCL1 and CXCL2 are chemokines secreted by the perivascular leukocytes to capture neutrophils.[210] CSF3 was specifically elevated in the CIA-CS group of the synchronized model and has a function of regulating neutrophil production, differentiation and functional activity at sites of inflammation.[210] CSF2 which was elevated in the CIA-CS group of the non-synchronized model has similar function as CSF3, especially in the context of severe inflammatory response when "emergency granulopoiesis" is required.[210] While IL-1α stimulates neutrophil migration by inducing CXCL1[211], IL-1β produced by neutrophils works in concert with CSF2 (G-CSF) downstream to augment neutrophil sustenance in the murine lung.[212] TNF is involved in regulating the actin skeleton to activate and prime neutrophils for the release of granular proteins in an inflammatory condition.[213] These results from the study support the elevated neutrophil infiltration in the lungs observed in both models. One interesting observation was the levels of the chemokine CCL4. In addition to its established role in inflammation, CCL4 binds to CCR5 on neutrophils and promotes a shift toward a $CCR5^{+}$ neutrophil phenotype, which has been reported in the literature to be pro-NETotic.[214] CCL4 levels were elevated in the CIA-CS group in both BALF and at both serum time points (pre- and post-LPS serum) in the synchronized model. Considering the increased neutrophil infiltration

and the potential presence of pro-NETotic CCR5^{+} neutrophils in the BALF, it is consistent that the CIA-CS group also exhibited the highest level of protein citrullination in the BALF samples.

In the synchronized model, NE abundance was significantly elevated in the CIA-CS group in both pre-LPS serum and BALF. However, this significance was no longer evident in the post-LPS serum collected at the study endpoint. Levels of mouse anti-collagen autoantibodies in the BALF or serum did not vary between CIA groups based on smoke exposure. It was notable that following the LPS injection on day 25, all mice began to exhibit joint swelling and disease symptoms. The onset of disease despite the absence of significantly increased mouse anti-collagen autoantibodies in the CIA-CS group, along with the elevated NE levels in BALF and in pre-LPS serum, suggests that CS exposure and CIA immunization may not exert an early synergistic effect. Instead, disease manifestation in this model may depend on the additional inflammatory stimulus provided by LPS. This interpretation is supported by observations from the non-synchronized model, where NE levels were not significantly elevated in any of the CIA groups, but mouse anti-collagen antibody levels were significantly higher in the BALF of CIA-CS mice, moderately elevated in day 14 serum, and lower again by day 58 (possibly reaching a plateau), implying that autoantibody production became systemic over time. However, in the absence of LPS-induced synchronization, disease incidence was variable between the CIA groups, with 83.33% of CIA-CS mice developing disease compared to only 33.33% in the CIA-FA group. This suggests that in the synchronized model, the interaction between CS exposure and collagen immunization contributed meaningfully to disease development, as others have shown.[171] No anti-collagen antibody differences were observed in the synchronized model, yet in the non-synchronized model, we observed markedly elevated antibodies in the BALF at day 58. This may indicate a delayed but important influx or local development of autoantibodies in the lungs without LPS administration, highlighting a possible mucosal site of immune activation in the CS-CIA group. Another notable observation is that in both models, disease symptoms appeared earlier in the CIA-FA group than in the CIA-CS group. This may be due to the effect of nicotine, which has been shown to delay the onset of collagen-induced arthritis in mice.[222]

It is worth noting that in the non-synchronized model, the incidence of inflammatory arthritis did not reach 100% in either of the CIA groups. It has been reported that with the DBA/1 strain, disease incidence can be as high as 80-100%.[225] However, only the synergy between the

CIA and CS exposure caused the 83.33% disease incidence in the CIA-CS group. Additionally, we observed that in the synchronized model that although all mice developed RA-like symptoms with swelling of the paws, joints, and digits, the highest total clinical score recorded for an individual mouse was 12, despite the maximum possible score being 16. While this reflects the findings of the present study, prior studies using the synchronized CIA model have reported mice reaching clinical scores as high as 15 at the study endpoint.[223,224] This outcome cannot be attributed to the delayed onset of arthritis caused by nicotine in CS as the same trend was observed in the CIA-FA group within the synchronized model. One plausible explanation may lie in the microenvironment of the animal housing facility. Although the mice were not housed under sterile conditions, it is well-established that housing conditions can influence the intestinal microenvironment. Notably, variations in gut microbiota composition have been linked to differential susceptibility to CIA in mice.[226–228] Therefore, repeating the experiment in a different facility and comparing disease outcomes could help determine whether the housing facility played a role in the overall lower clinical scores and disease incidence observed in this study.

Overall, the findings from this study indicate that CS plays a multifaceted role in enhancing neutrophil-mediated inflammation, NET formation, and citrullination during the development of RA-like symptoms in the CIA model. While previous studies have demonstrated that CS can induce lung neutrophilia by damaging airway epithelial cells[209], the precise mechanism by which CS triggers NET formation remains unclear. Recent evidence suggests that prolonged CS exposure can enhance neutrophil retention by promoting resistance to ferroptosis and inducing PAD4-dependent NET formation in the context of COPD.[229] Furthermore, factors such as exposure duration and the microbiome appear to influence the effects of CS in the CIA model. Collectively, data from both *in vitro* and *in vivo* experiments also highlight the contribution of cigarette smoke components, including AhR and nicotine, in modulating neutrophil functions.

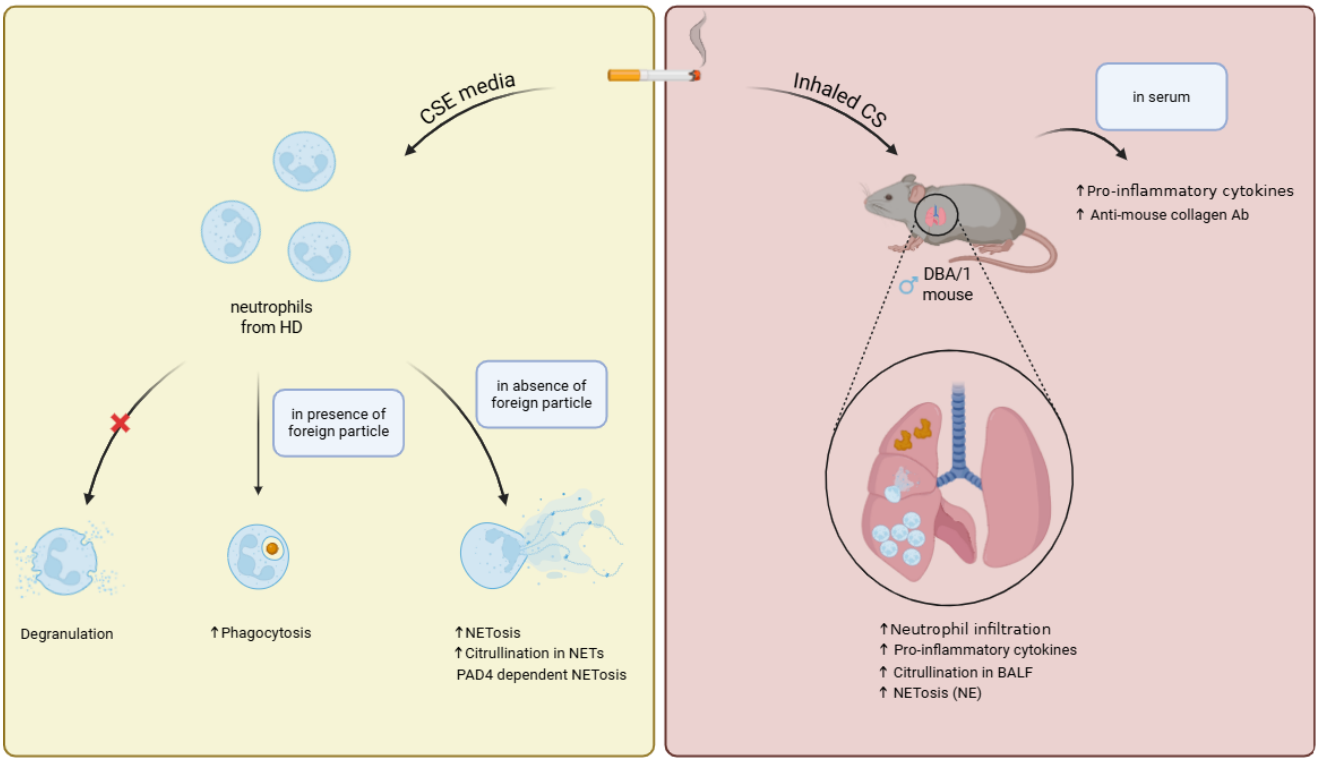

Figure 19: Graphic Summary of the Overall Results

Overall, the figure shows that *in vitro* CSE medium has effects on phagocytic and NETotic functions of neutrophils but not on degranulation and *in vivo* with CS exposure, there are increased neutrophil infiltration, inflammation, citrullination and NE in mice lungs while increased anti-mouse collagen antibodies and pro-inflammatory cytokines in serum. Image created with BioRender.com

5.2 Limitations

In this study, two different proteomic platforms were used: 48-plex panels for the synchronized model and a 96-plex panel for the non-synchronized model. As a result, we were unable to obtain paired data for several cytokines and chemokines that were absent from one panel or the other. This limitation may have prevented us from identifying important trends, such as the levels of CCL4 in the non-synchronized model. Although high levels of citrullination were detected in BALF samples, ACPA levels were not measured. Including this measurement could have added valuable insight, particularly given that only one study to date has assessed ACPA in the CS-CIA model.[230] Serum samples were collected on day 14 in the non-synchronized model and on day 23 in the synchronized model, making it challenging to directly compare cytokine levels, NE abundance, and mouse anti-collagen antibody responses between the two models, as the samples reflect different phases of disease progression. The day 14 time point was considered to possibly get further insights on the events that occur earlier in the CIA model when the experiment was repeated with the non-synchronized CIA model. Additionally, while comparisons were made between control groups (Saline-FA and Saline-CS) and CIA groups in the non-synchronized model, the small sample size of three mice per control group limits the reliability of these comparisons. Furthermore, sex disaggregation was not performed, as all mice used in both models were male, despite RA being approximately three times more prevalent in females than in males.[231] CSE medium used in the *in vitro* experiments and the CS exposure administered *in vivo* differ in chemical composition due to being in distinct phases (aqueous versus gaseous), which may complicate direct comparisons of their effects on neutrophils. In this study, a full-body smoking chamber was used for CS exposure. However, previous studies have shown that full-body exposure as opposed to nose-only exposure, can lead to increased lung inflammation.[232,233] It would therefore be valuable to investigate whether the mode of CS exposure has a significant impact on disease outcomes in the two CIA models.

Chapter 6: Future Directions

6.1 Elucidate the Potential Receptor of CSE component on Neutrophils that Induces NETosis

Although we demonstrate that CSE induces NETosis in neutrophils and propose potential components in the liquid phase that may act as triggers, the specific receptor(s) involved remain unidentified. It is known that neutrophils express aryl hydrocarbon receptors (AhR), which bind polycyclic aromatic hydrocarbons (PAHs), as well as nicotinic acetylcholine receptors (nAChRs), which interact with nicotine.[234,235] To determine whether these components in the CSE medium contribute to NET induction, future experiments could involve the use of AhR and nAChR antagonists. Additionally, whether these receptor-mediated effects are functionally relevant *in vivo* and influence disease outcomes could be explored using genetically modified mice deficient in genes encoding these receptors.

6.2 Mechanistic Studies of PAD Regulation with BB-Cl Amidine and a *PAD4* Deficient Mouse Model

In this study, we demonstrated the presence of NE and citrullinated proteins in the BALF along with elevated disease markers. However, the connection between NET formation and disease progression remains unclear. We have shown *in vitro* that CSE-induced NETosis is PAD4-dependent, and have observed lung citrullination in our preclinical model. Therefore, it would be appropriate to investigate how PAD4 inhibition impacts disease progression and whether NET formation plays a significant role in this process. The proposed experiment would involve oral administration of BB-Cl Amidine, following the experimental design outlined here. At the end of the study, clinical scores will be evaluated, and BALF will be analyzed for signs of pulmonary NET formation by measuring citH3-dsDNA complexes and total protein citrullination, as well as serum autoantibodies. Additionally, *PAD4*-deficient mice may be utilized to examine whether neutrophils or NETs contribute to disease development in the absence of PAD4.

6.3 Exploring Autoantibody Development Prior to Disease Manifestation

In the two models presented here, serum antibody levels were assessed at either the pre-LPS or day 14 time points, both of which represent phases prior to overt disease manifestation.

While the pre-LPS data in the synchronized model did not show a significant difference, in the non-synchronized model, day 14 serum autoantibody levels were significantly higher in the CIA-CS group compared to the CIA-FA group. However, antibody levels appeared to reach a plateau across groups by the end of the study. To better understand the kinetics of autoantibody development, it would be valuable to collect serum samples at multiple time points leading up to disease onset. This would help identify the earliest point at which autoantibodies begin to rise and when their levels stabilize and whether CS has any effect on the time and amount of autoantibody production. Additionally, given the observed citrullination within the lungs, it would be beneficial to check the ACPA levels.

6.4 Increase the Power of Analyses

Some of the analyses done here are underpowered (e.g. only 3 mice per control group in the non-synchronized model) and therefore need to be repeated to validate the findings from this study.

References

1. Scott DL, Wolfe F, Huizinga TWJ. Rheumatoid arthritis. *The Lancet*. 2010;376(9746):1094-1108. doi:10.1016/S0140-6736(10)60826-4/ASSET/FAFD7FCF-EE7B-4501-8F1B-02D05E110E3F/MAIN.ASSETS/GR4.JPG

2. Allan Gibofsky MJ. Epidemiology, Pathophysiology, and Diagnosis of Rheumatoid Arthritis: A Synopsis. 2014;20. Accessed May 14, 2025. https://www.ajmc.com/view/ace017_may14_ra-ce_gibofsky1_s128

3. Smolen JS, Aletaha D, McInnes IB. Rheumatoid arthritis. *The Lancet*. 2016;388(10055):2023-2038. doi:10.1016/S0140-6736(16)30173-8/ASSET/89E9F798-6386-4907-B9B3-A77319A4E1F3/MAIN.ASSETS/GR3.JPG

4. Catrina AI, Deane KD, Scher JU. Gene, environment, microbiome and mucosal immune tolerance in rheumatoid arthritis. *Rheumatology (Oxford)*. 2014;55(3):391. doi:10.1093/RHEUMATOLOGY/KEU469

5. Karlson EW, Deane K. Environmental and Gene-Environment Interactions and Risk of Rheumatoid Arthritis. *Rheumatic Disease Clinics of North America*. 2012;38(2):405-426. doi:10.1016/J.RDC.2012.04.002

6. Fresneda Alarcon M, McLaren Z, Wright HL. Neutrophils in the Pathogenesis of Rheumatoid Arthritis and Systemic Lupus Erythematosus: Same Foe Different M.O. *Front Immunol*. 2021;12:649693. doi:10.3389/FIMMU.2021.649693/XML/NLM

7. Edilova MI, Akram A, Abdul-Sater AA. Innate immunity drives pathogenesis of rheumatoid arthritis. *Biomed J*. 2020;44(2):172. doi:10.1016/J.BJ.2020.06.010

8. McInnes IB, Buckley CD, Isaacs JD. Cytokines in rheumatoid arthritis-shaping the immunological landscape. *Nat Rev Rheumatol*. 2016;12(1):63-68. doi:10.1038/NRRHEUM.2015.171;SUBJMETA=1670,256,2780,420,692,699;KWRD=IMMUNOPATHOGENESIS,INFLAMMATION,RHEUMATIC+DISEASES

9. Saferding V, Blüml S. Innate immunity as the trigger of systemic autoimmune diseases. *J Autoimmun*. 2020;110:102382. doi:10.1016/J.JAUT.2019.102382

10. Cecchi I, Arias de la Rosa I, Menegatti E, et al. Neutrophils: Novel key players in Rheumatoid Arthritis. Current and future therapeutic targets. *Autoimmun Rev*. 2018;17(11):1138-1149. doi:10.1016/J.AUTREV.2018.06.006

11. Cedergren J, Forslund T, Sundqvist T, Skogh T. Intracellular oxidative activation in synovial fluid neutrophils from patients with rheumatoid arthritis but not from other arthritis patients. *J Rheumatol*. 2007;34(11).

12. Liu X, Arfman T, Wichapong K, Reutelingsperger CPM, Voorberg J, Nicolaes GAF. PAD4 takes charge during neutrophil activation: Impact of PAD4 mediated NET formation on immune-mediated disease. *Journal of Thrombosis and Haemostasis*. 2021;19(7):1607. doi:10.1111/JTH.15313

13. Vossenaar ER, Nijenhuis S, Helsen MMA, et al. Citrullination of synovial proteins in murine models of rheumatoid arthritis. *Arthritis Rheum*. 2003;48(9):2489-2500. doi:10.1002/ART.11229

14. Suzuki A, Kochi Y, Shoda H, et al. Decreased severity of experimental autoimmune arthritis in peptidylarginine deiminase type 4 knockout mice. *BMC Musculoskelet Disord*. 2016;17(1):1-15. doi:10.1186/S12891-016-1055-2/FIGURES/7

15. Goldbach-Mansky R, Suson S, Wesley R, Hack CE, El-Gabalawy HS, Tak PP. Raised granzyme B levels are associated with erosions in patients with early rheumatoid factor positive rheumatoid arthritis. *Ann Rheum Dis*. 2005;64(5):715-721. doi:10.1136/ARD.2003.007039/ASSET/900FCF1B-F18F-44FD-BC22-1750966762DC/MAIN.ASSETS/GR2.JPG

16. Dalbeth N, Gundle R, Davies RJO, Lee YCG, McMichael AJ, Callan MFC. CD56bright NK Cells Are Enriched at Inflammatory Sites and Can Engage with Monocytes in a Reciprocal Program of Activation. *The Journal of Immunology*. 2004;173(10):6418-6426. doi:10.4049/JIMMUNOL.173.10.6418

17. Rodríguez-Carrio J, Hähnlein JS, Ramwadhdoebe TH, et al. Brief Report: Altered Innate Lymphoid Cell Subsets in Human Lymph Node Biopsy Specimens Obtained During the At-Risk and Earliest Phases of Rheumatoid Arthritis. *Arthritis and Rheumatology*. 2017;69(1):70-76. doi:10.1002/ART.39811;JOURNAL:JOURNAL:15290131;WGROUP:STRING:PUBLICATION

18. Takaki-Kuwahara A, Arinobu Y, Miyawaki K, et al. CCR6+ group 3 innate lymphoid cells accumulate in inflamed joints in rheumatoid arthritis and produce Th17 cytokines. *Arthritis Res Ther*. 2019;21(1):1-9. doi:10.1186/S13075-019-1984-X/FIGURES/5

19. Rauber S, Luber M, Weber S, et al. Resolution of inflammation by interleukin-9-producing type 2 innate lymphoid cells. *Nature Medicine 2017 23:8*. 2017;23(8):938-944. doi:10.1038/nm.4373

20. Luo P, Wang P, Xu J, et al. Immunomodulatory role of T helper cells in rheumatoid arthritis: a comprehensive research review. *Bone Joint Res*. 2022;11(7):426. doi:10.1302/2046-3758.117.BJR-2021-0594.R1

21. Zwerina J, Hayer S, Tohidast-Akrad M, et al. Single and Combined Inhibition of Tumor Necrosis Factor, Interleukin-1, and RANKL Pathways in Tumor Necrosis Factor-Induced Arthritis: Effects on Synovial Inflammation, Bone Erosion, and Cartilage Destruction. *Arthritis Rheum*. 2004;50(1):277-290. doi:10.1002/ART.11487;JOURNAL:JOURNAL:15290131;REQUESTEDJOURNAL:JOURNAL:15290131;WGROUP:STRING:PUBLICATION

22. Ikeuchi H, Kuroiwa T, Hiramatsu N, et al. Expression of interleukin-22 in rheumatoid arthritis: Potential role as a proinflammatory cytokine. *Arthritis Rheum*. 2005;52(4):1037-1046. doi:10.1002/ART.20965;PAGEGROUP:STRING:PUBLICATION

23. Wu F, Gao J, Kang J, et al. B Cells in Rheumatoid Arthritis：Pathogenic Mechanisms and Treatment Prospects. *Front Immunol*. 2021;12:750753. doi:10.3389/FIMMU.2021.750753

24. Panayi G. B cells: a fundamental role in the pathogenesis of rheumatoid arthritis? *Rheumatology*. 2005;44(suppl_2):ii3-ii7. doi:10.1093/RHEUMATOLOGY/KEH616

25. Volkov M, van Schie KA, van der Woude D. Autoantibodies and B Cells: The ABC of rheumatoid arthritis pathophysiology. *Immunol Rev*. 2019;294(1):148. doi:10.1111/IMR.12829

26. Yanaba K, Bouaziz JD, Haas KM, Poe JC, Fujimoto M, Tedder TF. A Regulatory B Cell Subset with a Unique CD1dhiCD5+ Phenotype Controls T Cell-Dependent Inflammatory Responses. *Immunity*. 2008;28(5):639-650. doi:10.1016/j.immuni.2008.03.017

27. MacGregor AJ, Snieder H, Rigby AS, et al. Characterizing the quantitative genetic contribution to rheumatoid arthritis using data from twins. *Arthritis Rheum*. 2000;43(1):30-37. doi:10.1002/1529-0131(200001)43:1<30::AID-ANR5>3.0.CO;2-B

28. Kurkó J, Besenyei T, Laki J, Glant TT, Mikecz K, Szekanecz Z. Genetics of Rheumatoid Arthritis — A Comprehensive Review. *Clin Rev Allergy Immunol*. 2013;45(2):170. doi:10.1007/S12016-012-8346-7

29. Gregersen PK, Silver J, Winchester RJ. The shared epitope hypothesis. an approach to understanding the molecular genetics of susceptibility to rheumatoid arthritis. *Arthritis Rheum*. 1987;30(11):1205-1213. doi:10.1002/ART.1780301102

30. Wagner U, Kaltenhäuser S, Pierer M, et al. Prospective analysis of the impact of HLA-DR and -DQ on joint destruction in recent-onset rheumatoid arthritis. *Rheumatology*. 2003;42(4):553-562. doi:10.1093/RHEUMATOLOGY/KEG190

31. Farragher TM, Goodson NJ, Naseem H, et al. Association of the HLA-DRB1 gene with premature death, particularly from cardiovascular disease, in patients with rheumatoid arthritis and inflammatory polyarthritis. *Arthritis Rheum*. 2008;58(2):359-369. doi:10.1002/ART.23149;JOURNAL:JOURNAL:15290131;REQUESTEDJOURNAL:JOURNAL:15290131;WGROUP:STRING:PUBLICATION

32. HLA-DRB1*0401/0404 genotype and rheumatoid arthritis: increased association in men, young age at onset, and disease severity. - Abstract - Europe PMC. Accessed May 19, 2025. https://europepmc.org/article/med/7674226

33. Gonzalez-Gay MA, Hajeer AH, Dababneh A, et al. Seronegative rheumatoid arthritis in elderly and polymyalgia rheumatica have similar patterns of HLA association. *J Rheumatol*. 2001;28(1).

34. Raychaudhuri S, Sandor C, Stahl EA, et al. Five amino acids in three HLA proteins explain most of the association between MHC and seropositive rheumatoid arthritis. *Nature Genetics 2012 44:3*. 2012;44(3):291-296. doi:10.1038/ng.1076

35. Han B, Diogo D, Eyre S, et al. Fine Mapping Seronegative and Seropositive Rheumatoid Arthritis to Shared and Distinct HLA Alleles by Adjusting for the Effects of Heterogeneity. *The American Journal of Human Genetics*. 2014;94(4):522-532. doi:10.1016/J.AJHG.2014.02.013

36. Stanford SM, Mustelin TM, Bottini N. Lymphoid tyrosine phosphatase and autoimmunity: human genetics rediscovers tyrosine phosphatases. *Semin Immunopathol*. 2010;32(2):127. doi:10.1007/S00281-010-0201-4

37. Begovich AB, Carlton VEH, Honigberg LA, et al. A missense single-nucleotide polymorphism in a gene encoding a protein tyrosine phosphatase (PTPN22) is associated with rheumatoid arthritis. *Am J Hum Genet*. 2004;75(2):330-337. doi:10.1086/422827

38. Bagheri-Hosseinabadi Z, Mirzaei MR, Esmaeili O, et al. Implications of Peptidyl Arginine Deiminase 4 gene transcription and polymorphisms in susceptibility to rheumatoid arthritis in an Iranian population. *BMC Med Genomics*. 2023;16(1):1-8. doi:10.1186/S12920-023-01532-9/TABLES/5

39. Ishigaki K, Sakaue S, Terao C, et al. Multi-ancestry genome-wide association analyses identify novel genetic mechanisms in rheumatoid arthritis. *Nat Genet*. 2022;54(11):1640-1651. doi:10.1038/S41588-022-01213-W;SUBJMETA=191,2018,205,208,2138,631;KWRD=GENE+EXPRESSION+PROFILING,GENOME-WIDE+ASSOCIATION+STUDIES

40. Sugiyama D, Nishimura K, Tamaki K, et al. Impact of smoking as a risk factor for developing rheumatoid arthritis: A meta-analysis of observational studies. *Ann Rheum Dis*. 2010;69(1):70-81. doi:10.1136/ARD.2008.096487/ASSET/BD00C085-D6AD-4FEC-A316-EF8E42895E5B/MAIN.ASSETS/GR4C.JPG

41. Di Giuseppe D, Discacciati A, Orsini N, Wolk A. Cigarette smoking and risk of rheumatoid arthritis: A dose-response meta-analysis. *Arthritis Res Ther*. 2014;16(2):1-7. doi:10.1186/AR4498/FIGURES/3

42. Hedström AK, Rönnelid J, Klareskog L, Alfredsson L. Complex Relationships of Smoking, HLA–DRB1 Genes, and Serologic Profiles in Patients With Early Rheumatoid Arthritis: Update From a Swedish Population-Based Case–Control Study. *Arthritis and Rheumatology*. 2019;71(9):1504-1511. doi:10.1002/ART.40852,

43. Wrangel O, Graff P, Bryngelsson IL, Fornander L, Wiebert P, Vihlborg P. Silica Dust Exposure Increases Risk for Rheumatoid Arthritis A Swedish National Registry Case–Control Study. *J Occup Environ Med*. 2021;63(11):951-955. doi:10.1097/JOM.0000000000002281,

44. Castranova V. Signaling pathways controlling the production of inflammatory mediators in response to crystalline silica exposure: Role of reactive oxygen/nitrogen species. *Free Radic Biol Med*. 2004;37(7):916-925. doi:10.1016/j.freeradbiomed.2004.05.032

45. Cassel SL, Eisenbarth SC, Iyer SS, et al. The Nalp3 inflammasome is essential for the development of silicosis. *Proc Natl Acad Sci U S A*. 2008;105(26):9035-9040. doi:10.1073/PNAS.0803933105/ASSET/51E411DD-847F-4578-B8C0-5ED5D0394147/ASSETS/GRAPHIC/ZPQ9990837210004.JPEG

46. Rizzi M, Carniato F, Tonello S, et al. Charged molecular silica trigger in vitro NETosis in human granulocytes via both oxidative and autophagic pathways. *Eur Rev Med Pharmacol Sci*. 2018;22(20):7058-7068. doi:10.26355/EURREV_201810_16178

47. Prisco LC, Martin LW, Sparks JA. Inhalants other than personal cigarette smoking and risk for developing rheumatoid arthritis. *Curr Opin Rheumatol*. 2020;32(3):279. doi:10.1097/BOR.0000000000000705

48. Cheng Z, Do T, Mankia K, et al. Dysbiosis in the oral microbiomes of anti-CCP positive individuals at risk of developing rheumatoid arthritis. *Ann Rheum Dis*. 2021;80(2):162-168. doi:10.1136/ANNRHEUMDIS-2020-216972,

49. Mankia K, Cheng Z, Do T, et al. Prevalence of Periodontal Disease and Periodontopathic Bacteria in Anti-Cyclic Citrullinated Protein Antibody-Positive At-Risk Adults Without Arthritis. *JAMA Netw Open*. 2019;2(6):e195394. doi:10.1001/JAMANETWORKOPEN.2019.5394,

50. Wegner N, Wait R, Sroka A, et al. Peptidylarginine deiminase from Porphyromonas gingivalis citrullinates human fibrinogen and α-enolase: Implications for autoimmunity in rheumatoid Arthritis. *Arthritis Rheum*. 2010;62(9):2662-2672. doi:10.1002/ART.27552,

51. Brewer RC, Lanz T V., Hale CR, et al. Oral mucosal breaks trigger anti-citrullinated bacterial and human protein antibody responses in rheumatoid arthritis. *Sci Transl Med*. 2023;15(684). doi:10.1126/SCITRANSLMED.ABQ8476,

52. van Delft MAM, Huizinga TWJ. An overview of autoantibodies in rheumatoid arthritis. *J Autoimmun*. 2020;110:102392. doi:10.1016/J.JAUT.2019.102392

53. Moura RA, Graca L, Fonseca JE. To B or Not to B the Conductor of Rheumatoid Arthritis Orchestra. *Clinical Reviews in Allergy & Immunology 2012 43:3*. 2012;43(3):281-291. doi:10.1007/S12016-012-8318-Y

54. Ingegnoli F, Castelli R, Gualtierotti R. Rheumatoid Factors: Clinical Applications. *Dis Markers*. 2013;35(6):727-734. doi:10.1155/2013/726598

55. de Brito Rocha S, Baldo DC, Andrade LEC. Clinical and pathophysiologic relevance of autoantibodies in rheumatoid arthritis. *Adv Rheumatol*. 2019;59(1):2. doi:10.1186/S42358-018-0042-8/FIGURES/5

56. Edwards JCW, Cambridge G. Rheumatoid arthritis: the predictable effect of small immune complexes in which antibody is also antigen. *Br J Rheumatol*. 1998;37(2):126-130. doi:10.1093/RHEUMATOLOGY/37.2.126

57. Song YW, Kang EH. Autoantibodies in rheumatoid arthritis: rheumatoid factors and anticitrullinated protein antibodies. *QJM: An International Journal of Medicine*. 2010;103(3):139-146. doi:10.1093/QJMED/HCP165

58. Maibom-Thomsen SL, Trier NH, Holm BE, et al. Immunoglobulin G structure and rheumatoid factor epitopes. *PLoS One*. 2019;14(6):e0217624. doi:10.1371/JOURNAL.PONE.0217624

59. Jónsson T, Arinbjarnarson S, Thorsteinsson J, et al. Raised IgA Rheumatoid Factor (RF) but not IgM RF or IgG RF is Associated with Extra-articular Manifestations in Rheumatoid Arthritis. *Scand J Rheumatol*. 1995;24(6):372-375. doi:10.3109/03009749509095183

60. Sokolove J, Johnson DS, Lahey LJ, et al. Rheumatoid factor as a potentiator of anti-citrullinated protein antibody-mediated inflammation in rheumatoid arthritis. *Arthritis and Rheumatology*. 2014;66(4):813-821. doi:10.1002/ART.38307;WEBSITE:WEBSITE:ACRJOURNALS;JOURNAL:JOURNAL:15290131;WGROUP:STRING:PUBLICATION

61. Rantapää-Dahlqvist S, De Jong BAW, Berglin E, et al. Antibodies Against Cyclic Citrullinated Peptide and IgA Rheumatoid Factor Predict the Development of Rheumatoid Arthritis. *Arthritis Rheum*. 2003;48(10):2741-2749. doi:10.1002/ART.11223;JOURNAL:JOURNAL:15290131;REQUESTEDJOURNAL:JOURNAL:15290131;WGROUP:STRING:PUBLICATION

62. Van De Stadt LA, De Koning MHMT, Van De Stadt RJ, et al. Development of the anti-citrullinated protein antibody repertoire prior to the onset of rheumatoid arthritis. *Arthritis Rheum*. 2011;63(11):3226-3233. doi:10.1002/ART.30537;PAGE:STRING:ARTICLE/CHAPTER

63. Jørgensen KT, Wiik A, Pedersen M, et al. Cytokines, autoantibodies and viral antibodies in premorbid and postdiagnostic sera from patients with rheumatoid arthritis: Case-control study nested in a cohort of Norwegian blood donors. *Ann Rheum Dis*. 2008;67(6):860-866. doi:10.1136/ARD.2007.073825/ASSET/91746182-A7CC-4FB0-8E56-3FAD98365D11/MAIN.ASSETS/GR1.JPG

64. Nielen MMJ, Van Schaardenburg D, Reesink HW, et al. Specific Autoantibodies Precede the Symptoms of Rheumatoid Arthritis: A Study of Serial Measurements in Blood Donors. *Arthritis Rheum*. 2004;50(2):380-386. doi:10.1002/ART.20018;REQUESTEDJOURNAL:JOURNAL:15290131;WGROUP:STRING:PUBLICATION

65. Rantapää-Dahlqvist S, De Jong BAW, Berglin E, et al. Antibodies Against Cyclic Citrullinated Peptide and IgA Rheumatoid Factor Predict the Development of Rheumatoid Arthritis. *Arthritis Rheum*. 2003;48(10):2741-2749. doi:10.1002/ART.11223;JOURNAL:JOURNAL:15290131;REQUESTEDJOURNAL:JOURNAL:15290131;WGROUP:STRING:PUBLICATION

66. Kim Y, Kim GT. Positive Effects of Biologics on Osteoporosis in Rheumatoid Arthritis. *Journal of Rheumatic Diseases*. 2023;30(1):3-17. doi:10.4078/JRD.22.0046

67. Bugatti S, Bogliolo L, Vitolo B, Manzo A, Montecucco C, Caporali R. Anti-citrullinated protein antibodies and high levels of rheumatoid factor are associated with systemic bone loss in patients with early untreated rheumatoid arthritis. *Arthritis Res Ther*. 2016;18(1). doi:10.1186/S13075-016-1116-9,

68. Harre U, Georgess D, Bang H, et al. Induction of osteoclastogenesis and bone loss by human autoantibodies against citrullinated vimentin. *J Clin Invest*. 2012;122(5):1791-1802. doi:10.1172/JCI60975

69. Laria A, Lurati A, Marrazza M, Mazzocchi D, Re KA, Scarpellini M. The macrophages in rheumatic diseases. *J Inflamm Res*. 2016;9:1-11. doi:10.2147/JIR.S82320,

70. Kurowska W, Slowinska I, Krogulec Z, Syrowka P, Maslinski W. Antibodies to citrullinated proteins (Acpa) associate with markers of osteoclast activation and bone destruction in the bone marrow of patients with rheumatoid arthritis. *J Clin Med*. 2021;10(8). doi:10.3390/JCM10081778,

71. Schellekens GA, De Jong BAW, Van Den Hoogen FHJ, Van De Putte LBA, Van Venrooij WJ. Citrulline is an essential constituent of antigenic determinants recognized by rheumatoid arthritis-specific autoantibodies. *Journal of Clinical Investigation*. 1998;101(1):273-281. doi:10.1172/JCI1316

72. Takizawa Y, Suzuki A, Sawada T, et al. Citrullinated fibrinogen detected as a soluble citrullinated autoantigen in rheumatoid arthritis synovial fluids. *Ann Rheum Dis*. 2006;65(8):1013-1020. doi:10.1136/ARD.2005.044743

73. Vossenaar ER, Després N, Lapointe E, et al. Rheumatoid arthritis specific anti-Sa antibodies target citrullinated vimentin. *Arthritis Res Ther*. 2004;6(2):R142. doi:10.1186/ar1149

74. Lundberg K, Kinloch A, Fisher BA, et al. Antibodies to citrullinated α-enolase peptide 1 are specific for rheumatoid arthritis and cross-react with bacterial enolase. *Arthritis Rheum*. 2008;58(10):3009-3019. doi:10.1002/ART.23936;PAGEGROUP:STRING:PUBLICATION

75. Khandpur R, Carmona-Rivera C, Vivekanandan-Giri A, et al. NETs are a source of citrullinated autoantigens and stimulate inflammatory responses in rheumatoid arthritis. *Sci Transl Med*. 2013;5(178). doi:10.1126/SCITRANSLMED.3005580,

76. Sokolove J, Zhao X, Chandra PE, Robinson WH. Immune complexes containing citrullinated fibrinogen costimulate macrophages via toll-like receptor 4 and Fcγ receptor. *Arthritis Rheum*. 2011;63(1):53-62. doi:10.1002/ART.30081,

77. Clavel C, Nogueira L, Laurent L, et al. Induction of macrophage secretion of tumor necrosis factor α through Fcγ receptor IIa engagement by rheumatoid arthritis-specific autoantibodies to citrullinated proteins complexed with fibrinogen. *Arthritis Rheum*. 2008;58(3):678-688. doi:10.1002/ART.23284,

78. Song W, Ye J, Pan N, Tan C, Herrmann M. Neutrophil Extracellular Traps Tied to Rheumatoid Arthritis: Points to Ponder. *Front Immunol*. 2021;11. doi:10.3389/FIMMU.2020.578129,

79. Ohmi Y, Ise W, Harazono A, et al. Sialylation converts arthritogenic IgG into inhibitors of collagen-induced arthritis. *Nat Commun*. 2016;7. doi:10.1038/NCOMMS11205,

80. Clavel C, Nogueira L, Laurent L, et al. Induction of macrophage secretion of tumor necrosis factor α through Fcγ receptor IIa engagement by rheumatoid arthritis–specific autoantibodies to citrullinated proteins complexed with fibrinogen. *Arthritis Rheum*. 2008;58(3):678-688. doi:10.1002/ART.23284

81. Kidd BA, Ho PP, Sharpe O, et al. Epitope spreading to citrullinated antigens in mouse models of autoimmune arthritis and demyelination. *Arthritis Res Ther*. 2008;10(5):1-12. doi:10.1186/AR2523/TABLES/2

82. Kuhn KA, Kulik L, Tomooka B, et al. Antibodies against citrullinated proteins enhance tissue injury in experimental autoimmune arthritis. *J Clin Invest*. 2006;116(4):961-973. doi:10.1172/JCI25422

83. Hashimoto M. Th17 in Animal Models of Rheumatoid Arthritis. *J Clin Med*. 2017;6(7):73. doi:10.3390/JCM6070073

84. Shi J, van Veelen PA, Mahler M, et al. Carbamylation and antibodies against carbamylated proteins in autoimmunity and other pathologies. *Autoimmun Rev*. 2014;13(3):225-230. doi:10.1016/J.AUTREV.2013.10.008

85. Verheul MK, Van Erp SJH, Van Der Woude D, et al. Anti-carbamylated protein antibodies: a specific hallmark for rheumatoid arthritis. Comparison to conditions known for enhanced carbamylation; renal failure, smoking and chronic inflammation. *Ann Rheum Dis*. 2016;75(8):1575-1576. doi:10.1136/ANNRHEUMDIS-2016-209248

86. van Delft MAM, Verheul MK, Burgers LE, et al. The isotype and IgG subclass distribution of anti-carbamylated protein antibodies in rheumatoid arthritis patients. *Arthritis Res Ther*. 2017;19(1):1-12. doi:10.1186/S13075-017-1392-Z/TABLES/3

87. Shi J, Knevel R, Suwannalai P, et al. Autoantibodies recognizing carbamylated proteins are present in sera of patients with rheumatoid arthritis and predict joint damage. *Proc*

Natl Acad Sci U S A. 2011;108(42):17372-17377. doi:10.1073/PNAS.1114465108/SUPPL_FILE/PNAS.201114465SI.PDF

88. Ajeganova S, Van Steenbergen HW, Verheul MK, et al. The association between anti-carbamylated protein (anti-CarP) antibodies and radiographic progression in early rheumatoid arthritis: a study exploring replication and the added value to ACPA and rheumatoid factor. *Ann Rheum Dis*. 2017;76(1):112-118. doi:10.1136/ANNRHEUMDIS-2015-208870

89. Brink M, Verheul MK, Rönnelid J, et al. Anti-carbamylated protein antibodies in the pre-symptomatic phase of rheumatoid arthritis, their relationship with multiple anti-citrulline peptide antibodies and association with radiological damage. *Arthritis Res Ther*. 2015;17(1):25. doi:10.1186/s13075-015-0536-2

90. Tigner A, Ibrahim SA, Murray I V. Histology, White Blood Cell. *StatPearls*. Published online November 14, 2022. Accessed May 21, 2025. https://www.ncbi.nlm.nih.gov/books/NBK563148/

91. Rowat AC, Jaalouk DE, Zwerger M, et al. Nuclear envelope composition determines the ability of neutrophil-type cells to passage through micron-scale constrictions. *Journal of Biological Chemistry*. 2013;288(12):8610-8618. doi:10.1074/JBC.M112.441535/ATTACHMENT/90A981A0-E63A-4E44-AAAA-47BB328BE873/MMC1.PDF

92. Olins AL, Zwerger M, Herrmann H, et al. The human granulocyte nucleus: Unusual nuclear envelope and heterochromatin composition. *Eur J Cell Biol*. 2008;87(5):279-290. doi:10.1016/J.EJCB.2008.02.007

93. Torres M, Coates TD. Function of the cytoskeleton in human neutrophils and methods for evaluation. *J Immunol Methods*. 1999;232(1-2):89-109. doi:10.1016/S0022-1759(99)00168-4

94. Othman A, Sekheri M, Filep JG. Roles of neutrophil granule proteins in orchestrating inflammation and immunity. *FEBS J*. 2021;289(14):3932. doi:10.1111/FEBS.15803

95. Lominadze G, Powell DW, Luerman GC, Link AJ, Ward RA, McLeish KR. Proteomic analysis of human neutrophil granules. *Molecular and Cellular Proteomics*. 2005;4(10):1503-1521. doi:10.1074/mcp.M500143-MCP200

96. Rørvig S, Østergaard O, Heegaard NHH, Borregaard N. Proteome profiling of human neutrophil granule subsets, secretory vesicles, and cell membrane: correlation with transcriptome profiling of neutrophil precursors. *J Leukoc Biol*. 2013;94(4):711-721. doi:10.1189/JLB.1212619

97. Maianski NA, Geissler J, Srinivasula SM, Alnemri ES, Roos D, Kuijpers TW. Functional characterization of mitochondria in neutrophils: A role restricted to apoptosis. *Cell Death Differ*. 2004;11(2):143-153. doi:10.1038/SJ.CDD.4401320;KWRD=LIFE+SCIENCES

98. Summers C, Rankin SM, Condliffe AM, Singh N, Peters AM, Chilvers ER. Neutrophil kinetics in health and disease. *Trends Immunol*. 2010;31(8):318-324. doi:10.1016/J.IT.2010.05.006/ASSET/C5AC01A8-92EC-4F00-BD35-6791C9CF3D4B/MAIN.ASSETS/GR3.JPG

99. Takeuchi O, Akira S. Pattern Recognition Receptors and Inflammation. *Cell*. 2010;140(6):805-820. doi:10.1016/j.cell.2010.01.022

100. Mayadas TN, Cullere X, Lowell CA. The Multifaceted Functions of Neutrophils. *Annu Rev Pathol*. 2013;9:181. doi:10.1146/ANNUREV-PATHOL-020712-164023

101. Bournazos S, Ravetch J V. Fcγ receptor pathways during active and passive immunization. *Immunol Rev*. 2015;268(1):88-103. doi:10.1111/IMR.12343,

102. Lee WL, Harrison RE, Grinstein S. Phagocytosis by neutrophils. *Microbes Infect*. 2003;5(14):1299-1306. doi:10.1016/J.MICINF.2003.09.014

103. Swanson JA. Shaping cups into phagosomes and macropinosomes. *Nat Rev Mol Cell Biol*. 2008;9(8):639-649. doi:10.1038/NRM2447;KWRD=LIFE+SCIENCES

104. Nauseef WM. Myeloperoxidase in human neutrophil host defence. *Cell Microbiol*. 2014;16(8):1146-1155. doi:10.1111/CMI.12312

105. Lehrer RI, Ganz T. Defensins of vertebrate animals. *Curr Opin Immunol*. 2002;14(1):96-102. doi:10.1016/S0952-7915(01)00303-X

106. Stapels DAC, Geisbrecht B V., Rooijakkers SHM. Neutrophil serine proteases in antibacterial defense. *Curr Opin Microbiol*. 2014;0:42. doi:10.1016/J.MIB.2014.11.002

107. Borregaard N, Cowland JB. Granules of the Human Neutrophilic Polymorphonuclear Leukocyte. *Blood*. 1997;89(10):3503-3521. doi:10.1182/BLOOD.V89.10.3503

108. Selvatici R, Falzarano S, Mollica A, Spisani S. Signal transduction pathways triggered by selective formylpeptide analogues in human neutrophils. *Eur J Pharmacol*. 2006;534(1-3):1-11. doi:10.1016/J.EJPHAR.2006.01.034

109. Ramadass M, Catz SD. Molecular mechanisms regulating secretory organelles and endosomes in neutrophils and their implications for inflammation. *Immunol Rev*. 2016;273(1):249. doi:10.1111/IMR.12452

110. Patel S, Kumar S, Jyoti A, et al. Nitric oxide donors release extracellular traps from human neutrophils by augmenting free radical generation. *Nitric Oxide*. 2010;22(3):226-234. doi:10.1016/J.NIOX.2010.01.001

111. Kaplan MJ, Radic M. Neutrophil extracellular traps (NETs): Double-edged swords of innate immunity. *J Immunol*. 2012;189(6):2689. doi:10.4049/JIMMUNOL.1201719

112. Juha M, Molnár A, Jakus Z, Ledó N. NETosis: an emerging therapeutic target in renal diseases. *Front Immunol*. 2023;14:1253667. doi:10.3389/FIMMU.2023.1253667/XML/NLM

113. Petretto A, Bruschi M, Pratesi F, et al. Neutrophil extracellular traps (NET) induced by different stimuli: A comparative proteomic analysis. *PLoS One*. 2019;14(7):e0218946. doi:10.1371/JOURNAL.PONE.0218946

114. de Bont CM, Boelens WC, Pruijn GJM. NETosis, complement, and coagulation: a triangular relationship. *Cell Mol Immunol*. 2019;16(1):19-27. doi:10.1038/S41423-018-0024-0;KWRD=BIOMEDICINE

115. Yang H, Biermann MH, Brauner JM, Liu Y, Zhao Y, Herrmann M. New insights into neutrophil extracellular traps: Mechanisms of formation and role in inflammation. *Front Immunol*. 2016;7(AUG). doi:10.3389/FIMMU.2016.00302,

116. Kaplan MJ, Radic M. Neutrophil Extracellular Traps: Double-Edged Swords of Innate Immunity. *The Journal of Immunology*. 2012;189(6):2689-2695. doi:10.4049/JIMMUNOL.1201719,

117. Metzler KD, Goosmann C, Lubojemska A, Zychlinsky A, Papayannopoulos V. Myeloperoxidase-containing complex regulates neutrophil elastase release and actin dynamics during NETosis. *Cell Rep*. 2014;8(3):883-896. doi:10.1016/J.CELREP.2014.06.044,

118. Thiam HR, Wong SL, Wagner DD, Waterman CM. Cellular Mechanisms of NETosis. *Annu Rev Cell Dev Biol*. 2020;36:191-218. doi:10.1146/ANNUREV-CELLBIO-020520-111016,

119. Thiama HR, Wong SL, Qiu R, et al. NETosis proceeds by cytoskeleton and endomembrane disassembly and PAD4-mediated chromatin decondensation and nuclear envelope rupture. *Proc Natl Acad Sci U S A*. 2020;117(13):7326-7337. doi:10.1073/PNAS.1909546117,

120. Speziale P, Pietrocola G. Staphylococcus aureus induces neutrophil extracellular traps (NETs) and neutralizes their bactericidal potential. *Comput Struct Biotechnol J*. 2021;19:3451. doi:10.1016/J.CSBJ.2021.06.012

121. Papayannopoulos V. Neutrophil extracellular traps in immunity and disease. *Nat Rev Immunol*. 2018;18(2):134-147. doi:10.1038/NRI.2017.105;SUBJMETA=1699,223,249,250,2504,254,631;KWRD=IMMUNOLOGICAL+DISORDERS,INFECTION,NEUTROPHILS

122. Zhou Y, Chen B, Mittereder N, et al. Spontaneous secretion of the citrullination enzyme PAD2 and cell surface exposure of PAD4 by neutrophils. *Front Immunol*. 2017;8(SEP):1200. doi:10.3389/FIMMU.2017.01200/FULL

123. Carmona-Rivera C, Zhao W, Yalavarthi S, Kaplan MJ. Neutrophil extracellular traps induce endothelial dysfunction in systemic lupus erythematosus through the activation of matrix metalloproteinase-2. *Ann Rheum Dis*. 2015;74(7):1417-1424. doi:10.1136/ANNRHEUMDIS-2013-204837,

124. Pratesi F, Dioni I, Tommasi C, et al. Antibodies from patients with rheumatoid arthritis target citrullinated histone 4 contained in neutrophils extracellular traps. *Ann Rheum Dis*. 2014;73(7):1414-1422. doi:10.1136/ANNRHEUMDIS-2012-202765,

125. Garcia-Romo GS, Caielli S, Vega B, et al. Netting neutrophils are major inducers of type I IFN production in pediatric systemic lupus erythematosus. *Sci Transl Med*. 2011;3(73). doi:10.1126/SCITRANSLMED.3001201,

126. Sur Chowdhury C, Giaglis S, Walker UA, Buser A, Hahn S, Hasler P. Enhanced neutrophil extracellular trap generation in rheumatoid arthritis: Analysis of underlying signal transduction pathways and potential diagnostic utility. *Arthritis Res Ther*. 2014;16(3). doi:10.1186/AR4579,

127. Hakkim A, Fürnrohr BG, Amann K, et al. Impairment of neutrophil extracellular trap degradation is associated with lupus nephritis. *Proc Natl Acad Sci U S A*. 2010;107(21):9813-9818. doi:10.1073/PNAS.0909927107/-/DCSUPPLEMENTAL/PNAS.200909927SI.PDF

128. Firestein GS, McInnes IB. Immunopathogenesis of Rheumatoid Arthritis. *Immunity*. 2017;46(2):183-196. doi:10.1016/j.immuni.2017.02.006

129. Källberg H, Ding B, Padyukov L, et al. Smoking is a major preventable risk factor for rheumatoid arthritis: Estimations of risks after various exposures to cigarette smoke. *Ann Rheum Dis*. 2011;70(3):508-511. doi:10.1136/ARD.2009.120899,

130. Hedström AK, Rönnelid J, Klareskog L, Alfredsson L. Complex Relationships of Smoking, HLA–DRB1 Genes, and Serologic Profiles in Patients With Early Rheumatoid Arthritis: Update From a Swedish Population-Based Case–Control Study. *Arthritis and Rheumatology*. 2019;71(9):1504-1511. doi:10.1002/ART.40852,

131. Costenbader KH, Feskanich D, Mandl LA, Karlson EW. Smoking Intensity, Duration, and Cessation, and the Risk of Rheumatoid Arthritis in Women. *American Journal of Medicine*. 2006;119(6). doi:10.1016/j.amjmed.2005.09.053

132. Sopori M. Effects of cigarette smoke on the immune system. *Nat Rev Immunol*. 2002;2(5):372-377. doi:10.1038/NRI803,

133. Yeager RP, Kushman M, Chemerynski S, et al. Proposed Mode of Action for Acrolein Respiratory Toxicity Associated with Inhaled Tobacco Smoke. *Toxicological Sciences*. 2016;151(2):347-364. doi:10.1093/TOXSCI/KFW051

134. García-Sánchez A, Miranda-Díaz AG, Cardona-Muñoz EG. The Role of Oxidative Stress in Physiopathology and Pharmacological Treatment with Pro- and Antioxidant Properties in Chronic Diseases. *Oxid Med Cell Longev*. 2020;2020:2082145. doi:10.1155/2020/2082145

135. Quintana FJ, Basso AS, Iglesias AH, et al. Control of Treg and TH17 cell differentiation by the aryl hydrocarbon receptor. *Nature*. 2008;453(7191):65-71. doi:10.1038/NATURE06880,

136. Valderrama A, Ortiz-Hernández P, Agraz-Cibrián JM, et al. Particulate matter (PM10) induces in vitro activation of human neutrophils, and lung histopathological alterations in a mouse model. *Scientific Reports 2022 12:1*. 2022;12(1):1-11. doi:10.1038/s41598-022-11553-6

137. Maisha JA, El-Gabalawy HS, O'Neil LJ. Modifiable risk factors linked to the development of rheumatoid arthritis: evidence, immunological mechanisms and prevention. *Front Immunol*. 2023;14:1221125. doi:10.3389/FIMMU.2023.1221125/XML/NLM

138. Heijink IH, Pouwels SD, Leijendekker C, et al. Cigarette smoke-induced damage-associated molecular pattern release from necrotic neutrophils triggers proinflammatory mediator release. *Am J Respir Cell Mol Biol*. 2015;52(5):554-562. doi:10.1165/RCMB.2013-0505OC,

139. Imai Y, Kuba K, Neely GG, et al. Identification of Oxidative Stress and Toll-like Receptor 4 Signaling as a Key Pathway of Acute Lung Injury. *Cell*. 2008;133(2):235-249. doi:10.1016/J.CELL.2008.02.043

140. Takeuchi O, Akira S. Pattern Recognition Receptors and Inflammation. *Cell*. 2010;140(6):805-820. doi:10.1016/J.CELL.2010.01.022

141. Doz E, Noulin N, Boichot E, et al. Cigarette Smoke-Induced Pulmonary Inflammation Is TLR4/MyD88 and IL-1R1/MyD88 Signaling Dependent. *The Journal of Immunology*. 2008;180(2):1169-1178. doi:10.4049/JIMMUNOL.180.2.1169

142. Damgaard D, Friberg Bruun Nielsen M, Gaunsbaek MQ, Palarasah Y, Svane-Knudsen V, Nielsen CH. Smoking is associated with increased levels of extracellular peptidylarginine deiminase 2 (PAD2) in the lungs. *Clin Exp Rheumatol*. 2015;33(3):405-408. Accessed May 25, 2025. https://www.clinexprheumatol.org/abstract.asp?a=8516

143. Robays LJ, Maes T, Joos GF, Vermaelen KY. Between a cough and a wheeze: Dendritic cells at the nexus of tobacco smoke-induced allergic airway sensitization. *Mucosal Immunol*. 2009;2(3):206-219. doi:10.1038/MI.2009.7;KWRD=BIOMEDICINE

144. Lubberts E. The IL-23-IL-17 axis in inflammatory arthritis. *Nat Rev Rheumatol*. 2015;11(7):415-429. doi:10.1038/NRRHEUM.2015.53,

145. Barceló B, Pons J, Ferrer JM, Sauleda J, Fuster A, Agustí AGN. Phenotypic characterisation of T-lymphocytes in COPD: abnormal CD4+CD25+ regulatory T-lymphocyte response to tobacco smoking. *European Respiratory Journal*. 2008;31(3):555-562. doi:10.1183/09031936.00010407

146. Chiappori A, Folli C, Balbi F, et al. CD4+CD25highCD127-regulatory T-cells in COPD: Smoke and drugs effect. *World Allergy Organization Journal*. 2016;9(1). doi:10.1186/s40413-016-0095-2

147. Rangel-Moreno J, Hartson L, Navarro C, Gaxiola M, Selman M, Randall TD. Inducible bronchus-associated lymphoid tissue (iBALT) in patients with pulmonary complications of rheumatoid arthritis. *Journal of Clinical Investigation*. 2006;116(12):3183-3194. doi:10.1172/JCI28756,

148. Zong D, Liu X, Li J, Ouyang R, Chen P. The role of cigarette smoke-induced epigenetic alterations in inflammation. *Epigenetics & Chromatin 2019 12:1*. 2019;12(1):1-25. doi:10.1186/S13072-019-0311-8

149. Reynisdottir G, Karimi R, Joshua V, et al. Structural changes and antibody enrichment in the lungs are early features of anti-citrullinated protein antibody-positive rheumatoid arthritis. *Arthritis and Rheumatology*. 2014;66(1):31-39. doi:10.1002/ART.38201,

150. Demoruelle MK, Weisman MH, Simonian PL, et al. Airways abnormalities and rheumatoid arthritis-related autoantibodies in subjects without arthritis: Early injury or initiating site of autoimmunity? *Arthritis Rheum*. 2012;64(6):1756-1761. doi:10.1002/ART.34344,

151. Catrina AI, Jimmy Ytterberg A, Reynisdottir G, Malmström V, Klareskog L. Lungs, joints and immunity against citrullinated proteins in rheumatoid arthritis. *Nature Reviews Rheumatology 2014 10:11*. 2014;10(11):645-653. doi:10.1038/nrrheum.2014.115

152. Gosset P, Tsicopoulos A, Wallaert B, et al. Increased secretion of tumor necrosis factor α and interleukin-6 by alveolar macrophages consecutive to the development of the late asthmatic reaction. *Journal of Allergy and Clinical Immunology*. 1991;88(4):561-571. doi:10.1016/0091-6749(91)90149-I

153. Bendstrup E, Møller J, Kronborg-White S, Prior TS, Hyldgaard C. Interstitial Lung Disease in Rheumatoid Arthritis Remains a Challenge for Clinicians. *J Clin Med*. 2019;8(12):2038. doi:10.3390/JCM8122038

154. Does ACPA Increase the Risk of Interstitial Lung Disease? | RheumNow. Accessed May 25, 2025. https://rheumnow.com/content/does-acpa-increase-risk-interstitial-lung-disease

155. Trentham DE, Townes AS, Kang AH. Autoimmunity to type II collagen an experimental model of arthritis. *J Exp Med*. 1977;146(3):857. doi:10.1084/JEM.146.3.857

156. Brand DD, Latham KA, Rosloniec EF. Collagen-induced arthritis. *Nat Protoc*. 2007;2(5):1269-1275. doi:10.1038/NPROT.2007.173;KWRD=LIFE+SCIENCES

157. Rosloniec EF, Cremer M, Kang AH, Myers LK, Brand DD. Collagen-Induced Arthritis. *Curr Protoc Immunol*. 2010;89(1):15.5.1-15.5.25. doi:10.1002/0471142735.IM1505S89

158. Rooney CM, Mankia K, Emery P. The Role of the Microbiome in Driving RA-Related Autoimmunity. *Front Cell Dev Biol*. 2020;8:538130. doi:10.3389/FCELL.2020.538130

159. Scher JU, Sczesnak A, Longman RS, et al. Expansion of intestinal Prevotella copri correlates with enhanced susceptibility to arthritis. *Elife*. 2013;2013(2). doi:10.7554/ELIFE.01202.001

160. Tanaka S, Toki T, Akimoto T, Morishita K. Lipopolysaccharide accelerates collagen-induced arthritis in association with rapid and continuous production of inflammatory mediators and anti-type II collagen antibody. *Microbiol Immunol*. 2013;57(6):445-454. doi:10.1111/1348-0421.12052,

161. Chujo S, Okamoto S, Sunahara R, et al. Cigarette smoke condensate extracts augment collagen-induced arthritis in mice. *Int Immunopharmacol*. 2010;10(10):1194-1199. doi:10.1016/J.INTIMP.2010.06.026,

162. Okamoto S, Adachi M, Chujo S, et al. Etiological role of cigarette smoking in rheumatoid arthritis: Nasal exposure to cigarette smoke condensate extracts augments the development of collagen-induced arthritis in mice. *Biochem Biophys Res Commun*. 2011;404(4):1088-1092. doi:10.1016/j.bbrc.2010.12.118

163. Lindblad SS, Mydel P, Jonsson IM, Senior RM, Tarkowski A, Bokarewa M. Smoking and nicotine exposure delay development of collagen-induced arthritis in mice. *Arthritis Res Ther*. 2009;11(3). doi:10.1186/AR2728,

164. Wu S, Luo H, Xiao X, Zhang H, Li T, Zuo X. Attenuation of collagen induced arthritis via suppression on Th17 response by activating cholinergic anti-inflammatory pathway with nicotine. *Eur J Pharmacol*. 2014;735(1):97-104. doi:10.1016/j.ejphar.2014.04.019

165. He Z, Chen Y, Hou C, He W, Chen P. Cigarette Smoke Extract Changes Expression of Endothelial Nitric Oxide Synthase (eNOS) and p16(INK4a) and is Related to Endothelial Progenitor Cell Dysfunction. *Med Sci Monit*. 2017;23:3224. doi:10.12659/MSM.902746

166. Clark SR, Ma AC, Tavener SA, et al. Platelet TLR4 activates neutrophil extracellular traps to ensnare bacteria in septic blood. *Nat Med*. 2007;13(4):463-469. doi:10.1038/NM1565;KWRD=BIOMEDICINE

167. Bicker KL, Subramanian V, Chumanevich AA, Hofseth LJ, Thompson PR. Seeing citrulline: Development of a phenylglyoxal-based probe to visualize protein citrullination. *J Am Chem Soc*. 2012;134(41):17015-17018. doi:10.1021/JA308871V/SUPPL_FILE/JA308871V_SI_001.PDF

168. Liu X, Arfman T, Wichapong K, Reutelingsperger CPM, Voorberg J, Nicolaes GAF. PAD4 takes charge during neutrophil activation: Impact of PAD4 mediated NET formation on immune-mediated disease. *Journal of Thrombosis and Haemostasis*. 2021;19(7):1607. doi:10.1111/JTH.15313

169. Hemshekhar M, Anaparti V, Hitchon C, Mookherjee N. Buprenorphine Alters Inflammatory and Oxidative Stress Molecular Markers in Arthritis. *Mediators Inflamm*. 2017;2017:2515408. doi:10.1155/2017/2515408

170. Brand DD, Latham KA, Rosloniec EF. Collagen-induced arthritis. *Nat Protoc*. 2007;2(5):1269-1275. doi:10.1038/NPROT.2007.173;KWRD=LIFE+SCIENCES

171. Kang J, Jeong SH, Lee K, et al. Exacerbation of symptomatic arthritis by cigarette smoke in experimental arthritis. *PLoS One*. 2020;15(3):e0230719. doi:10.1371/JOURNAL.PONE.0230719

172. Kilkenny C, Browne WJ, Cuthill IC, Emerson M, Altman DG. Improving Bioscience Research Reporting: The ARRIVE Guidelines for Reporting Animal Research. *PLoS Biol*. 2010;8(6):e1000412. doi:10.1371/JOURNAL.PBIO.1000412

173. Chow LNY, Choi KYG, Piyadasa H, et al. Human cathelicidin LL-37-derived peptide IG-19 confers protection in a murine model of collagen-induced arthritis. *Mol Immunol*. 2014;57(2):86-92. doi:10.1016/J.MOLIMM.2013.08.011

174. Galligan CL, Siminovitch KA, Keystone EC, Bykerk V, Perez OD, Fish EN. Fibrocyte activation in rheumatoid arthritis. *Rheumatology*. 2010;49(4):640-651. doi:10.1093/RHEUMATOLOGY/KEP265

175. Song W, Ye J, Pan N, Tan C, Herrmann M. Neutrophil Extracellular Traps Tied to Rheumatoid Arthritis: Points to Ponder. *Front Immunol*. 2021;11:578129. doi:10.3389/FIMMU.2020.578129

176. Weirich E, Rabin RL, Maldonado Y, Benitz W, Modler S, Herzenberg LA. Neutrophil CD11b expression as a diagnostic marker for early-onset neonatal infection. *J Pediatr*. 1998;132(3):445-451. doi:10.1016/S0022-3476(98)70018-6

177. Wang Y, Jönsson F. Expression, role, and regulation of neutrophil Fcγ receptors. *Front Immunol*. 2019;10(AUG):474374. doi:10.3389/FIMMU.2019.01958/XML

178. Zhang Y, Boesen CC, Radaev S, et al. Crystal structure of the extracellular domain of a human FcγRIII. *Immunity*. 2000;13(3):387-395. doi:10.1016/S1074-7613(00)00038-8

179. Källquist L, Hansson M, Persson AM, et al. The tetraspanin CD63 is involved in granule targeting of neutrophil elastase. *Blood*. 2008;112(8):3444-3454. doi:10.1182/BLOOD-2007-10-116285

180. Skubitz KM, Campbell KD, Skubitz APN. CD63 associates with CD11/CD18 in large detergent-resistant complexes after translocation to the cell surface in human neutrophils. *FEBS Lett*. 2000;469(1):52-56. doi:10.1016/S0014-5793(00)01240-0

181. Hart SP, Alexander KM, Dransfield I. Immune Complexes Bind Preferentially to FcγRIIA (CD32) on Apoptotic Neutrophils, Leading to Augmented Phagocytosis by Macrophages and Release of Proinflammatory Cytokines. *The Journal of Immunology*. 2004;172(3):1882-1887. doi:10.4049/JIMMUNOL.172.3.1882,

182. Lacy P. Mechanisms of Degranulation in Neutrophils. *Allergy, Asthma & Clinical Immunology*. 2006;2(3):1-11. doi:10.1186/1710-1492-2-3-98/FIGURES/2

183. Opasawatchai A, Amornsupawat P, Jiravejchakul N, et al. Neutrophil activation and early features of net formation are associated with dengue virus infection in human. *Front Immunol*. 2019;10(JAN):419111. doi:10.3389/FIMMU.2018.03007/BIBTEX

184. Tsuk AG, Oster G. Determination of enzyme activity by a linear measurement. *Nature*. 1961;190(4777):721-722. doi:10.1038/190721A0;KWRD=SCIENCE

185. Wang Y, Jönsson F. Expression, Role, and Regulation of Neutrophil Fcγ Receptors. *Front Immunol*. 2019;10(AUG):1958. doi:10.3389/FIMMU.2019.01958

186. Korkmaz B, Horwitz MS, Jenne DE, Gauthier F. Neutrophil Elastase, Proteinase 3, and Cathepsin G as Therapeutic Targets in Human Diseases. *Pharmacol Rev*. 2010;62(4):726. doi:10.1124/PR.110.002733

187. Luzhetskaya OP, Sedykh SE, Nevinsky GA. How Human H1 Histone Recognizes DNA. *Molecules*. 2020;25(19):4556. doi:10.3390/MOLECULES25194556

188. Neuenfeldt F, Schumacher JC, Grieshaber-Bouyer R, et al. Inflammation induces pro-NETotic neutrophils via TNFR2 signaling. *Cell Rep*. 2022;39(3):110710. doi:10.1016/J.CELREP.2022.110710

189. Chemicals in Tobacco Products and Your Health | FDA. Accessed August 7, 2025. https://www.fda.gov/tobacco-products/health-effects-tobacco-use/chemicals-tobacco-products-and-your-health

190. Zhang Y, Geng S, Prasad GL, Li L. Suppression of Neutrophil Antimicrobial Functions by Total Particulate Matter From Cigarette Smoke. *Front Immunol*. 2018;9(OCT):2274. doi:10.3389/FIMMU.2018.02274

191. PRYOR WA, STONE K. Oxidants in Cigarette Smoke Radicals, Hydrogen Peroxide, Peroxynitrate, and Peroxynitrite. *Ann N Y Acad Sci*. 1993;686(1):12-27. doi:10.1111/J.1749-6632.1993.TB39148.X,

192. Pryor WA, Prier DG, Church DF. Electron-spin resonance study of mainstream and sidestream cigarette smoke: Nature of the free radicals in gas-phase smoke and in cigarette tar. *Environ Health Perspect*. 1983;Vol. 47:345-355. doi:10.1289/EHP.8347345,

193. CTRP. Accessed August 7, 2025. https://ctrp.uky.edu/products/gallery/Reference%20Cigarettes/detail/937

194. Jaimes EA, DeMaster EG, Tian RX, Raij L. Stable compounds of cigarette smoke induce endothelial superoxide anion production via NADPH oxidase activation. *Arterioscler Thromb Vasc Biol*. 2004;24(6):1031-1036. doi:10.1161/01.ATV.0000127083.88549.58/ASSET/FFA357A6-DCF7-432A-9BF7-8B80D8DB122B/ASSETS/GRAPHIC/8FF6.JPEG

195. Manfredi AA, Ramirez GA, Rovere-Querini P, Maugeri N. The Neutrophil's Choice: Phagocytose vs Make Neutrophil Extracellular Traps. *Front Immunol*. 2018;9(FEB):288. doi:10.3389/FIMMU.2018.00288

196. Poli V, Zanoni I. Neutrophil Intrinsic And Extrinsic Regulation Of NETosis In Health And Disease. *Trends Microbiol*. 2022;31(3):280. doi:10.1016/J.TIM.2022.10.002

197. Lin JH, Taggart M, Borthwick L, et al. Acute cigarette smoke or extract exposure rapidly activates TRPA1-mediated calcium influx in primary human airway smooth muscle cells. *Sci Rep*. 2021;11(1):1-15. doi:10.1038/S41598-021-89051-4;SUBJMETA=443,631,80;KWRD=CELL+BIOLOGY,PHYSIOLOGY

198. Yao K, Dou B, Zhang Y, et al. Inflammation—the role of TRPA1 channel. *Front Physiol*. 2023;14:1093925. doi:10.3389/FPHYS.2023.1093925/XML

199. Bautista DM, Jordt SE, Nikai T, et al. TRPA1 Mediates the Inflammatory Actions of Environmental Irritants and Proalgesic Agents. *Cell*. 2006;124(6):1269-1282. doi:10.1016/J.CELL.2006.02.023/ATTACHMENT/6B32D956-82BF-44CB-B6A6-8042D17957D7/MMC1.PDF

200. Talavera K, Gees M, Karashima Y, et al. Nicotine activates the chemosensory cation channel TRPA1. *Nat Neurosci*. 2009;12(10):1293-1299. doi:10.1038/NN.2379;KWRD=BIOMEDICINE

201. Yao K, Dou B, Zhang Y, et al. Inflammation—the role of TRPA1 channel. *Front Physiol*. 2023;14:1093925. doi:10.3389/FPHYS.2023.1093925/XML

202. Jensen JA, Goodson WH, Hopf HW, Hunt TK. Cigarette Smoking Decreases Tissue Oxygen. *Archives of Surgery*. 1991;126(9):1131-1134. doi:10.1001/ARCHSURG.1991.01410330093013

203. Fricker M, Goggins BJ, Mateer S, et al. Chronic cigarette smoke exposure induces systemic hypoxia that drives intestinal dysfunction. *JCI Insight*. 2018;3(3):e94040. doi:10.1172/JCI.INSIGHT.94040

204. Lodge KM, Vassallo A, Liu B, et al. Hypoxia Increases the Potential for Neutrophil-mediated Endothelial Damage in Chronic Obstructive Pulmonary Disease. *Am J Respir Crit Care Med*. 2022;205(8):903-916. doi:10.1164/RCCM.202006-2467OC/SUPPL_FILE/DISCLOSURES.PDF$AUTHORDISCLOSURES

205. Dölling M, Eckstein M, Singh J, et al. Hypoxia Promotes Neutrophil Survival After Acute Myocardial Infarction. *Front Immunol*. 2022;13:726153. doi:10.3389/FIMMU.2022.726153/BIBTEX

206. Thatcher TH, McHugh NA, Egan RW, et al. The Role of CXCR2 in Cigarette Smoke-Induced Lung Inflammation. *Am J Physiol Lung Cell Mol Physiol*. 2005;289(2):L322. doi:10.1152/AJPLUNG.00039.2005

207. Aoshiba K, Nagai A, Yasui S, Konno K. Nicotine prolongs neutrophil survival by suppressing apoptosis. *Journal of Laboratory and Clinical Medicine*. 1996;127(2):186-194. doi:10.1016/S0022-2143(96)90077-3

208. Csiszar A, Podlutsky A, Wolin MS, Losonczy G, Pacher P, Ungvari Z. Oxidative stress and accelerated vascular aging: implications for cigarette smoking. *Front Biosci*. 2009;14(14):3128. doi:10.2741/3440

209. Tsioumpekou M, Krijgsman D, Leusen JHW, Olofsen PA. The Role of Cytokines in Neutrophil Development, Tissue Homing, Function and Plasticity in Health and Disease. *Cells*. 2023;12(15):1981. doi:10.3390/CELLS12151981

210. Lee PY, Kumagai Y, Xu Y, et al. IL-1α Modulates Neutrophil Recruitment in Chronic Inflammation Induced by Hydrocarbon Oil. *The Journal of Immunology*. 2011;186(3):1747-1754. doi:10.4049/JIMMUNOL.1001328

211. Song Z, Bhattacharya S, Huang G, et al. NADPH oxidase 2 limits amplification of IL-1β–G-CSF axis and an immature neutrophil subset in murine lung inflammation. *Blood Adv*. 2022;7(7):1225. doi:10.1182/BLOODADVANCES.2022007652

212. McLeish KR, Merchant ML, Creed TM, et al. Frontline Science: Tumor necrosis factor-α stimulation and priming of human neutrophil granule exocytosis. *J Leukoc Biol*. 2017;102(1):19-29. doi:10.1189/JLB.3HI0716-293RR/-/DC1

213. Neuenfeldt F, Schumacher JC, Grieshaber-Bouyer R, et al. Inflammation induces pro-NETotic neutrophils via TNFR2 signaling. *Cell Rep*. 2022;39(3). doi:10.1016/J.CELREP.2022.110710/ATTACHMENT/118B6654-A597-454F-9297-62CCCEB648AF/MMC2.PDF

214. Wheeler JLH, Martin KC, Lawrence BP. Novel cellular targets of AhR underlie alterations in neutrophilic inflammation and iNOS expression during influenza virus infection. *J Immunol*. 2012;190(2):659. doi:10.4049/JIMMUNOL.1201341

215. Teske S, Bohn AA, Hogaboam JP, Lawrence BP. Aryl Hydrocarbon Receptor Targets Pathways Extrinsic to Bone Marrow Cells to Enhance Neutrophil Recruitment during Influenza Virus Infection. *Toxicol Sci*. 2007;102(1):89. doi:10.1093/TOXSCI/KFM282

216. Neff-LaFord H, Teske S, Bushnell TP, Lawrence BP. Aryl Hydrocarbon Receptor Activation during Influenza Virus Infection Unveils a Novel Pathway of IFN-γ Production by Phagocytic Cells. *The Journal of Immunology*. 2007;179(1):247-255. doi:10.4049/JIMMUNOL.179.1.247

217. Burns AR, Smith CW, Walker DC. Unique structural features that influence neutrophil emigration into the lung. *Physiol Rev*. 2003;83(2):309-336. doi:10.1152/PHYSREV.00023.2002/ASSET/IMAGES/LARGE/9J0230233109.JPEG

218. Wagner JG, Roth RA. Neutrophil migration mechanisms, with an emphasis on the pulmonary vasculature. *Pharmacol Rev*. 2000;52(3):349-374. doi:10.1016/S0031-6997(24)01456-X

219. Lakhan SE, Kirchgessner A. Anti-inflammatory effects of nicotine in obesity and ulcerative colitis. *J Transl Med*. 2011;9(1). doi:10.1186/1479-5876-9-129,

220. Mahmoudzadeh L, Froushani SMA, Ajami M, Mahmoudzadeh M. Effect of Nicotine on Immune System Function. *Adv Pharm Bull*. 2022;13(1):69. doi:10.34172/APB.2023.008

221. Lindblad SS, Mydel P, Jonsson IM, Senior RM, Tarkowski A, Bokarewa M. Smoking and nicotine exposure delay development of collagen-induced arthritis in mice. *Arthritis Res Ther*. 2009;11(3):R88. doi:10.1186/AR2728

222. Hemshekhar M, Piyadasa H, Mostafa D, Chow LNY, Halayko AJ, Mookherjee N. Cathelicidin and Calprotectin Are Disparately Altered in Murine Models of Inflammatory Arthritis and Airway Inflammation. *Front Immunol*. 2020;11:557260. doi:10.3389/FIMMU.2020.01932/BIBTEX

223. Hemshekhar M, Anaparti V, Hitchon C, Mookherjee N. Buprenorphine Alters Inflammatory and Oxidative Stress Molecular Markers in Arthritis. *Mediators Inflamm*. 2017;2017:2515408. doi:10.1155/2017/2515408

224. Rajaiah R, Moudgil KD. Animal Models. *Rheumatoid Arthritis*. Published online January 1, 2009:218-224. doi:10.1016/B978-032305475-1.50031-8

225. Horta-Baas G, Romero-Figueroa MDS, Montiel-Jarquín AJ, Pizano-Zárate ML, García-Mena J, Ramírez-Durán N. Intestinal Dysbiosis and Rheumatoid Arthritis: A Link between Gut Microbiota and the Pathogenesis of Rheumatoid Arthritis. *J Immunol Res*. 2017;2017:4835189. doi:10.1155/2017/4835189

226. Liu X, Zeng B, Zhang J, et al. Role of the Gut Microbiome in Modulating Arthritis Progression in Mice. *Sci Rep*. 2016;6:30594. doi:10.1038/SREP30594

227. Rogier R, Evans-Marin H, Manasson J, et al. Alteration of the intestinal microbiome characterizes preclinical inflammatory arthritis in mice and its modulation attenuates established arthritis. *Sci Rep*. 2017;7(1):15613. doi:10.1038/S41598-017-15802-X

228. Wang L, Zhu L, Tang Y, Wen Z, Peng L, Ci X. Long-Term Cigarette Smoke Exposure Promotes Neutrophil Ferroptosis Resistance, Inducing Neutrophil Extracellular Trap Formation and Driving Glucocorticoid Resistance in Chronic Obstructive Pulmonary Disease. *Research*. 2025;8:0751. doi:10.34133/RESEARCH.0751

229. Kang J, Jeong SH, Lee K, et al. Exacerbation of symptomatic arthritis by cigarette smoke in experimental arthritis. *PLoS One*. 2020;15(3):e0230719. doi:10.1371/JOURNAL.PONE.0230719

230. Differences Between the Sexes in Rheumatic Disease. Accessed July 17, 2025. https://rheumatology.org/patient-blog/differences-between-the-sexes-in-rheumatic-disease

231. Serré J, Tanjeko AT, Mathyssen C, et al. Enhanced lung inflammatory response in whole-body compared to nose-only cigarette smoke-exposed mice. *Respir Res*. 2021;22(1):1-15. doi:10.1186/S12931-021-01680-5/FIGURES/7

232. Serré J, Ajimé TT, Mathyssen C, et al. Comparison of the immune response in a mouse model of whole body and nose-only cigarette smoke-exposure. *European Respiratory Journal*. 2017;50(suppl 61):OA4827. doi:10.1183/1393003.CONGRESS-2017.OA4827

233. Teske S, Bohn AA, Hogaboam JP, Lawrence BP. Aryl Hydrocarbon Receptor Targets Pathways Extrinsic to Bone Marrow Cells to Enhance Neutrophil Recruitment during Influenza Virus Infection. *Toxicol Sci*. 2007;102(1):89. doi:10.1093/TOXSCI/KFM282

234. Xu M, Scott JE, Liu KZ, et al. The influence of nicotine on granulocytic differentiation - Inhibition of the oxidative burst and bacterial killing and increased matrix metalloproteinase-9 release. *BMC Cell Biol*. 2008;9(1):1-14. doi:10.1186/1471-2121-9-19/FIGURES/8